MEASUREMENTS OF THE MICROWAVE CONDUCTIVITY OF N-TYPE GERMANIUM

MEASUREMENTS OF THE MICROWAVE CONDUCTIVITY OF N-TYPE GERMANIUM

By

MOHAMMAD HASIBUR RAHMAN, B.SC. ENGG.,

M.SC. ENGG., M.ENG.

A Thesis

Submitted to the Faculty of Graduate Studies

in Partial Fulfilment of the Requirements

for the Degree

Doctor of Philosopy

McMaster University

March 1969

DOCTOR OF PHILOSOPHY (1969) McMaster University

(ELECTRICAL ENGINEERING) Hamilton, Ontario

TITLE: Measurements of the Microwave Conductivity of N-type Germanium

AUTHOR: Mohammad Hasibur Rahman, B.Sc.Engg. (East Pakistan University of Engg. & Technology)

M.Sc.Engg. (East Pakistan University of Engg. & Technology)

M.Eng. (McMaster University)

SUPERVISORS: Professor M.W. Gunn

Professor C.K. Campbell

NUMBER OF PAGES: xv, 182

SCOPE AND CONTENTS:

An investigation of the microwave reflections from the surface of a medium with complex permittivity at the open end of a rectangular waveguide has been made and a convenient method of measuring the microwave conductivity and dielectric constant of semiconductors is described.

The theory of operation of a microwave reflection bridge together with a method for the correction of the measurement error is presented.

In addition, a study has been made of the anisotropy of the small-signal microwave conductivity of n-type germanium in the presence of a high electric field.

ABSTRACT

An investigation has been made of the microwave reflections from the surface of a semiconducting medium with complex permittivity ($\hat{\varepsilon} = \varepsilon_r\varepsilon_o - j\frac{\sigma}{\omega}$) at the open end of an empty rectangular waveguide. The approximate and exact solutions of the reflection coefficients at the surfaces of both finite and semi-infinite media have been found as a function of the complex permittivity of the medium. The computations of the reflection coefficients are made at the 10 and 35 GHz ranges. Measurements, which confirm these calculations, have been performed with n-type germanium, selectron, and air at the open end of a rectangular waveguide using a reflection type microwave bridge. The investigation has shown that it is possible to devise a convenient method of measuring the conductivity and dielectric constant of semiconductors.

The theory of operation of the microwave reflection bridge together with the setting-up (matching) procedure of a practical form of the bridge has been presented. A method is also described for the correction of the measurement error which arises from the scattering coefficients at the input ports of the precision attenuator.

A theoretical and experimental study has also been made of the small-signal microwave conductivity of n-type germanium at room temperature in the presence of a high electric field, directed at an angle Θ to the microwave field. The study has shown that at frequencies such as 10 GHz, the microwave conductivity becomes anisotropic with respect to the direction of the d.c. field vector. Measurements are made on an 11.4 ohm cm, n-type germanium sample at 9.381 GHz with applied electric fields up to 1.8 KV/cm for $\theta = 0^{\circ}$, 40°, and 90°. The "open-end-waveguide measuring technique", which allows the angle between the microwave and d.c. field vectors to be varied, was employed to measure the microwave conductivity. The results of measurements which agree with predictions, confirm the feasibility of operation of a new microwave device based on the anisotropic effect.

ACKNOWLEDGEMENT

The author expresses his deep sense of gratitude to Professor M.W. Gunn for his helpful advice and criticism during the progress of a major portion of this work.

The author also expresses his sincere gratitude to Professor C.K. Campbell for his help and criticism during the progress of the work and in particular, during the preparation of this thesis.

The author is indebted to the Government of Canada for the receipt of a Commonwealth Scholarship and to the Defence Research Board of Canada for an equipment grant.

The author is also grateful to Dr. S.H. Chisholm for the loan of a few I.F. amplifiers, to Dr. J. Shewchun for his kind permission to use the facilities in the sample preparation laboratory, and to Dr. H.C. Bezner of the University of Waterloo for the loan of a piece of selectron.

Special thanks are due to the friends who helped the author with the project and in particular, to B. Clarke, F. Vallo, J.A. Carson and M.Y. Dimyan in the preparation of some semiconductor samples.

Finally, the author expresses his sincere thanks to Miss Barbara Coverdale for typing the manuscript in a very short time.

TABLE OF CONTENTS

LIST OF FIGURES

FIGURE		PAGE
4.7	Polar Plots of the Reflection Coefficients at Plane z=0 of the Waveguide Structure shown in Figure 4.1a as functions of Resistivity and Dielectric constant of the Medium in the half-space for 9.522 GHz. The circles represent the Measured Values for n-type Germanium, Selectron and Air---	76
4.8	The Skin Depth of Germanium as a Function of Resistivity----------------------------	77
5.1	A Rectangular Waveguide in a Ground Plane Covered by a Lossy Medium-----------------	84
5.2	The Change of Variables in the Equation 5.41--------------------------------------	84
5.3	A Rectangular Waveguide in a Ground Plane Covered by a Semiconductor-Metal Sandwich	94
5.4	Theoretically predicted Effects of the Slab Thickness on the Reflection Coefficients of Germanium in the Waveguide Structure of Figure 1.3---------	106
5.5	Resistivity versus Voltage Standing Wave Ratio for Various Values of Slab Thickness of Germanium in the Waveguide Structure of Figure 5.3 at 9.35 GHz------------------------------------	107
5.6	Polar Plots of the Reflection Coefficients as Functions of Resistivity and Slab Thickness of Germanium in the Waveguide Structure of Figure 5.3 at 9.35 GHz-------	108
5.7	Resistivity versus Voltage Standing Wave Ratio of Germanium in the Waveguide System of Figure 5.3 at 34.5 GHz_________	109
5.8	Polar Plots of the Computed Reflection Coefficients as Functions of Resisitivity and Slab Thickness of Germanium in the Waveguide System of Figure 5.3 for 34.5 GHz--------------------------------------	110

LIST OF TABLES

CHAPTER I

INTRODUCTION

The properties of semiconductors such as relative permittivity ε_r and conductivity σ play an important role in the design and operation of semiconductor devices. Ever since Bardeen and Brattain[1] discovered the transistor in 1948, great interest has been shown in the study of the properties of semiconductors. With their evergrowing importance in the field of practical science, semiconductors of different materials are being investigated carefully to discover their properties for use in newer branches of technology.

The investigation of the microwave properties of semiconductors is a relatively recent development, having begun only about a decade ago[2-17]. Within this period, the measurement of semiconductor properties by microwave methods has proved to be advantageous over the d.c. methods. Moreover, in recent years, the semiconductor devices have found important applications at microwave frequencies. The gradual displacement of the microwave power tubes by solid state devices is an example[18].

The problem of microwave propagation through semiconductors in the presence of a high d.c. electric field is another recent development[19-34]. From a study of the microwave conductivity data at high electric fields one can infer the variation of relaxation time with electric fields and hence the nature of the scattering processes. Also, the microwave conductivity at high electric field levels becomes anisotropic with respect to the direction of the d.c. and microwave field vectors. This effect can be useful in the design of microwave devices[25-26, 56-57].

The objectives of this thesis are three-fold, as follows:

(i) Since a microwave reflection bridge is suitable for the measurement of the electrical properties of semiconductors, its practical setting-up (matching) procedure, giving the most accurate results, has been desired for some time. The measurement accuracy in such a bridge depends mainly on the matching of the input ports of the 'hybrid tee', a basic unit of the reflection bridge. Also a significant error arises from the scattering coefficients at the input ports of the rotary-vane precision attenuator, the standard component of the bridge. Although a theory of this bridge[13] is available, its practical setting-up procedure and a method for correcting these errors have not been reported in the literature.

This thesis describes a theory together with the practical setting-up procedure of a reflection type bridge and a method for correcting the measurement error which arises from the scattering coefficients at the input ports of the precision attenuater. This bridge to be discussed in chapter II, has been used to confirm the theories developed in this thesis.

(ii) The second objective is the study of microwave reflections from the surface of a bulk semiconductor. This study was motivated in part by a need to devise a method of measuring the microwave properties of semiconductors. A number of techniques for measuring microwave conductivity and dielectric constant has been reported in the literature (2-7, 10-17). The well-known techniques involve the measurement of VSWR[5-6], transmission coefficient[10] and reflection coefficient[13] at the air-sample interface in a completely filled waveguide, which require the samples to be cut to the cross-section of the waveguide. Of these, the accuracy of the reflection method of measurement is comparatively good when the resistivity of the semiconductor is relatively high. At low resistivities the unavoidable gap present between the semiconductor and the walls of the waveguide introduces error in the results of measurement[12].

Resonant cavity perturbation techniques have been used for measuring the properties of low resistivity semiconductors[11]. The lossy wall[14] and partially filled guide[15] have been developed very recently. The former technique is suitable for measurement when $\sigma = \omega \varepsilon_o \varepsilon_r$ while the latter for low resistivity measurement.

Besides the above mentioned techniques a number of authors[2, 7] measured resistivity by pressing a thin slab of semiconductors backed by a short-circuit plate at the open end of a rectangular waveguide. This is a convenient physical arrangement for measuremnt. However, the accuracy of the method is affected by the undesired radiation which propagates through the semiconductor parallel to the short-circuit plate. The intensity of this radiation depends on the dimensions and the resistivity of the semiconductor sample. Moreover the measuring method was based on the use of a slotted line which lacks precision at high frequencies because of the perturbing influence of the slot and probe on the fields and because of the mechanical inaccuracies.

None of the techniques mentioned above provides an accurate means of measuring ε_r and σ at the high end of the resistivitiy range. Not only that, but different techniques of measurement are required, depending on the resistivity of the semiconductor. Thus the development of a new method that could provide an accurate means of measuring ε_r and σ over the entire range of resistivity is desirable. Such a method based on the reflections of microwaves from a piece of semiconductor placed at the end of a rectangular waveguide, has been described.

Chapters III to V of this thesis are devoted to the theory of microwave reflections giving experimental verifications wherever possible. To be specific, the theoretical solutions of the reflection coefficient of a semiconductor block at the end of a rectangular waveguide are developed. The following waveguide configurations were considered for the analysis:

(a) A semiconductor slab placed inside a rectangular waveguide and terminated by a short-circuit plate (Fig. 1.1);

(b) A semiconductor slab pressed at the end of a rectangular waveguide opening onto a metal flange and terminated by a short-circuit plate (Fig. 1.2);

(c) A semiconductor slab placed at the end of a rectangular waveguide opening onto a metal flange and followed by free space (Fig. 1.3).

The approximate solutions of the reflection coefficient at plane z=0 of these configurations for a finite semiconductor medium are developed in Chapter III. The exact solutions of the reflection coefficient for a semi-infinite and finite medium at plane z=0 of the configurations (b) and (c) are developed in Chapters IV and V, respectively. Numerical computations for each case were made at the 10 and 35 GHz ranges and confirmed experimentally for n-type germanium, selectron and air.

The result of this analysis has been utilised to devise a method of measurement which involves the placement of a semiconductor sample at the open end of a rectangular waveguide. This method which has been termed the "open-end-waveguide measuring technique" is not only suitable for the normal measurement of the microwave properties of semiconductors but it is also advantageous for high-field measurements. The principal advantages of this method over the previous ones are that the samples are not required to be cut to the cross-section of the waveguide, the measurement accuracy is fairly high in the entire range of resistivity and the rotation of the sample position with respect to the microwave field vector in high-field measurements is easy.

(iii) The last objective of this thesis is the study and measurement of the anisotropy of the microwave conductivity in n-type germanium subjected to a high d.c. electric field. Gunn[25] has stated from physical reasoning that the small-signal microwave conductivity of a semiconductor sample for parallel d.c. and microwave fields is given by the incremental conductivity $\frac{\partial J}{\partial F}$ whereas the conductivity of the same sample for perpendicular fields is given by the d.c. conductivity $\frac{J}{F}$. Although a theory and the experimental verifications of the parallel conductivity have been described by a number of authors[19-29], a satisfactory theory together with experimental confirmations for the perpendicular case has not been reported in literature. In particular, a confirmation of the dependence of the microwave conductivity on the angle between microwave and d.c. field vectors has remained an unsolved problem. Moreover, a definite conclusion of the existence of this anisotropy would confirm the feasibility of operation of a new microwave device, namely "the hot electron microwave rotator". The theoretical performance of such a rotator has been investigated elsewhere by the author[57].

This thesis gives a simple derivation of the small-signal microwave conductivity of semiconductors, in terms of parallel and perpendicular conductivities and the angle between the microwave and d.c. field vectors. An analysis has also been made of the parallel and perpendicular conductivities of n-type germanium by solving the Boltzmann equation in the same manner as used by Nag and Das[23]. Numerical calculations have been made of the microwave conductivity and the angle of rotation of the microwave current vector for an n-type germanium sample at 9.381 GHz. To confirm these calculations, measurements have been made of the conductance as a function of the electric field intensity in the same germanium sample at d.c. and 9.381 GHz. A new method of measuring microwave conductivity in high electric fields, which allows the angle between the microwave and d.c. field vectors to be varied, has been devised. The results of measurement agree with those calculated by the theory.

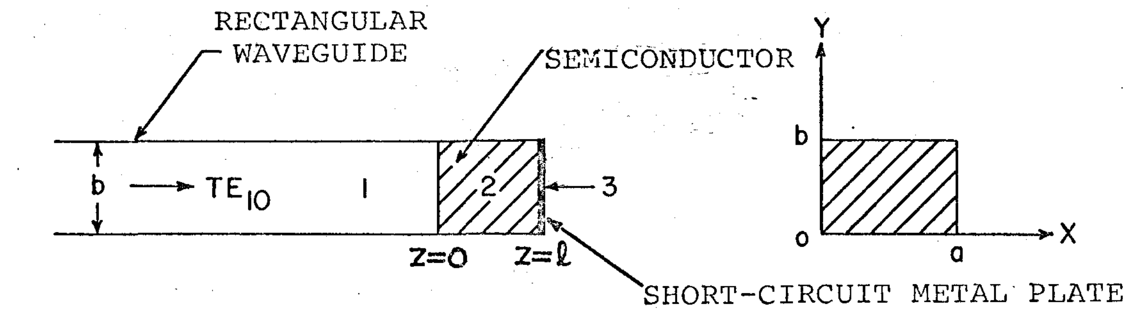

FIGURE 1.1: A Semiconductor Sample Placed inside a Rectangular Waveguide and Terminated by a Short-Circuit Metal Plate.

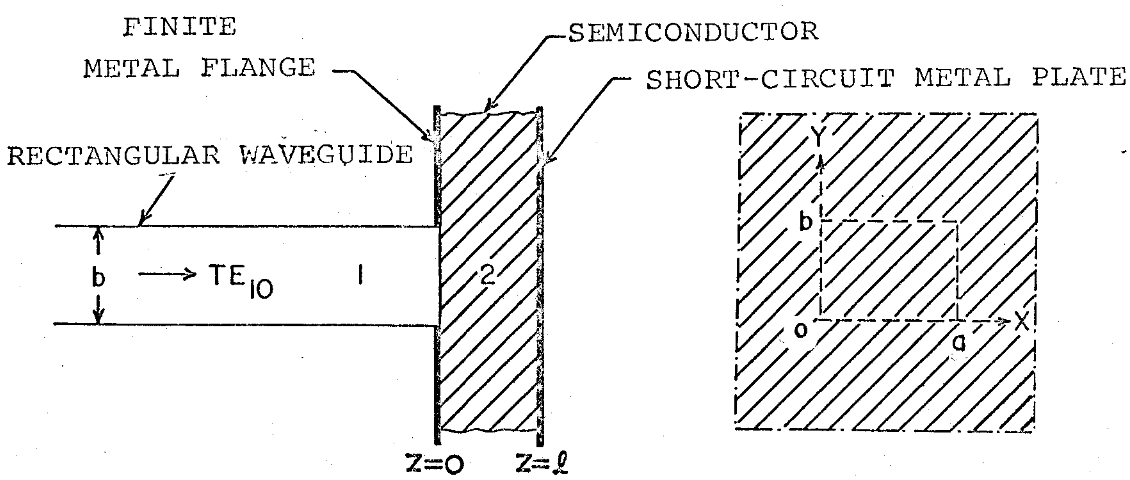

FIGURE 1.2: A Semiconductor Sample Placed across the End of a Rectangular Waveguide Opening onto a Metal Flange and Terminated by a Short-Circuit Metal Plate.

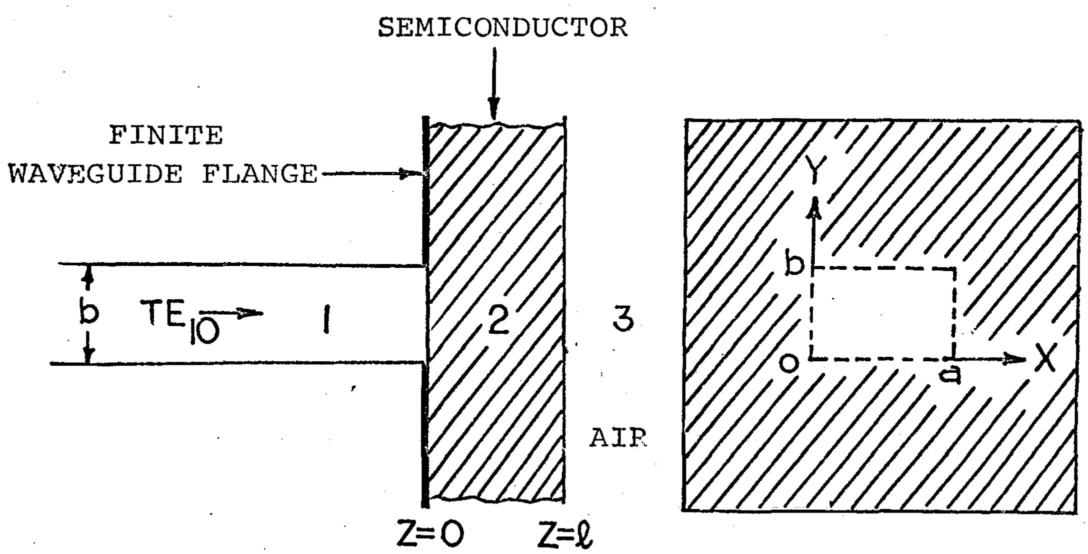

FIGURE 1.3: A Semiconductor Sample Placed across the End of a Rectangular Waveguide Opening onto a Metal Flange and Followed by Air.

CHAPTER II

THE MICROWAVE REFLECTION BRIDGE

2.1 Introduction

A microwave reflection bridge[13, 35] is most suitable for accurate measurements of the electrical properties of semiconductors (σ, ε_r) in the microwave frequency range. Such measurements normally involve the precise determination of the reflection coefficient of a waveguide filled or partially filled with semiconductors and for this the bridge has some advantages over a slotted line. At the higher end of the microwave frequency range, slotted lines become subject to errors because of the difficulty of maintaining the required mechanical tolerances.

A basic unit of a microwave reflection bridge is a hybrid tee and in Section 2.2.1, the properties of the 'hybrid tee', 'symmetric tee', and 'magic tee' are described. The magic tee with it's terminal conditions is also discussed in Section 2.2.1, and in Section 2.2.2, a theory of operation of a reflection bridge is presented. In Section 2.2.3, a method is described for the correction of the measurement error. Finally, in Section 2.3, the details of the setting-up procedure of a practical form of a reflection bridge are discussed.

2.2 Theory

A microwave junction with four ports as shown in Fig. 2.1 is defined as a hybrid tee. A tee that appears matched looking into each arm in turn with matched terminations on the other arms is called a 'matched tee'. A matched tee may or may not be symmetric and when compensated for asymmetry is called a 'magic tee'.

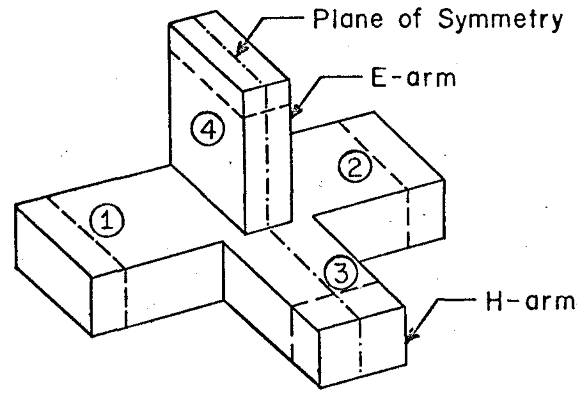

Figure 2.1: The three Dimensional View of a Hybrid Tee

2.2.1 The Microwave Tees

(a) The Hybrid T: The essential properties of a hybrid tee are expressed in the form of a scattering matrix [S]. With reference to ports 1, 2, 3, and 4 in Fig. 2.1 the scattering matrix of a hybrid tee is defined as

$$[b] = [S]\,[a]$$

where a is the incident wave and b is the scattered wave.

or,

$$\begin{bmatrix} b_1 \\ b_2 \\ b_3 \\ b_4 \end{bmatrix} = \begin{bmatrix} S_{11} & S_{12} & S_{13} & S_{14} \\ S_{21} & S_{22} & S_{23} & S_{24} \\ S_{31} & S_{32} & S_{33} & S_{34} \\ S_{41} & S_{42} & S_{43} & S_{44} \end{bmatrix} \begin{bmatrix} a_1 \\ a_2 \\ a_3 \\ a_4 \end{bmatrix}$$

When the propagation medium is air,

$$S_{12} = S_{21}$$

$$S_{13} = S_{31}$$

$$S_{34} = S_{43} \text{ etc. so that}$$

$$\begin{bmatrix} b_1 \\ b_2 \\ b_3 \\ b_4 \end{bmatrix} = \begin{bmatrix} S_{11} & S_{12} & S_{13} & S_{14} \\ S_{12} & S_{22} & S_{23} & S_{24} \\ S_{13} & S_{23} & S_{33} & S_{34} \\ S_{14} & S_{24} & S_{34} & S_{44} \end{bmatrix} \begin{bmatrix} a_1 \\ a_2 \\ a_3 \\ a_4 \end{bmatrix} \qquad (2.1)$$

(b) The Symmetric T: A hybrid tee becomes a symmetric tee if it has a symmetrical structure with reference planes placed symmetrically and at equal distances from the plane of symmetry. Further, a symmetric tee has the following additional characteristics.

$$S_{34} = 0$$

$$S_{43} = 0$$

$$S_{13} = S_{23}$$

$$S_{11} = S_{22}$$

$$S_{14} = -S_{24}$$

If the reference planes in the side arms are not equidistant from the plane of symmetry, then

$$S_{13} = S_{23}\, e^{j\psi}$$

where ψ = difference in electrical phase change over the lengths of the side arms.

(c) The Magic T: A symmetric tee becomes a magic tee when ports 3 and 4 are matched i.e. $S_{33} = S_{44} = 0$. The matching of ports 3 and 4 ensures

$$S_{11} = S_{22} = S_{12} = 0$$

and $|S_{13}|^2 = |S_{14}|^2 = 1/2$, automatically, provided the following condition is satisfied:

"The walls are perfect conductors or approximately so; for long side arms, this condition may not be satisfied[36]".

The magic tee has, therefore, the following additional characteristics to the symmetric tee:

$$S_{33} = S_{44} = 0$$

$$S_{11} = S_{22} = S_{12} = 0$$

If a TE_{10} wave $E_3 \angle 0^\circ$ is incident on port 3 of a magic tee while all other ports are terminated in loads having reflection coefficents R_1, R_2, and R_4 at reference ports, the output waves at these ports are expressed respectively as[36]

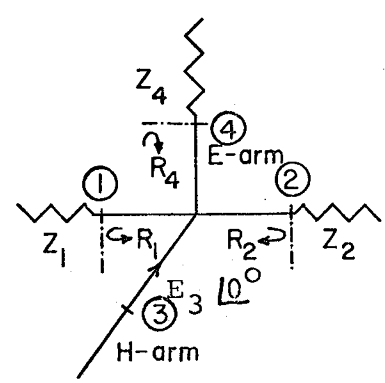

Figure 2.2: A Magic Tee with Unmatched Terminal Loads Z_1, Z_2 and Z_4.

$$E_1' = \sqrt{2}\ \frac{(1-R_2R_4)\ E_3 \angle 0^\circ}{2 - R_4\ (R_1 + R_2)} \qquad (2.1a)$$

$$E_2' = \sqrt{2}\ \frac{(1-R_1R_4)\ E_3 \underline{|0^\circ}}{2 - R_4\ (R_1 + R_2)} \tag{2.1b}$$

$$E_3' = \frac{(R_1 + R_2 - 2\ R_1R_2R_4)\ E_3\underline{|0^\circ}}{2 - R_4\ (R_1 + R_2)} \tag{2.1c}$$

$$E_4' = \frac{(R_1 - R_2)\ E_3\underline{|0^\circ}}{2 - R_4\ (R_1 + R_2)} \tag{2.1d}$$

These equations give the following important conditions:

(i) If $R_4 = 0$ and $R_1 \neq R_2$,

$$E_4' = (R_1 - R_2)\ E_3/2,$$

$$E_1' = E_2' = E_3/\sqrt{2}$$

i.e. the power outputs are equal in side arms with an output E_4' in port 4 and

$$E_3' = (R_1 + R_2)\ E_3/2$$

i.e. the power is reflected into port 3.

(ii) If $R_4 \neq 0$ or $R_4 = 0$ and $R_1 = R_2$,

$$E_4' = 0$$

$$E_1' = E_2' = E_3/\sqrt{2}$$

i.e. the power outputs are equal in side arms with zero output in port 4 and

$$E_3' = R_1E_3$$

i.e. for a short circuit ($R_1 = -1$), all the power is reflected into arm 3. Thus for a magic tee when the bridge is balanced $R_1 = R_2$ whether or not $R_4 = 0$ and the power outputs are equal in the side arms.

2.2.2 The Reflection Bridge

The schematic diagram of a reflection bridge circuit is shown in Fig. 2.3. The bridge element can be a 'hybrid tee', a 'symmetric tee' or a 'magic tee'. The ports 1 and 2 of the bridge element lie in the reference and sample arms, while ports 3 and 4 lie in the H and E arms, respectively. Z_1 is the reference load and Z_2 is the unknown load, the reflection coefficient of which is to be determined.

(a) The Bridge with a Hybrid Tee:

With a 'hybrid tee' in Fig. 2.3 the scattering matrix with reference to ports 1, 2, 3 and 4 is given by equation (2.1). Also, at reference ports 1 and 2,

$$R_1 = \frac{a_1}{b_1} \tag{2.2}$$

$$R_2 = \frac{a_2}{b_2} \tag{2.3}$$

where R_1 and R_2 are reflection coefficients at ports 1 and 2, respectively. Noting that $a_4 = b_4 = 0$ for a null condition, R_2 can be obtained from equations (2.1), (2.2) and (2.3) and is given by[13],

$$R_2 = \frac{\alpha\ R_1 - \delta}{\gamma\ R_1 - 1} \tag{2.4}$$

where

$$\alpha = \left[\frac{S_{11}\ S_{34} - S_{13}\ S_{14}}{S_{22}\ S_{34} - S_{23}\ S_{24}}\right] \tag{2.5a}$$

$$\delta = \left[\frac{S_{34}}{S_{22}\ S_{34} - S_{23}\ S_{24}}\right] \qquad (2.5b)$$

and

$$\gamma = \left[\frac{(S_{11}\ S_{22} - S_{12}^2)\ S_{34} + (S_{13}\ S_{12} - S_{23}\ S_{11})\ S_{24}}{S_{22}\ S_{34} - S_{23}\ S_{24}} + \frac{(S_{12}\ S_{23} - S_{13}\ S_{22})\ S_{14}}{S_{22}\ S_{34} - S_{23}\ S_{24}}\right] \qquad (2.5c)$$

(b) The Bridge with a Symmetric Tee:

When the 'hybrid tee' is symmetric,

$$S_{34} = 0$$
$$S_{43} = 0$$
$$S_{11} = S_{22}$$
$$S_{13} = S_{23}$$
$$S_{24} = -S_{14}$$
$$S_{12} = S_{21} \quad \text{etc.}$$

and the equations (2.4) and (2.5) give

$$\alpha = \left[\frac{0 - S_{13}\ S_{14}}{0 - S_{23}\ S_{24}}\right]$$

$$= -1$$

$$\delta = 0$$

$$\gamma = \frac{(S_{13}\ S_{12} - S_{23}\ S_{11})\ S_{24} + (S_{12}\ S_{23} - S_{13}S_{22})\ S_{14}}{-S_{23}\ S_{24}}$$

$$= 0$$

$$\therefore\ R_2 = R_1 \qquad (2.6)$$

(c) The Bridge with a Matched Tee:

When the input ports of the 'hybrid tee' are matched,

$$S_{11} = S_{22} = S_{12} = 0$$

$$S_{34} = S_{43} \neq 0$$

which give from equation (2.5c)

$$\gamma = 0$$

$$\therefore R_2 = -R_1 \alpha + \delta \tag{2.7}$$

(d) The Bridge with a Magic Tee:

When the 'hybrid tee' is magic,

$$S_{34} = S_{43} = 0$$

$$S_{11} = S_{22} = S_{12} = 0$$

$$S_{13} = S_{23}$$

$$S_{14} = - S_{24}$$

which give

$$\alpha = \frac{0 - S_{13} S_{14}}{0 - S_{23} S_{24}}$$

$$= -1$$

$$\delta = 0$$

$$\gamma = 0$$

$$\therefore R_2 = R_1 \tag{2.8}$$

which is the same as obtained in the symmetric bridge (Equation 2.6)

(e) The Bridge with either a Symmetric or a Magic Tee:

Consider the bridge circuit of Fig. 2.3 with the tuning stub removed from the slotted section for the balanced condition in which the reflection coefficient R_1 at the plane 1 is made equal to R_2 at the plane 2, by suitable adjustment of the standard rotary vane attenuator and short-circuit. For a given attenuator setting (A_1), R_1 can be written[36]

$$R_1 = S_{11}\ (A_1) + \frac{S_{16}^2\ (A_1)\ R_6}{1 - S_{66}\ (A_1)\, R_6}$$

$$\doteqdot S_{11}\ (A_1) + S_{16}^2\ (A_1)\ R_6 \qquad (2.9)$$

on the reasonable assumption that $S_{66}\ (A_1)\ R_6 \ll 1$. The scattering coefficient[37] $S_{16} = K_A e^{-A_1}$ where the constant K_A represents the constant insertion loss and phase shift in the attenuator. Also the reflection coefficient $R_6 = K_s\ e^{-j2\beta \ell_1}$ where K_s is the complex constant containing the fixed loss in the short circuit and β is the phase constant in the empty waveguide. The readings of the precision rotary vane attenuator and the precision short circuit are taken as A_1 and ℓ_1 respectively, thus

$$R_1 = S_{11}\ (A_1) + K_A^2\ K_s\ e^{-2(A_1\ + j\beta \ell_1)} \qquad (2.10)$$

If the unknown impedence is replaced by a short circuit, then $R_2 = -1$ and a null balance will be obtained with the attenuator and short circuit settings A_o and ℓ_o respectively. This gives

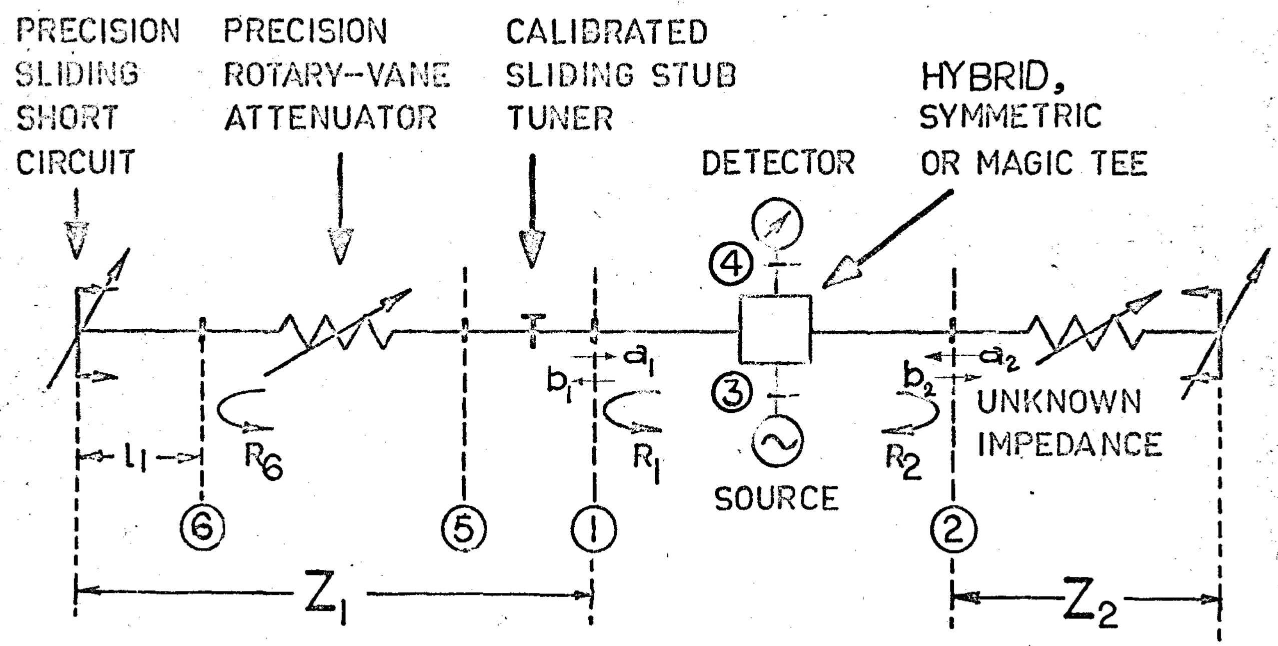

FIGURE 2.3: A Microwave Reflection Bridge Circuit.

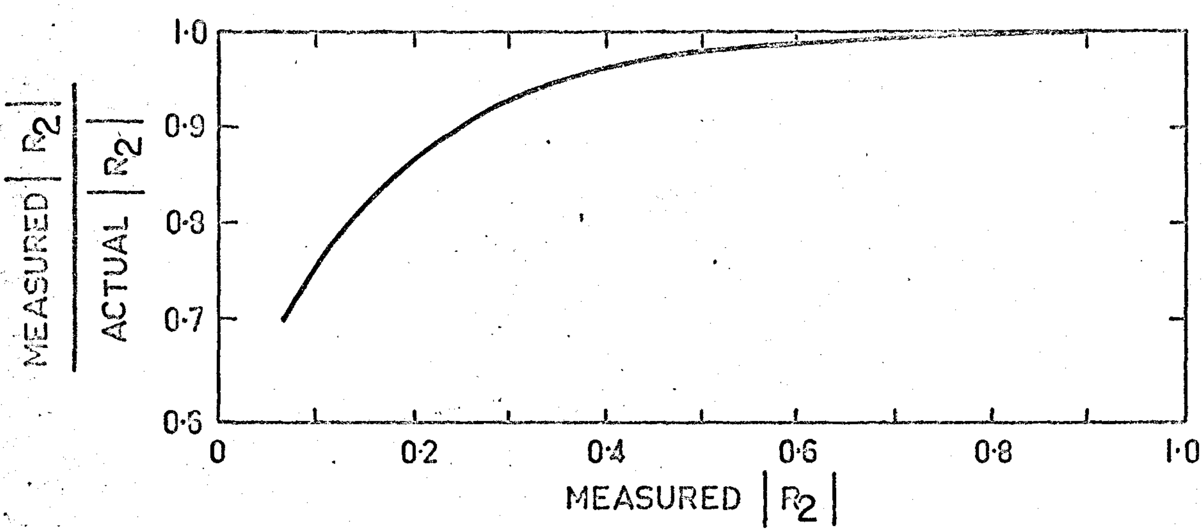

FIGURE 2.4: The Relative Error in the Magnitude of the Reflection Coefficient $|R_2|$ due to the Scattering Coefficient S_{11}.

the equation

$$-1 = S_{11}\ (A_0) + K_A^2\ K_s\ e^{-2\ (A_0 + j\beta \ell_0)} \tag{2.11}$$

Equations (2.10) and (2.11) then give for a null balance with the unknown impedence at plane 2

$$\begin{aligned} R_2 &= R_1 \\ &\doteq -\left[1 + S_{11}(A_0)\right]\ e^{-(A + j\phi)} + S_{11}\ (A_1) \\ &\doteq -\ e^{-(A + j\phi)} + S_{11}\ (A_1) \end{aligned} \tag{2.12}$$

where $A=2\ (A_1 - A_0)$, $\phi = 2\beta\ (\ell_1 - \ell_0)$ and $S_{11}\ (A_0) \ll 1$.

In a precision attenuator, due to the finite thickness of the absorbing vane S_{11} is not zero but it is small. Under conditions of measurement in which the term $S_{11}\ (A_1)$ is significant, the usual practice of neglecting it by some microwave engineers may resultin a serious error. In the measurement of a large reflection coefficient, however, $\left| e^{-(A + j\phi)} \right| \gg \left| S_{11}(A_1) \right|$ so that

$$R_2 \doteq -e^{-(A+j\phi)} \tag{2.13}$$

For the purposes of measurement, particularly with materials of low reflection coefficient, the equation (2.12) was used in conjunction with a calibrated tuner in the reference arm to tune out $S_{11}(A_1)$ to zero. This ultimately made it possible to use the much simpler equation (2.13).

Accurate results can also be obtained with equation (2.12) only if the magnitude and phase of S_{11} are known.

Unfortunately it is very difficult to measure precisely both phase and magnitude of such a small scattering coefficient by a conventional slotted line technique. In the following section a method has been described for such measurement using the bridge circuit of Fig. 2.3.

2.2.3 The Measurement Errors

The accuracy of the reflection bridge measurements depends to a large extent on the quality of the variable impendance standard arm components, which comprise a precision rotary vane attenuator and a precision variable short-circuit. One source of error in such measurements results from the scattering coefficients at the input ports of the attenuator and the magnitude of this error is a function of the attenuator setting. This error becomes significant in measurements of low reflection coefficients which require an attenuator setting greater than a few dB, for example the measurement of the reflection coefficient at the open end of a rectangular waveguide.

Holm, et.al.[38] have derived an expression for the associated scattering matrix of a rotary-vane attenuator which is useful for the calculation of the scattering coefficient. For the attenuator - stub tuner combination shown in Fig. 2.3 with the tuning stub removed from the slotted section of guide, their expression for the scattering coefficient S_{11} at the measuring plane 1 is

$$S_{11} = A_{11} + B_{11} \sin^2\theta + C_{11} \sin 2\theta \qquad (2.14)$$

The vane angle θ is related to the attenuator setting in dB by the expression $dB = -20 \log_{10} (\cos^2 \theta)$ and A_{11}, B_{11} and C_{11} are complex constants. The authors verified Eq. (2.14) by using the reflectometer technique of Engen and Beatty[39] which measures the magnitude but not the phase of S_{11}. The constants in Eq. (2.14) were determined, after assuming A_{11} real, from measurements of the magnitude of S_{11} at five values of attenuator setting.

We wish to describe a procedure of eliminating errors due to S_{11} by using a calibrated sliding stub tuner at the input port of the rotary-vane attenuator. The method also gives a means of measuring not only the magnitude but also the phase of S_{11} as a function of attenuator setting. The determination of the constants A_{11}, B_{11}, and C_{11} has also been simplified as measurements of both phase and magnitude of S_{11} at three attenuator settings only are required.

Consider now the case of the Fig. 2.3 in which a tuning stub is introduced into the slotted section of the guide between planes 1 and 5. For any given setting of the attenuator, this tuner can be adjusted to make $S_{11}(A_1) = 0$. For the same unknown impedance, this matched condition of the attenuator will result in new readings A_m and ϕ_m instead of the A and ϕ in Eq. (2.12). The scattering coefficient $S_{11}(A_1)$ can then be obtained from the equation

$$S_{11}(A_1) = -\bar{e}^{(A_m + j\phi_m)} + \bar{e}^{(A + j\phi)} \qquad (2.15)$$

Measurements have been made of S_{11} (A_1) for several commercially available X band (10GHz) rotary vane attenuators, using the bridge circuit of Figure 2.3. For the preliminary measurements, matched loads were placed at planes 6 and 2 and the calibrated sliding stub tuner was adjusted to give a null output for different settings of the attenuator. These calibrated readings then allowed S_{11} (A_1) to be made zero as required in the subsequent measurements.

The reflection coefficient of a variable unknown impedance at plane 2, comprising a variable attenuator and variable short circuit, was then measured with and without the tuning stub, that is for the conditions S_{11} $(A_1) = 0$, S_{11} $(A_1) \neq 0$. These measurements gave the scattering coefficient S_{11} (A_1) as a function of attenuation, through equation (2.15). Measurements with the rotary vane attenuator at three angles (θ) enabled the constants A_{11}, B_{11}, and C_{11} in equation (2.14) to be calculated.

Measured values of the magnitude and phase of S_{11} for the two rotary vane attenuators are given in Figure 2.5 (H.P. x 382A) and Figure 2.6 (Elliott A167/44). Calculated curves from equation (2.14) based on the experimentally determined constants, can be seen to be in good agreement with the measured values. Relative errors in measured magnitudes of the reflection coefficient due to S_{11} are indicated in Figure 2.4.

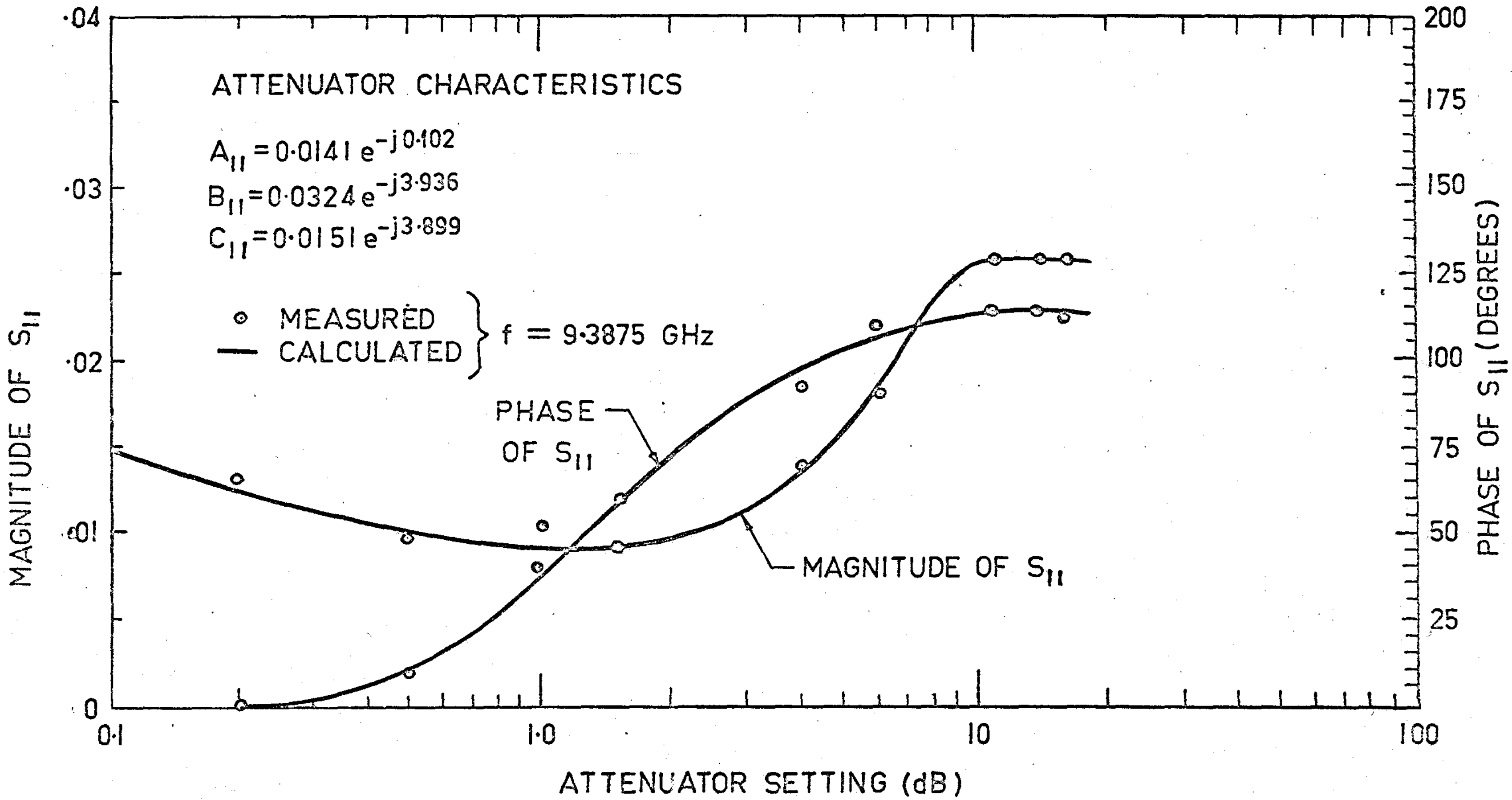

FIGURE 2.5: The Measured and Calculated Values of S_{11} with HP x 382A Attenuator

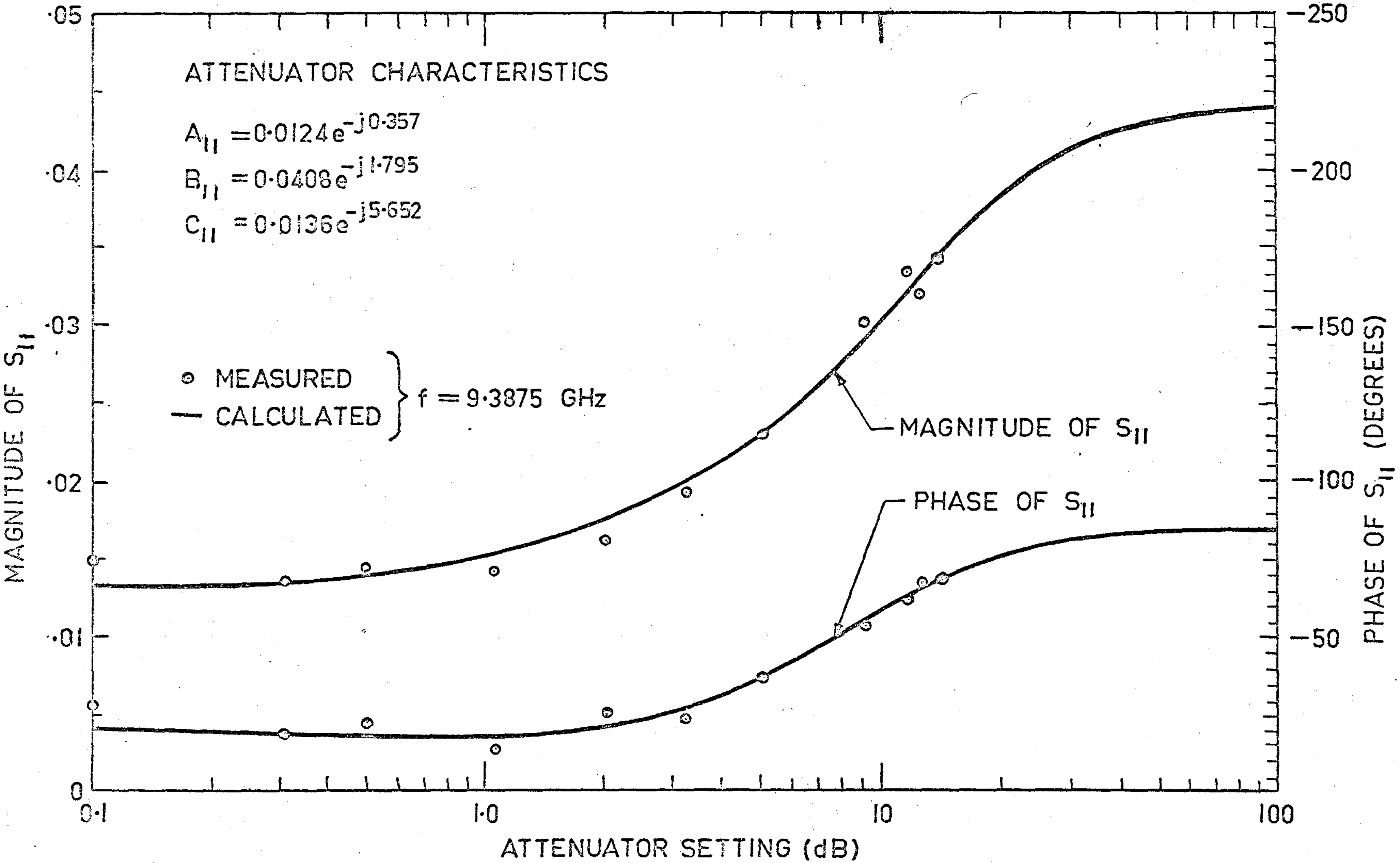

FIGURE 2.6: The Measured and Calculated Values of S_{11} with Elliot A167/44 Attenuator

2.3 The Practical Reflection Bridge

The performance of a reflection bridge depends also on the bridge element, which can either be a 'hybrid tee' or a 'magic tee'. The bridge with a hybrid tee described in Section 2.2.2 requires three preliminary calibration readings, two with short-circuits and one with a matched termination. This is to be compared to the one short reading for a symmetric tee or a magic tee for measurement.

The use of a hybrid tee involves not only the time consuming calibration procedure, but also the calculation of the reflection coefficient, which is usually cumbersome. This difficulty is avoided by using a magic tee, which gives an expression for the required reflection coefficient in a much simpler form (cf. Eqs. 2.4 and 2.8). The magic tee is also perferred to a symmetric tee for the following reasons:

(a) A symmetric tee is very difficult to obtain in practice due its unequal side arm lengths, dimensions and losses in side arms;

(b) The equality of both magnitudes and phases of S_{13}, S_{23} and S_{11}, S_{22}, which are required properties of the symmetric tee, is difficult to achieve in practice.

The magnitudes of these coefficients, however, in a 'practical magic tee' approach zero, so that the equality of the phases does not become so important. Since it is practically impossible to obtain either an ideal symmetric or magic tee, it is best to make a tee symmetric as well as matched as far as possible, in order to approach the ideal case.

The schematic diagram of a practical form of a reflection bridge is shown in Figure 2.7. The side arms of the 'original tee' are not often convenient for measurement purposes and additional waveguide sections are added to one side arm. This results in the 'modified tee' shown in the figure. The modified tee is first changed into a magic tee by matching the E and H arms with two slide screw or E-H tuners in E and H arms and then compensating the asymmetry, if any, with a tuner in one of the side arms. The precision attenuator and precision short which provide the 'reference arm' are coupled to port 1. A calibrated tuner is used in the reference arm to cancel out the attenuator reflection.

2.3.1 Details of the Setting-up Procedure

(A) MATCHING THE INPUT PORTS OF THE 'MODIFIED HYBRID TEE'

The input ports of the modified hybrid tee are matched with screw tuners in E and H arms at the frequency of operation. The matching procedure is as follows:

A tuner and a matched detector are coupled into the E and H arms respectively, while the side arms are terminated in matched loads. The tuner in the E arm in conjunction with a slotted line is adjusted to obtain maximum output in the matched detector. The VSWR at port 4 is minimum under this condition and can be made less than 1.02. This corresponds to a magnitude of the reflection coefficient looking into E arm of $|S_{44}| \leq .01$. This completes the matching procedure of E arm.

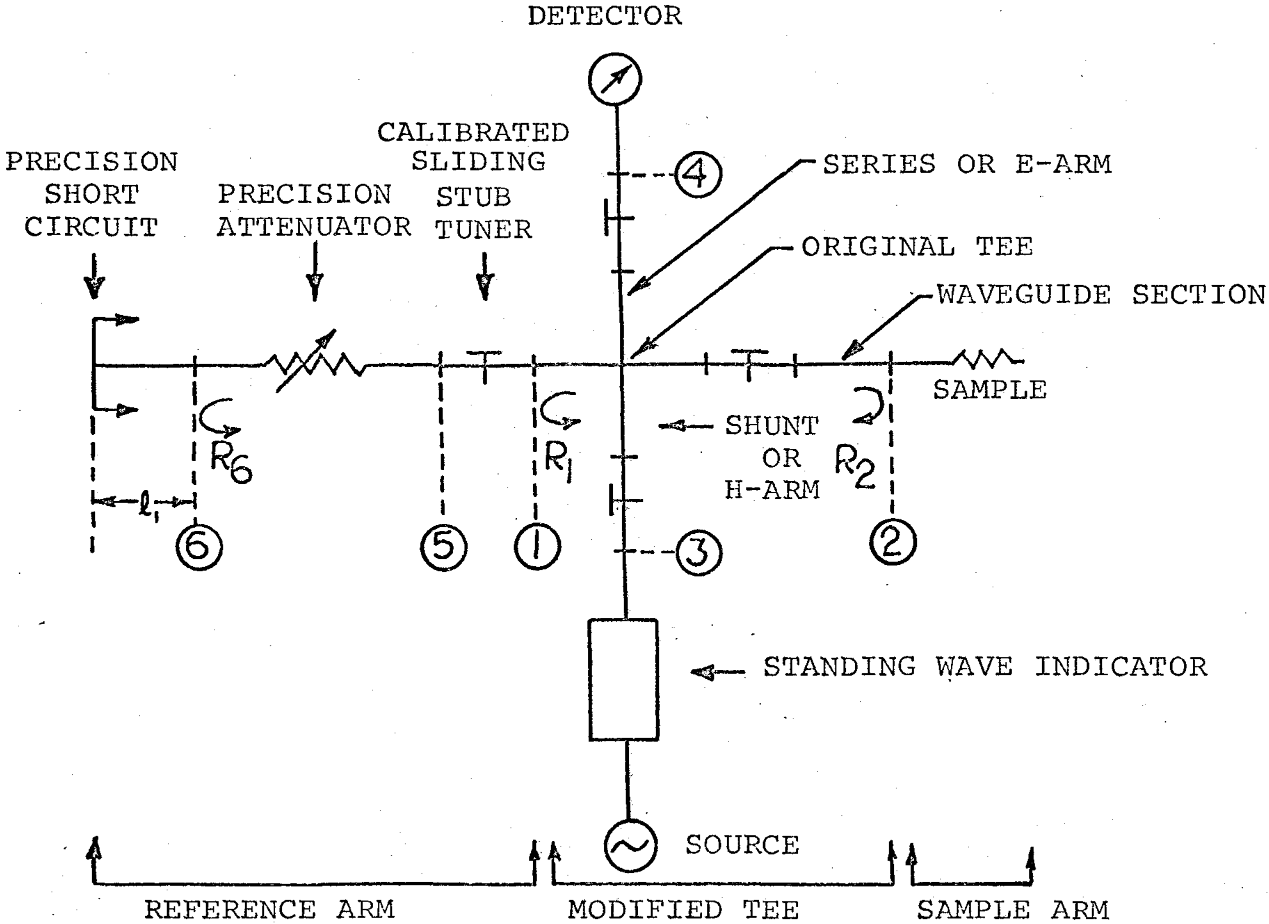

FIGURE 2.7: A Practical Microwave Reflection Bridge Circuit.

Similarly, the H arm is matched by adjusting a tuner in H arm and observing the maximum output in E arm while the side arms are terminated in matched loads. The magnitude of the reflection coefficient looking into H arm $|S_{33}|$, can also be made $\leq$ .01.

If the tee is symmetric and lossless , the above procedure automatically ensures that side arm ports 1 and 2 are matched also.

(B) COMPENSATING FOR ASYMMETRY IN THE TEE

Cross coupling can exist between the H and E arms even when the side arms are terminated in matched loads because of the asymmetry in the construction of the tee. For such a condition an input to the H arm will give an output in the E arm varying from a few tens of microvolts to a few millivolts, depending on the quality of the tee and power input to H arm (about 30 to 40 dB isolation). This T-asymmetry results from a number of factors such as unequal electrical lengths of the side arms from the plane of symmetry, incorrect waveguide width and unequal losses in the side arms. The power output in E arm due to these features can be minimised by adjusting a screw tuner in one of the side arms, which are terminated in matched loads.

The vector diagram[40] of the output E_{m1} at the detector in E arm is shown in Figure 2.8 where E_{m1} and E_{m2} are the reflected waves from the imperfect matched terminations in ports 1 and 2 respectively, E_t is the reflected wave from

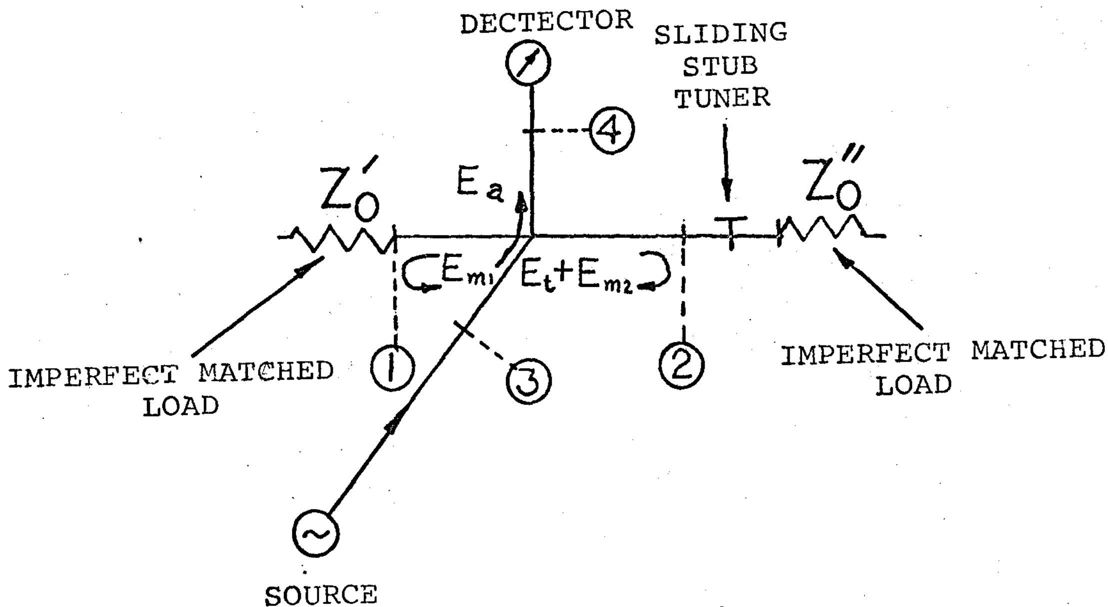

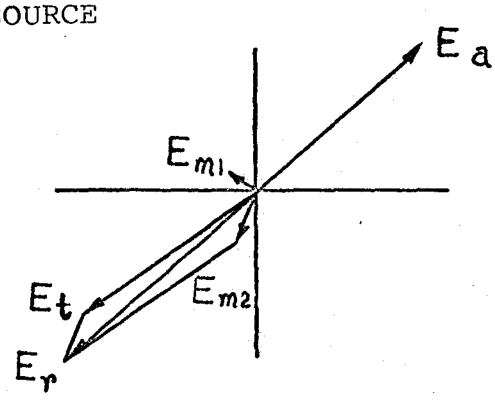

VECTOR DIAGRAM

FIGURE 2.8: Cancellation of the Tee-asymmetry by adjusting a Stub-tuner in the Side Arm.

the tuner in the side arm 2, E_r is the resultant of E_t and E_{m2} and E_a is the transmitted wave from port 3 to port 4 due to asymmetry of the tee. If the bridge is compensated for asymmetry, E_a cancels E_r and the null output, caused from the sliding matched load reflection E_{ml}, does not change with the position of the matched load, since E_{ml} is variable in phase but not in magnitude. If the bridge is not compensated, the output E_{ml} will vary with the position, since E_{ml} will now add to or subtract from the unbalanced signal.

For the waveguide systems used, the magnitudes of the transmission coefficient from ports 3 to 4, the reflection coefficients at ports 1 and 2 and the cross coupling coefficient from ports 1 to 2 were measured and found to be $|S_{43}| = |S_{34}| = 0.0000023$, $|S_{11}| = |S_{22}| = 0.01$, and $|S_{12}| = |S_{21}| = 0.03$. A compromise between $|S_{12}|$ and $|S_{44}|$ could, however, be made by decreasing $|S_{12}|$ from 0.03 to 0.01 on adjusting the tuner in the E arm at the expense of an increased $|S_{44}|$ from 0.01 to 0.025.

(C) MATCHING THE PRECISION ATTENUATOR

This has been described in Section 2.2.3. The reflection from the attenuator due to the finite thickness of the absorbing vane, as mentioned earlier, varies with the attenuator settings. A calibrated tuner was, therefore, required to cancel out the attenuator reflection for any given attenuator setting. The calibration was performed by noting the position and penetration of the screw tuner with increasing attenuator settings required to give minimum output in the E arm with ports 2 and 6 terminated in matched loads.

2.4 Discussion

The waveguide sections which have been included in one side arm of the bridge as shown in Figure 2.7 should be lossless or approximately so, to satisfy the conditions of a matched and symmetric tee $|S_{11}| = |S_{22}| = |S_{12}| \rightarrow 0$ (Section 2.2.1). It has, however, been found that a lossy waveguide section is necessary in the sample arm particularly for the preliminary measurement with a short-circuit in order to balance the insertion loss of the precision attenuator in the reference arm. This unavoidable loss in the sample arm should be as small as possible.

The tee chosen for use in the bridge should not be highly non-symmetric. If it is so, the required depth of penetration of the tuner in one of the side arms to compensate asymmetry may destroy the matching looking into the side arms i.e. $|S_{11}| \neq |S_{22}| \neq 0$. Care should, therefore, be taken in choosing the tee and the microwave components for the side arms, which are not too lossy and have a minimum number of bends with consequent small reflections.

The waveguide component flanges must be accurately aligned and the waveguide connections must be tight to avoid unwanted reflections. Particular care is required in the connections to the side arms which should be firm and aligned to avoid large errors.

2.5 Photographs of the Microwave Reflection Bridge

The set-ups of the microwave reflection bridge which were used to confirm the theories developed in this thesis are shown in Figures 2.9 through 2.12. Figures 2.9 and 2.10 show the set-ups used to verify the theoretical predictions of Section 4.2 at 35 and 10 GHz, respectively. Figure 2.11 is the part of an x-band reflection bridge used to verify the theoretical predictions of Section 5.3, while Figure 2.12 shows the complete apparatus used for measuring the microwave conductivity of a germanium sample subjected to a high d.c. electric field.

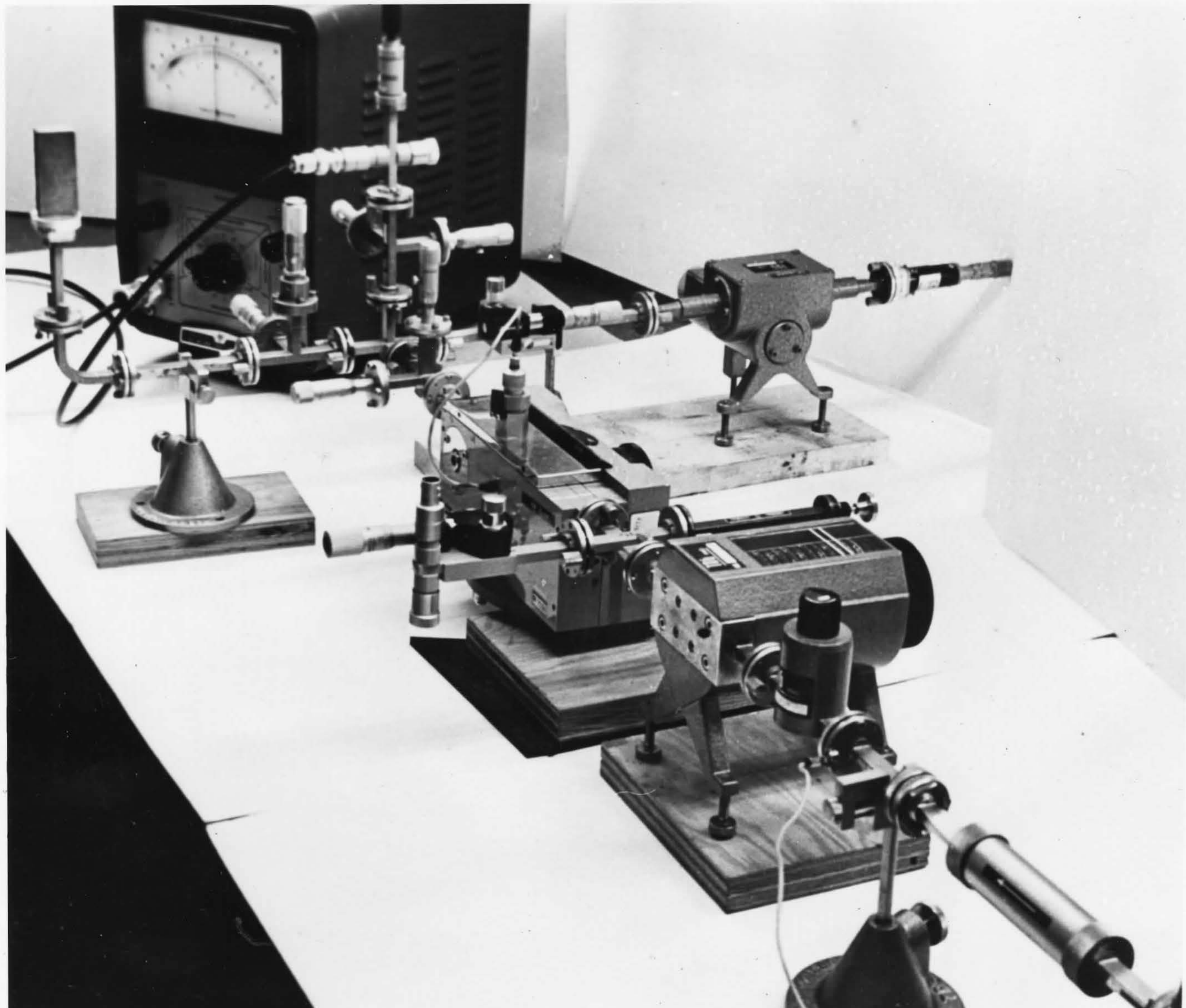

FIGURE 2.9: Rear View of the 35 GHz Set-up of the Microwave Reflection Bridge showing the Measurement of the Reflection Coefficient of a Block of Germanium in One Side Arm of the Bridge.

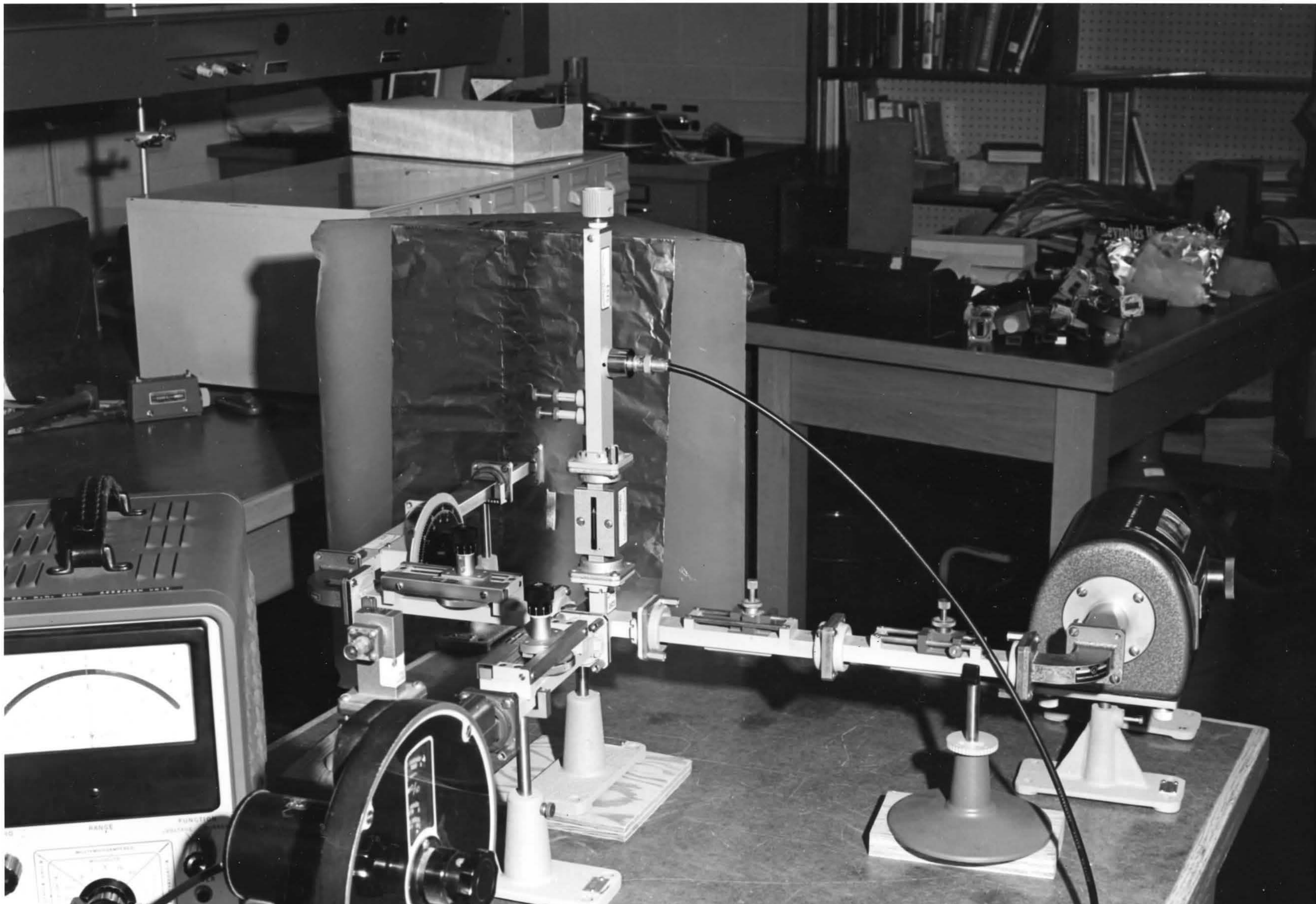

FIGURE 2.10: Rear View of the 10 GHz Set-up of the Microwave Reflection Bridge showing the Measurement of the Reflection Coefficient of a Piece of Selectron in One Side Arm of the Bridge.

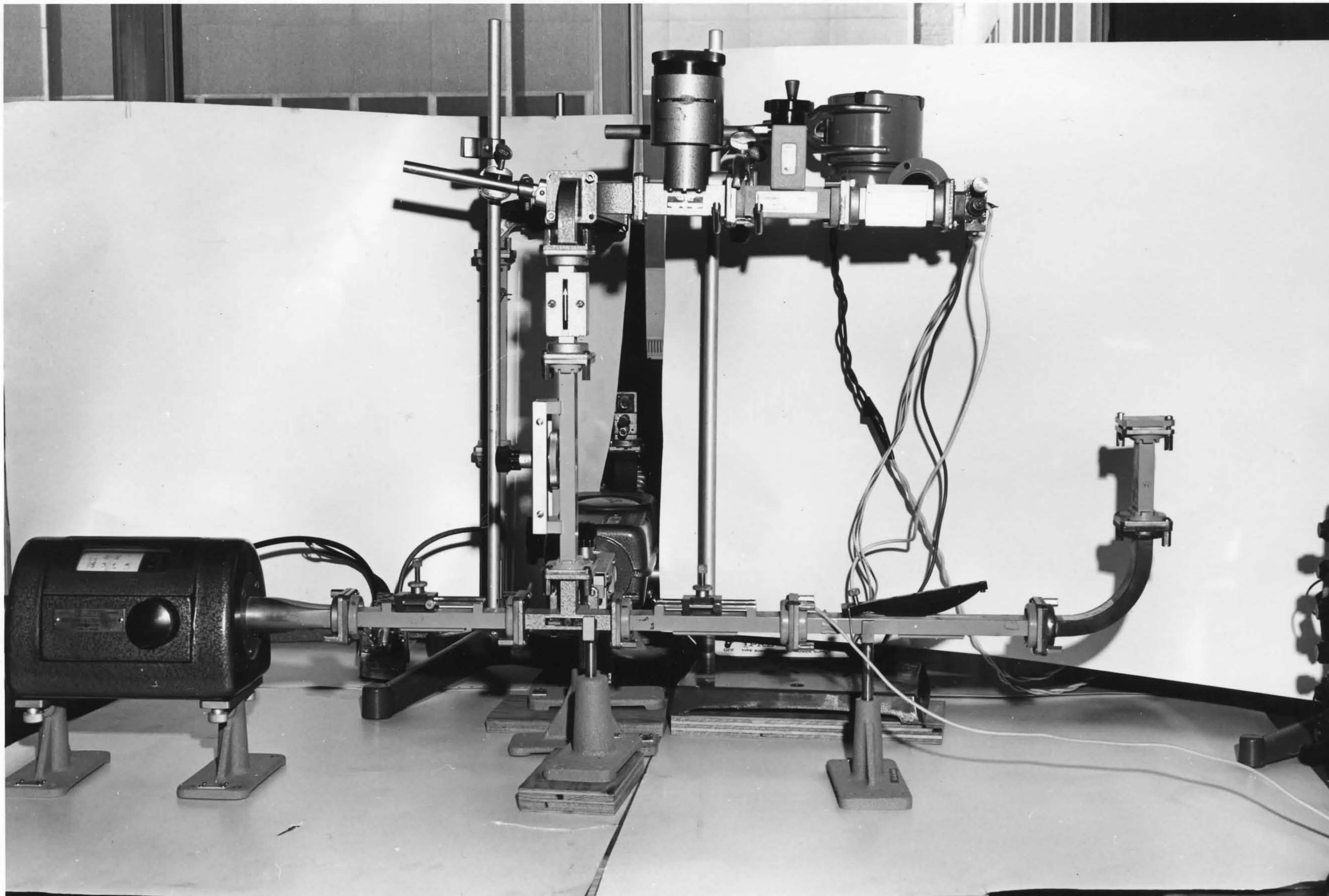

FIGURE 2.11: Front View of the 10 GHz Set-up of the Microwave Reflection Bridge showing the Sample Holder containing a Slab of Germanium between the Waveguide Flange and the Precision Short-Circuit Plate.

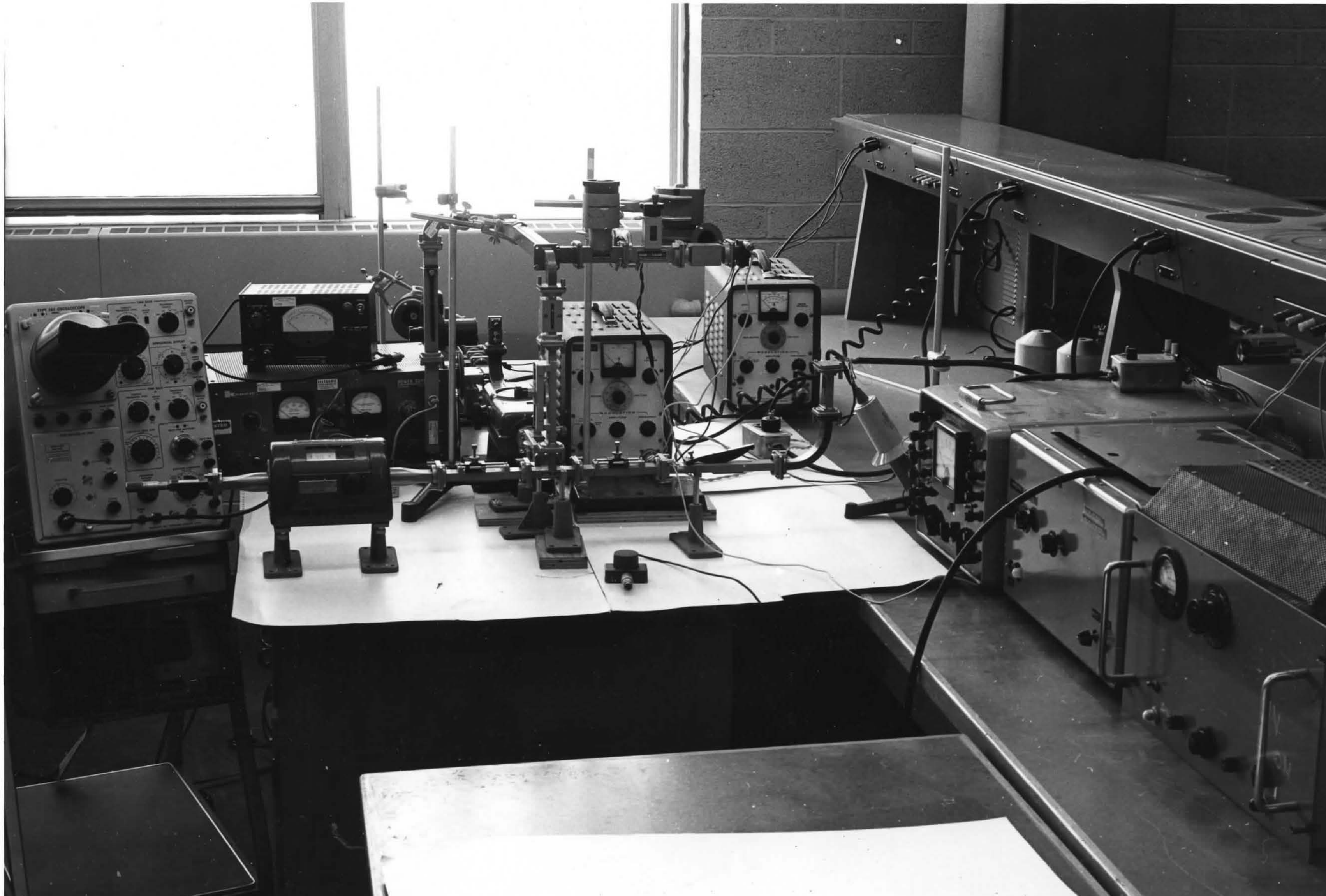

FIGURE 2.12: General View of the Complete Apparatus for measuring the Microwave Conductivity of an 11.4 ohm cm N-type Germanium Sample subjected to a High D.C. Electric Field.

CHAPTER III

MICROWAVE REFLECTIONS FROM THE SURFACE OF A FINITE SEMICONDUCTOR MEDIUM (APPROXIMATE SOLUTIONS)

3.1 Introduction

This chapter contains a theoretical analysis of the wave reflections together with the development of the approximate solutions for the input impedance and the reflection coefficient at the surface of a finite block of semiconductor.

The reflection coefficient at the plane $z = 0$ of a finite block of semiconductor placed in a rectangular waveguide as shown in Figure 1.1 can be calculated exactly and the appropriate equations are derived in Section 3.2. The reflection coefficients at the surface of a finite block of semiconductor placed at the open end of a rectangular waveguide as shown in Figures 1.2 and 1.3 are also calculated on the assumption of a z-directed TEM wave in the semiconductor region. The solution is approximate, as the radiative propagating wave in the semiconductor region is neither a complete TE_{10} wave nor a TEM wave. The appropriate equations are derived in Sections 3.3 and 3.4.

3.2 The Reflection Coefficient of a Finite Semiconductor Block Inside A Rectangular Waveguide

The input impedance at the air-semiconductor interface plane $z = 0$ of a rectangular waveguide of Figure 1.1 can be expressed as[41]

$$Z_{in} = Z_2 \frac{Z_3 + Z_2 \tanh \gamma_2 \ell}{Z_2 + Z_3 \tanh \gamma_2 \ell} \tag{3.1}$$

where Z_2 = the wave impedance of the semiconductor loaded waveguide i.e. of region 2; Z_3 = the wave impedance of the material terminating the waveguide i.e. of region 3; ℓ = the length of the semiconductor sample in axial direction and γ_2 = the propagation coefficient of the semiconductor loaded waveguide. If the waveguide is terminated by a short-circuit metal plate, $Z_3 = 0$ and the input impedance simplifies to the following form

$$Z_{in} = Z_2 \tanh \gamma_2 \ell \tag{3.2}$$

The reflection coefficient R at the air-sample interface may therefore be written as

$$R = \frac{Z_2 \tanh \gamma_2 \ell - Z_1}{Z_2 \tanh \gamma_2 \ell + Z_1} \tag{3.3}$$

where Z_1 = the wave impedance of the empty waveguide, i.e. of region 1. If we assume that the TE_{10} wave propagates in regions 1 and 2 of the structure of Figure 1.1, the propagation coefficients and the wave impedances of the empty guide and semiconductor loaded guide are given by the following expressions:†

---

† The conductivity is assumed to follow the field at 10 and 35 GHz. At higher frequencies, σ should be replaced by[42] $\hat{\sigma}(\omega) = \frac{\sigma}{1 + \omega^2 <\tau>^2} - j\omega \frac{\sigma <\tau>}{1 + \omega^2 <\tau>^2}$ where τ is relaxation time of carriers and ω is the radian frequency of the microwave field.

$$\gamma_1 = \left[\left(\frac{\pi}{a}\right)^2 - \omega^2 \mu \varepsilon_o \right]^{1/2} \tag{3.4}$$

$$\gamma_2 = \left[\left(\frac{\pi}{a}\right)^2 - \omega^2 \mu \varepsilon + j\omega\mu\sigma \right]^{1/2} \tag{3.5}$$

$$Z_1 = \frac{j\omega\mu}{\gamma_1} = \frac{Z_o}{\left[1 - (f_c/f)^2\right]^{1/2}} \tag{3.6}$$

and
$$Z_2 = \frac{j\omega\mu}{\gamma_2} = \frac{Z_o}{\left[\hat{\varepsilon}_r - (f_c/f)^2\right]^{1/2}} \tag{3.7}$$

where f_c = cut off frequency of the TE_{10} mode, a = width of the waveguide,

$$Z_o = \sqrt{\mu_o/\varepsilon_o}, \quad \varepsilon = \varepsilon_o \varepsilon_r, \text{ and } \quad \hat{\varepsilon}_r = \varepsilon_r - j\,\frac{\sigma}{\omega\varepsilon_o}\,.$$

Thus equation (3.3) can be rewritten as

$$R = \frac{1 - \left[\dfrac{\hat{\varepsilon}_r - (f_c/f)^2}{1 - (f_c/f)^2}\right]^{1/2} \coth \gamma_2 \ell}{1 + \left[\dfrac{\hat{\varepsilon}_r - (f_c/f)^2}{1 - (f_c/f)^2}\right]^{1/2} \coth \gamma_2 \ell} \tag{3.8}$$

It is noted that equation (3.3) can be transformed to the following form:

$$R = \frac{(Z_2 - Z_1) \,/\, (Z_2 + Z_1) - e^{2\gamma_2 \ell}}{1 - (Z_2 - Z_1) \,/\, (Z_2 + Z_1)\; e^{-2\gamma_2 \ell}} \tag{3.9}$$

which is the same as derived by Lindmayer and Kutsko [7].

3.3 The Reflection Coefficient of a Finite Semiconductor-Metal Block at the Open End of a Rectangular Waveguide

If the semiconductor block is placed at the end of the guide instead of inside as followed by Lindmayer and Kutsko (Figure 1.2), the incident TE_{10} wave is transformed into a radiated propagating wave in the semiconductor region, which is neither a completely TE_{10} wave nor a TEM wave. An approximate solution can be obtained which is based on the assumption of either of the two modes of propagation. If the TE_{10} wave is assumed, the results of equation (3.8) are obtained. However, if the TEM wave that propagates only in the z-direction (no transverse propagation!) is assumed, the propagation coefficient in the semiconductor region differs from equation (3.5) by the following expression:

$$\gamma_2 = \left[-\omega^2 \mu\varepsilon + j\omega\mu\sigma \right]^{1/2} \tag{3.10}$$

The error introduced by this assumption is large for semiconductors with high resistivity and low dielectric constants. With this value of the propagation coefficient in equation (3.3) the reflection coefficient can be written as

$$R = \frac{1 - \left[\dfrac{\hat{\varepsilon}_r}{1 - (f_c/f)^2} \right]^{1/2} \coth \gamma_2 \ell}{1 + \left[\dfrac{\hat{\varepsilon}_r}{1 - (f_c/f)^2} \right]^{1/2} \coth \gamma_2 \ell} \tag{3.11}$$

The equations (3.8) and (3.11) are identical for the condition $\varepsilon_r \gg (f_c/f)^2$ which is, in fact, true for Ge and Si. When the length of the lossy material is large compared to the skin depth δ, the backing of the sample with a short-circuit has little effect. If $\ell \geq 5\,\delta$, coth $\gamma_2 \ell \simeq 1.0$. Thus equation (3.11) reduces to the expression

$$R = \frac{1 - \left[\dfrac{\hat{\varepsilon}_r}{1 - (f_c/f)^2}\right]^{1/2}}{1 + \left[\dfrac{\hat{\varepsilon}_r}{1 - (f_c/f)^2}\right]^{1/2}} \tag{3.12}$$

This reflection coefficient R can be considered as that of a semi-infinite medium and may be measured with a microwave reflection bridge. With a magic tee in such a bridge, the reflection coefficient may be written from the equation (2.13) as

$$R = -e^{-(A + j\phi)} \tag{3.13}$$

where $A = 2(A_1 - A_o)$ in neper; $\phi = 2\beta(\ell_1 - \ell_o)$ in radian; A_1, ℓ_1 are readings of the precision attenuator and precision short, respectively with the sample in the sample arm and A_o, ℓ_o are similar readings with fixed short in the sample arm. Equating the real and imaginary parts of the identity formed from equations (3.12) and (3.13), it can be shown that (Appendix A)

$$\varepsilon_r = \left[1 - (f_c/f)^2\right] \left[\frac{\cosh A + \cos\phi}{\cosh A - \cos\phi}\right] \ldots$$

$$\cos\left[2\tan^{-1}\frac{\sin\phi}{\sinh A}\right] \quad (3.14a)$$

$$\sigma = \left[1 - (f_c/f)^2\right] \left[\frac{\cosh A + \cos\phi}{\cosh A - \cos\phi}\right] \ldots$$

$$\sin\left[2\tan^{-1}\frac{\sin\phi}{\sinh A}\right]\omega\varepsilon_o \quad (3.14b)$$

Thus a measurement of A, ϕ, and f enables the values of ε_r and σ to be determined.

3.4 The Reflection Coefficient of a Finite Semiconductor Block at the Open End of a Rectangular Waveguide

If the semiconductor block is followed by air as shown in Figure 1.3,

$$Z_3 = \sqrt{\frac{\mu_o}{\varepsilon_o}} \quad (3.15)$$

so that equation (3.1) becomes

$$Z_{in} = Z_2 \frac{\sqrt{\frac{\mu_o}{\varepsilon_o}} + Z_2 \tanh\gamma_2\ell}{Z_2 + \sqrt{\frac{\mu_o}{\varepsilon_o}} \tanh\gamma_2\ell} \quad (3.16)$$

Substituting equations (3.10) and (3.7) for γ_2 and Z_2 respectively, the reflection coefficient at the plane $z = 0$ can be written as

$$R = \frac{Z_{in} - Z_1}{Z_{in} + Z_1}$$

$$= \frac{1 - \left[\dfrac{\hat{\varepsilon}_r}{1-(f_c/f)^2}\right]^{1/2} \dfrac{1+\sqrt{\hat{\varepsilon}_r}\tanh\gamma_2\ell}{\sqrt{\hat{\varepsilon}_r}+\tan\gamma_2\ell}}{1 + \left[\dfrac{\hat{\varepsilon}_r}{1-(f_c/f)^2}\right]^{1/2} \dfrac{1+\sqrt{\hat{\varepsilon}_r}\tanh\gamma_2\ell}{\sqrt{\hat{\varepsilon}_r}+\tanh\gamma_2\ell}} \qquad (3.17)$$

where equation (3.6) has been used for Z_1. As expected, this equation reduces to equation (3.12) for $\ell \geq .5\,\delta$ ie. when $\tanh\gamma_2\ell \simeq 1$.

3.5 Numerical Results For Germanium and Their Intrepretations

Equation (3.12) has been evaluated numerically on a CDC 6400 Digital Computer. Numerical computations were obtained for germanium for the following two cases:

(a) a = 2.286cm, b = 1.016 cm, f = 9.522 GHz

(b) a = 0.712 cm, b = 0.356 cm, f = 34.5 GHz

The results of these calculations are shown in Table 4.1 for comparison. Inspection of the table shows that equation (3.12) gives an error in the phase of R for high resistivity semiconductors ($\sigma < 2\omega\varepsilon_0\,\varepsilon_r$, above 1.6 ohm cm at 34.5 GHz).

The σ and ε_r have also been calculated from the measured values of A and ϕ using equation (3.14). The results show that this equation gives reasonable accuracy of the resistivity measurement at the low end of the resistivity range and that of the dielectric constant measurement at the high end. However, the accuracy of ε_r measurement at low range and that of resistivity measurement at high range are found to be inaccurate. This is because of the nature of the equation (3.14) and the breakdown of its validity in the high resistivity range where equation (3.12) introduces a large phase error, as mentioned earlier.

CHAPTER IV

MICROWAVE REFLECTIONS FROM THE SURFACE OF A SEMI-INFINITE MEDIUM (EXACT SOLUTIONS).

4.1 Introduction

The exact solutions for the input admittance and the reflection coefficient of an infinite block of semi-conductor are developed in this Chapter for the following waveguide configurations:

(a) the rectangular waveguide in an infinite ground plane (Figure 4.1);

(b) the rectangular waveguide in bounded ground planes (Figure 4.2);

(c) the parallel-plate waveguide in bounded ground planes (Figure 4.3).

The original formulation by Lewin[43] for the admittance of a rectangular waveguide in an infinite ground plane radiating into a lossless half-space has been modified for the case of a lossy semi-infinite medium. The admittance for the configurations (b) and (c) are then deduced from the new formulation as special cases.

Numerical calculations are made and discussed. Measurements which confirm the theory have been carried out with a microwave reflection bridge at 9.522 and 34.5 GHz. The results of measurements with n-type germanium and also with air and selectron at the end of a rectangular waveguide opening onto a metal flange, are given.

4.2 The Reflection Coefficient of a Semi-Infinite Block of Semiconductor at the End of a Rectangular Waveguide Opening onto an Infinite Ground Plane

In the structure of Figure 4.1a the region 1 is the interior of the air filled guide and region 2 is the semi-infinite half-space filled with a material of complex permittivity $\hat{\varepsilon}$. If a TE_{10} mode is excited in region 1 of such a structure, the energy is radiated from the guide into half space $(z > 0)$. Since the ground metal flange is taken to be infinite, radiation is confined to the half-space $(z > 0)$. We wish to determine the electric and magnetic fields in regions 1 and 2.

In a source free homogeneous medium such as region 1 or 2, the electric and magnetic fields are satisfied by the following equations[44]

$$E = \frac{\nabla(\nabla.A)}{j\omega\hat{\varepsilon}} - j\omega\mu A - \nabla \times F \tag{4.1a}$$

and

$$H = \frac{\nabla(\nabla.F)}{j\omega\mu} - j\omega\hat{\varepsilon}F + \nabla \times A \tag{4.1b}$$

where μ is the permeability of the medium, $\hat{\varepsilon}$ is the complex permittivity of the medium and the quantity F is called an electric vector potential in analogy to the magnetic vector potential A. The electric and magnetic fields can also be described in terms of either A or F, regardless of its actual source. There is a great deal of arbitrariness in the choice of the vector potential. If we choose A = 0, the equations (4.1a) and (4.1b) may be written as

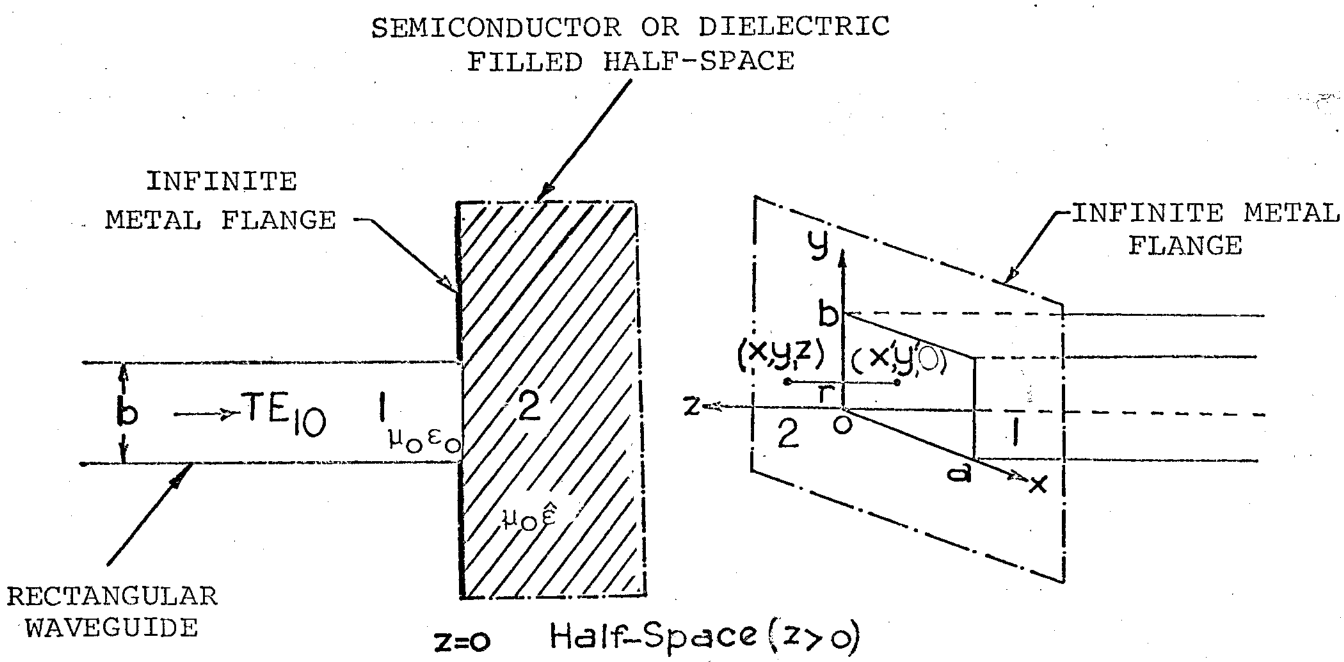

(a)

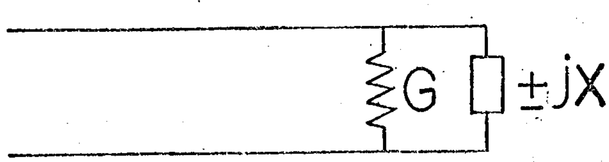

(b)

FIGURE 4.1a: A Semi-infinite Block of Semiconductor or Dielectric Sample at the End of a Rectangular Waveguide Opening onto an Infinite Metal Flange

FIGURE 4.1b: The Electrical Equivalent Circuit of the Above Waveguide System.

$$E = -\nabla \times F \qquad (4.2a)$$

$$H = \frac{1}{j\omega\mu}\left[\nabla(\nabla . F) + \hat{k}^2 F\right] \qquad (4.2b)$$

where $\hat{k}^2 = \omega^2\hat{\mu}\hat{\varepsilon}$.

If F is taken to have only a single component F_x, we obtain a field with no electric field in the x-direction. This is otherwise known as the TE to x mode or TE_x mode. Thus the field components are

$$E_x = 0 \quad (a) \qquad H_x = \frac{1}{j\omega\mu}\left[\frac{\partial^2}{\partial x^2} + \hat{k}^2\right] F_x \quad (d)$$

$$E_y = -\frac{\partial F_x}{\partial z} \quad (b) \qquad H_y = \frac{1}{j\omega\mu}\,\frac{\partial^2 F_x}{\partial x\,\partial y} \quad (c) \qquad (4.3)$$

$$E_z = +\frac{\partial F_x}{\partial y} \quad (c) \qquad H_z = \frac{1}{j\omega\mu}\,\frac{\partial 2 F_x}{\partial x\,\partial z} \quad (f)$$

Equating the y-components of the electric fields in the two regions at the aperture z = 0,

$$E_{y(1)}\Big|_{z=0} = E_{y(2)}\Big|_{z=0} \qquad (4.4)$$

There will be an incident wave plus a reflected wave plus the higher order modes in region 1 and a radiated wave in region 2. For z<0, we have for dominant mode†

$$E_{y(1)} = \left[e^{-jk_1 z} + R\, e^{+jk_1 z}\right] \sin\frac{\pi x}{a} \qquad (4.5)$$

† Page 542, Reference 41.

where k_1 is the propagation coefficient in region 1 and is given by $k_1 = \left[k_o^2 - (\frac{\pi}{a})^2 \right]^{1/2}$, k_o is the propagation coefficient in free space and R is the voltage reflection coefficient. By equations (4.3b) and (4.5),

$$F_{x(1)} = -\int_o^z E_{y(1)} \, dz$$

$$= -\frac{1}{jk_1} \left[-e^{-jk_1 z} + R\, e^{jk_1 z} \right] \sin\left(\frac{\pi x}{a}\right) \quad (4.6)$$

The vector potential F_x can be rewritten for region 1 with the addition of higher order modes. Thus

$$F_{x(1)} = \frac{1}{jk_1} \left[e^{-jk_1 z} - R\, e^{jk_1 z} \right] \sin\left(\frac{\pi x}{a}\right)$$
$$+ \sum_1^\infty {\sum_o^\infty}' A_{mn} \operatorname{Sin}\left(\frac{m\pi}{a} x\right) \cos\left(\frac{n\pi}{b} y\right) e^{\gamma_{mn} z} \quad (4.7)$$

where A_{mn} = a constant, $\gamma_{mn} = \left[(\frac{m\pi}{a})^2 + (\frac{n\pi}{b})^2 - k_o^2 \right]^{1/2}$ and $\sum'$ denotes the term m = 1, n = 0 is omitted from the double series as it is already included in the first term.

$$E_Y(1) \bigg|_{z=0} = -\frac{\partial F_{x(1)}}{\partial z} \bigg|_{z=0}$$

$$= (1 + R) \sin\left(\frac{\pi x}{a}\right) - \sum_1^\infty {\sum_0^\infty}' A_{mn} \gamma_{mn} \sin\left(\frac{m\pi}{a} x\right) \cos\left(\frac{n\pi}{b} y\right)$$

(4.8)

The field in region 2 corresponds to a field radiated outwards from the plane z = 0. Thus

$$F_{x(2)} = \frac{1}{2\pi} \int_0^a \int_0^b E(x', y') \frac{e^{-j\hat{k}r}}{r} dx' dy' \quad (4.9)$$

where x' and y' denote the coordinates in the aperture; r, the distance between a point at z = 0 plane and a fixed point at (x, y, z), i.e. $r = \left[(x - x')^2 + (y - y')^2 + z^2 \right]^{1/2}$; E(x', y') the aperture field; $\hat{k}$ the wave vector in region 2 and the factor $1/2\pi$ has been included for convenience only. The boundary conditions for the electric fields at z = 0 are such that they are zero at the metal flange and continuous and equal to E(x, y) in the aperture. Thus from equation (4.4)

$$E(x, y) = E_{y(1)} \Big|_{z=0} = E_{y(2)} \Big|_{z=0} \quad (4.10)$$

and from equation (4.8)

$$E(x, y) = (1 + R) \sin(\frac{\pi x}{a}) - \sum_{1}^{\infty} \sum_{0}^{\infty}{}' A_{mn} \gamma_{mn} \sin(\frac{m\pi}{a} x) \cos(\frac{n\pi}{b} y)$$

which, in terms of aperture coordinates, assumes the form

$$E(x',y') = (1 + R) \sin(\frac{\pi x'}{a}) - \sum_{1}^{\infty} \sum_{0}^{\infty}{}' A_{mn} \gamma_{mn} \sin(\frac{m\pi}{a} x') \cos(\frac{n\pi}{b} y') \quad (4.11)$$

The coefficients (1 + R) and $-A_{mn} \gamma_{mn}$ of this Fourier Series can be found in terms of the aperture field

$$1 + R = \frac{2}{ab} \int_0^a \int_0^b E(x', y') \sin(\frac{\pi}{a} x') dx' dy' \quad (4.12)$$

and

$$-\gamma_{mn}A_{mn} = \frac{4\ \varepsilon_{mn}}{ab} \int_o^a \int_o^b E(x', y')\ \sin\left(\frac{m\pi}{a}x'\right)\cos\left(\frac{n\pi}{b}y'\right)dx'dy' \tag{4.13}$$

where the integration has been taken over the aperture and ε_{mn} is 1 unless n = 0, when it equals 1/2.

The remaining boundary condition to be satisfied is the continuity of the x-component of the magnetic field in the two regions at the aperture z = 0.

$$H_{x(1)}\Big|_{z=0} = H_{x(2)}\Big|_{z=0}$$

or

$$\left(\frac{\partial 2}{\partial_x 2} + k_o^2\right) F_{x(1)}\Big|_{z=0} = \left(\frac{\partial 2}{\partial_x 2} + \hat{k}^2\right) F_{x(2)}\Big|_{z=0} \tag{4.14}$$

An expression for 1 - R can be obtained by substituting equations (4.7), (4.9) and (4.13) in equation (4.14) and using equation (4.12) for 1 + R, the normalized waveguide admittance Y_n at plane z = 0, can be shown to be equal to (Appendix B)

$$Y_n = \frac{1 - R}{1 + R}$$

$$= \frac{j\ ab}{2k_1D_1D_1} \int_0^a \int_0^b \int_0^a \int_0^b \sin\left(\frac{\pi x}{a}\right)\ E(x', y')\cdots$$

$$G(x, y, x', y')dxdydx'dy' \tag{4.15}$$

where

$$D_1 = \int_0^a \int_0^b E(x', y') \sin(\frac{\pi}{a}x')dx'dy' \qquad (4.16)$$

$$D_2 = \int_0^a \int_0^b \sin^2(\frac{\pi x}{a})dxdy \qquad (4.17)$$

and

$$G(x,y,x',y') = \frac{1}{2\pi}\left(\frac{\partial^2}{\partial_x^2} + \hat{k}^2\right) \frac{e^{-j\hat{k}r}}{r} + \sum_1^{\infty} \sum_0^{\infty}{}' \frac{4}{ab} \frac{\varepsilon_{mn}}{\gamma_{mn}} \left(\frac{\partial^2}{\partial x^2} + k_o^2\right) \cdots$$

$$\sin(\frac{m\pi}{a} x') \cos(\frac{n\pi}{b} y') \sin(\frac{m\pi}{a} x) \cos(\frac{n\pi}{b} y) \qquad (4.18)$$

The aperture field as described by the equation (4.11) contains higher order modes excited by the discontinuity at $z = 0$. The amplitudes of these higher order modes may be assumed small compared to that of the dominant mode and the aperture field can thus be equal to the field of the dominant incident mode. Thus if

$$E(x', y') = \sin(\frac{\pi x'}{a}) \qquad (4.19)$$

then $D_1 = D_2 = ab/2$ and all terms of the double series in G of equation (4.15) integrate out to zero since

$\int_0^a \sin(\frac{\pi x'}{a}) \sin(m\frac{\pi x'}{a}) dx' = 0$. This allows one to write

equation (4.15) as

$$Y_n = \frac{j}{\pi k_1 ab} \int_0^a \int_0^a \int_0^b \int_0^b \sin(\frac{\pi x}{a}) \sin(\frac{\pi x'}{a}) (\frac{\partial^2}{\partial x^2} + \hat{k}^2) \frac{e^{-j\hat{k}r}}{r} dxdx'dydy' \qquad (4.20)$$

This is a quadruple integral that can be transformed into a double integral by the change of variables as described in Appendix C. Thus

$$Y_n = \frac{\left[\hat{\varepsilon}_r - (f_c/f)^2\right]}{\left[1 - (f_c/f)^2\right]} \frac{4j}{ab\lambda_g} \int_{u=0}^{a} \int_{v=0}^{b} (b - v) \left[(a - u) \cos(\frac{\pi}{a} u) + \frac{a}{\pi} \sin(\frac{\pi}{a} u) \frac{\hat{k}^2 + (\frac{\pi}{a})^2}{\hat{k}^2 - (\frac{\pi}{a})^2}\right] \frac{e^{-j\hat{k}\left[u^2 + v^2\right]^{1/2}}}{\left[u^2 + v^2\right]^{1/2}} \, dudv \tag{4.21}$$

If the region 2 contains air ($\hat{\varepsilon}_r = 1$) instead of a semiconductor or dielectric material, the above equation simplifies to an expression analogous to that described by Lewin[43].

To facilitate numerical integration, equation (4.21) has been simplified to the following form:

$$Y_n = \frac{j4(\frac{a}{\lambda})}{a^2 b} \left[\frac{\hat{\varepsilon}_r - 0.25/(\frac{a}{\lambda})^2}{1 - 0.25/(\frac{a}{\lambda})^2}\right]^{1/2} \int_{u=0}^{a} \int_{v=0}^{b} (b-v) \left[(a-u)\cos(\frac{\pi}{a} u) + \frac{a}{\pi} \sin(\frac{\pi}{a} u) \frac{4(\frac{a}{\lambda})^2 \hat{\varepsilon}_r + 1}{4(\frac{a}{\lambda})^2 \hat{\varepsilon}_r - 1}\right] \frac{e^{-j\frac{2\pi}{a}(\frac{a}{\lambda})\sqrt{\hat{\varepsilon}_r}\left[u^2 + v^2\right]^{1/2}}}{\left[u^2 + v^2\right]^{1/2}} \, dudv \tag{4.22}$$

The voltage reflection coefficient of the waveguide structure at the plane z = 0 can be written as

$$R = \frac{1 - Y_n}{1 + Y_n} \tag{4.23}$$

The solution presented above is not completely an exact solution and has been obtained on the basis of an assumption that the aperture field is equal to the field of the dominant incident mode. The possible generation of higher modes excited by the discontinuity at z = 0 has not been taken into account in the theoretical solution.

4.3 THE REFLECTION COEFFICIENT OF A SEMI-INFINITE BLOCK OF SEMICONDUCTOR AT THE END OF A RECTANGULAR WAVEGUIDE OPENING ONTO BOUNDED GROUND PLANES

The geometry of the problem is given in Figure 4.2. The equation (4.21), after some algebra, gives

$$Y_{in} = Y_n Y_o$$

$$= \frac{\left[\hat{\varepsilon}_r - (f_c/f)^2\right]}{\sqrt{\frac{\mu_o}{\varepsilon_o}}} \frac{4j}{b\lambda} \int_{v=0}^{b} (b-v) \left\{ \int_{u=0}^{a} \left[(1 - \frac{u}{a}) \cos(\frac{\pi}{a} u) + \frac{1}{\pi} \sin(\frac{\pi}{a} u) \frac{\hat{k}^2 + (\frac{\pi}{a})^2}{\hat{k}^2 + (\frac{\pi}{a})^2} \right] \frac{e^{-j\hat{k}\sqrt{u^2+v^2}}}{\sqrt{u^2+v^2}} du \right\} dv \qquad (4.24)$$

For the configuration of Figure 4.2 we assume that the x-directed wave propagation at z>0 is negligible. Since 'a' becomes infinite at z>0 and the variable u is small in comparison with a, the terms involving $\frac{u}{a}$ in equation (4.24) approach zero.

With this assumption,

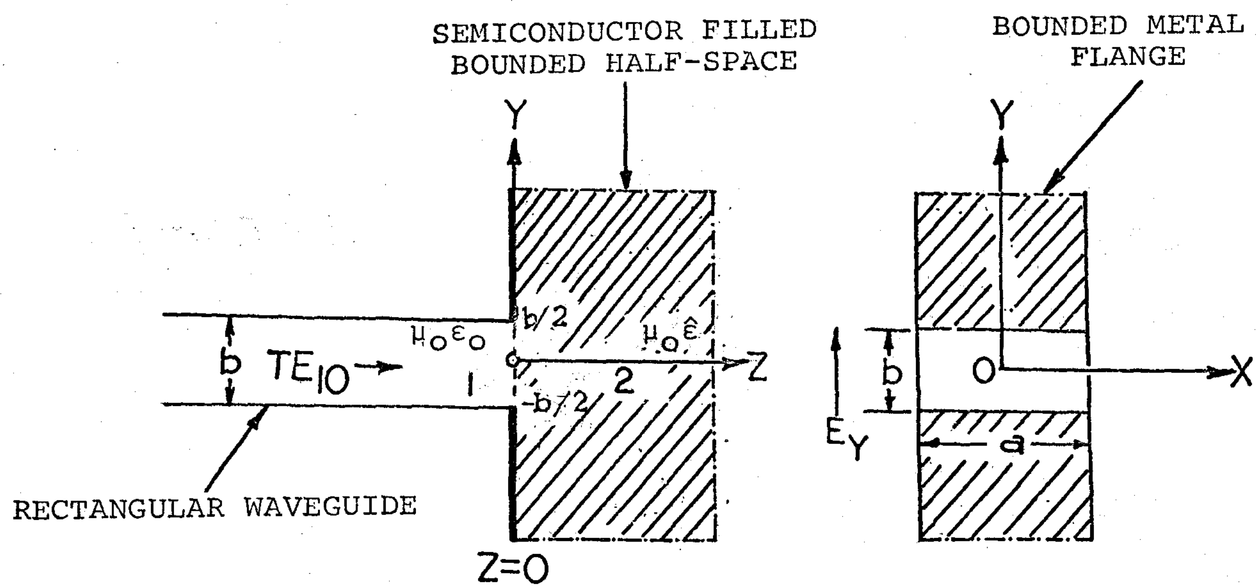

FIGURE 4.2: A Semi-Infinite Block of Semiconductor at the End of a Rectangular Waveguide in Bounded Ground Planes.

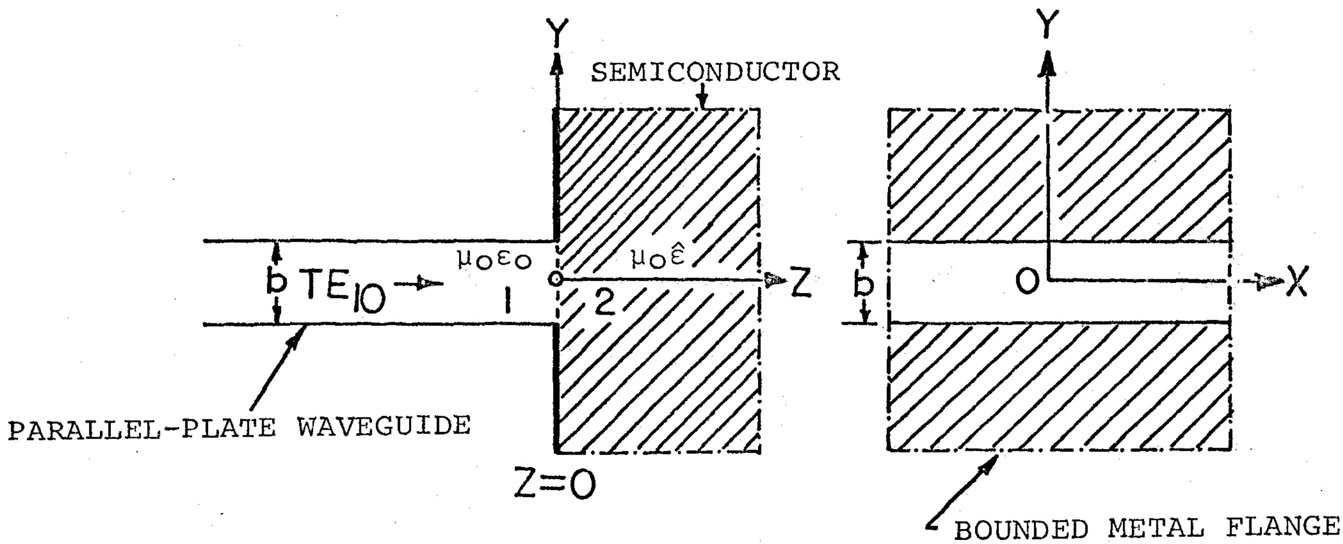

FIGURE 4.3: A Parallel-Plate Waveguide in Bounded Ground Planes Covered by a Semi-Infinite Block of Semiconductor.

$$Y_{in} = \frac{\left[\hat{\varepsilon}_r - (f_c/f)^2\right]}{\sqrt{\frac{\mu_o}{\varepsilon_o}}} \frac{2\pi}{b\lambda} \int_{v=0}^{b} (b-v) \left[\frac{2j}{\pi} \int_{u=0}^{\infty} \frac{e^{-j\hat{k}\sqrt{u^2+v^2}}}{\sqrt{u^2+v^2}} du \right] dv \tag{4.25}$$

The integral[45] in the parenthesis of equation (4.25) is equal to $H_o^{(2)}(\hat{k}v)$ so that

$$Y_{in} = \frac{\left[\hat{\varepsilon}_r - (f_c/f)^2\right]}{\sqrt{\frac{\mu_o}{\varepsilon_o}}} \frac{2\pi}{b\lambda} \int_o^b (b-v)\ H_o^{(2)}\ (\hat{k}v)\ dv \tag{4.26}$$

which becomes, after normalising with respect to the characteristic admittance $Y_o = \dfrac{\left[1-(f_c/f)^2\right]^{1/2}}{\sqrt{\frac{\mu_o}{\varepsilon_o}}}$,

$$Y_n = \frac{\left[\hat{\varepsilon}_r - (f_c/f)^2\right]}{\left[1 - (f_c/f)^2\right]} \frac{2\pi}{b\lambda_g} \int_o^b (b-v)\ H_o^{(2)}\ (\hat{k}v)\, dv \tag{4.27}$$

To check the validity of equation (4.27), the admittance can be simplified for air at the end of the guide for which case $\hat{\varepsilon}_r = 1$, $\hat{k} = k_o$
so that

$$Y_n = \frac{2\pi}{b\lambda_g} \int_o^b (b-v)\ H_o^{(2)}\ (k_o v)\ dv \tag{4.28}$$

This agrees with the result given by Lewin[43].

4.3.1 An Alternative Solution of the Admittance for the System of Figure 4.2

If we assume that the total electric field in the aperture z=0 is that of the dominant TE_{10} mode, then

$$E_y \Big|_{z=0} = \begin{cases} \sqrt{\frac{2}{ab}} \quad \text{Cos} \frac{\pi x}{a} & |y| < b/2 \\ o & |y| > b/2 \end{cases} \qquad (4.29)$$

and $$E_x \Big|_{z=0} = 0 \qquad (4.30)$$

The latter equation gives us tranverse electric to x mode i.e. TE_x mode. For this mode, the x-component of the magnetic field in region 1 is given by†

$$H_x = \frac{1}{j\omega\mu} \left[k^2 - k_x^2 \right] \psi$$

$$= E_y \frac{k^2 - (\pi/a)^2}{j\omega\mu \quad jk_z}$$

The transform of this field at z=0 plane may be written as

$$\bar{H}_x \Big|_{z=0} = - \bar{E}_y \Big|_{z=0} \frac{\hat{k}^2 - (\pi/a)^2}{\omega\mu \quad k_z} \qquad (4.31)$$

where $k \Big|_{z=0} = \hat{k} = \omega\sqrt{\mu\varepsilon}$ and k_z is the z-directed wave vector

at z>0 for the structure of Figure 4.2, which can be written approximately as

$$K_z = \sqrt{\hat{k}^2 - k_x^2 - k_y^2}$$
$$\simeq \sqrt{\hat{k}^2 - k_y^2} \qquad (4.31a)$$

---

† Page 181, Reference 44

with k_z is chosen so that

$$\mathrm{Re}\,[k_z] > 0, \quad \mathrm{Im}[k_z] < 0 \tag{4.32}$$

The transform of the electric field E_y at z=0 plane is expressed as†

$$\bar{E}_y \Big|_{z=0} = \int_{-\infty}^{\infty} dy \int_{-\infty}^{\infty} dx \quad E_y(x,y,0)\, e^{-jk_y y}\, e^{-jk_x x} \tag{4.33}$$

Since the x-directed wave propagation is assumed to be negligible at z>0, equation (4.33) can be rewritten as†

$$\bar{E}_y \Big|_{z=0} = \int_{-\infty}^{\infty} E_y(x,y,0)\, e^{-jk_y y}\, dy \tag{4.34}$$

which becomes on substituting equation (4.29)

$$\bar{E}_y \Big|_{z=0} = \sqrt{\frac{2}{ab}} \cos\frac{\pi x}{a} \int_{-b/2}^{b/2} e^{-jk_y y}\, dy$$

$$= \sqrt{\frac{2}{ab}} \cos\frac{\pi x}{a}\, \frac{2}{k_y} \sin(k_y b/2) \tag{4.35}$$

The complex power leaving a region is defined as

$$P = \oiint E \times H^{*} . dS \tag{4.36}$$

---

† Page 181, Reference 44

The z-component of the complex power transmitted at the z=0 plane of the waveguide system as shown in Figure 4.2 can be written as

$$P = \int_{-a/2}^{a/2} dx \int_{-\infty}^{\infty} \begin{vmatrix} a_x & a_y & a_z \\ 0 & E_y & E_z \\ H_x^* & H_y^* & H_z^* \end{vmatrix} dy$$

$$= -\int_{-a/2}^{a/2} dx \int_{-\infty}^{\infty} E_y \, H_x^* \Big|_{z=0} dy \qquad (4.37)$$

To evaluate this complex power, we shall make use of the integral form of the Parseval's theorem†, which is

$$\int_{-\infty}^{\infty} f(x)\; g(x)^* \; dx = \frac{1}{2\pi} \int_{-\infty}^{\infty} \bar{f}(k)\; \bar{g}^*\; (k)\; dk \qquad (4.38)$$

Application of this theorem on equation (4.37) yields

$$P = -\frac{1}{2\pi} \int_{-a/2}^{a/2} dx \int_{-\infty}^{\infty} \bar{E}_y \; \bar{H}_x^* \Big|_{z=0} dk_y \qquad (4.39)$$

The complex conjugate power can be written as

$$P^* = -\frac{1}{2\pi} \int_{-a/2}^{a/2} dx \int_{-\infty}^{\infty} \bar{E}_y^* \; \bar{H}_x \Big|_{z=0} dk_y \qquad (4.40)$$

† Page 458, Reference 44

Substituting equations (4.31) and (4.35) for $\overline{H}_x$ and $\overline{E}_y$ respectively, we obtain

$$P^* = \frac{4}{2\pi} \frac{\hat{k}^2 - (\pi/a)^2}{\omega\mu} \frac{2}{ab} \int_{-a/2}^{a/2} \cos^2 \frac{\pi x}{a}\, dx \int_{-\infty}^{\infty} \frac{\sin^2 (k_y b/2)}{k_y^2 k_z}\, dk_y$$

$$= \frac{4}{\pi b} \frac{\hat{k}^2 - (\pi/a)^2}{\omega\mu} \int_{o}^{\infty} \frac{\sin^2 (k_y b/2)}{k_y^2 k_z}\, dk_y \qquad (4.41)$$

The waveguide admittance at the plane z=0 is defined as

$$Y = \frac{P^*}{|V|^2} \qquad (4.42)$$

where $|V|$ is the magnitude of the aperture voltage and can be found as follows

$$V = \int_{-b/2}^{b/2} E_y \Big|_{z=0} dy \int_{a/2}^{a/2} E_y \Big|_{z=0} dx$$

$$= \frac{2}{ab} \int_{-b/2}^{b/2} dy \int_{-a/2}^{a/2} \cos^2 \frac{\pi x}{a}\, dx = 1 \qquad (4.43)$$

With $|V|$ is unity in equation (4.42),

$$Y = \frac{4}{\pi b} \frac{[\hat{k}^2 - (\pi/a)^2]}{\omega\mu} \int_{o}^{\infty} \frac{\sin^2 (k_y b/2)}{k_y^2 k_z}\, dk_y \qquad (4.44)$$

It is convenient at this point to normalize equation (4.44) with respect to the characteristic admittance of the waveguide, which is

$$Y_o = \frac{[1 - (f_c/f)^2]^{1/2}}{\sqrt{\mu/\varepsilon_o}} \tag{4.45}$$

Thus

$$Y_n = \frac{Y}{Y_o} = \frac{8}{b\lambda} \frac{[\hat{\varepsilon}_r - (f_c/f)^2]}{[1 - (f_c/f)^2]^{1/2}} \int_0^\infty \frac{\sin^2 (k_y b/2)}{k_y^2 k_z} dk_y \tag{4.46}$$

For a lossy medium, $\hat{k}$ has an imaginary part so that

$$k_z = + \sqrt{\hat{k}^2 - k_y^2} \tag{4.47}$$

which satisfies equation (4.32). For a lossless medium, however, proper values of k_z must be chosen with $\hat{k} = k$. Thus

$$\begin{aligned} k_z &= \sqrt{k^2 - k_y^2} \qquad |k_y| < k \\ k_z &= -j \sqrt{k_y^2 - k^2} \quad |k_y| > k \end{aligned} \tag{4.48}$$

With these values of k_z, the admittance for a lossless medium becomes

$$Y_n = \frac{8}{b\lambda} \frac{[\varepsilon_r - (f_c/f)^2]}{[1 - (f_c/f)^2]^{1/2}} \left[\int_o^k \frac{\sin^2 (k_y b/2)}{k_y^2 \sqrt{k^2 - k_y^2}} dk_y + j \int_k^\infty \frac{\sin^2 (k_y b/2)}{k_y^2 \sqrt{k_y^2 - k^2}} dk_y \right] \tag{4.49}$$

If a metal plate is placed at distance ℓ from the z=0 plane, equation (4.46) assumes the following form:

$$Y_n = \frac{8}{b\lambda} \frac{[\hat{\varepsilon}_r - (f_c/f)^2]}{[1 - (f_c/f)^2]^{1/2}} \int_0^\infty \left[\frac{1 + e^{-j2k_z\ell}}{1 - e^{-j2k_z\ell}}\right] \frac{\sin^2(k_y b/2)}{k_y^2 \sqrt{\hat{k}^2 - k_y^2}} dk_y \tag{4.50}$$

which simplifies to the original equation (4.46) for the case $\ell=\infty$. To simplify further, equation (4.46) can be written as

$$Y_n = \frac{8\pi}{b\lambda} \frac{[\hat{\varepsilon}_r - (f_c/f)^2]}{[1 - (f_c/f)^2]^{1/2}} \frac{1}{2\pi} \int_{-\infty}^{\infty} f_1(k_y) f_2(k_y) dk_y \tag{4.51}$$

where
$$f_1(k_y) = \frac{1}{\sqrt{\hat{k}^2 - k_y^2}} \tag{4.52}$$

$$f_2(k_y) = \frac{\sin^2(k_y b/2)}{k_y^2} \tag{4.53}$$

Taking the transforms of $f_1(k_y)$ and $f_2(k_y)$,

$$F_1(y) = \frac{1}{2\pi} \int_{-\infty}^{\infty} \frac{e^{-jk_y y}}{\sqrt{\hat{k}^2 - k_y^2}} dk_y$$

$$= \frac{1}{2} H_o^{(2)}(\hat{k}\, y) \tag{4.54}$$

$$F_2(y) = \frac{1}{2\pi} \int_{-\infty}^{\infty} \frac{1}{k_y^2} \sin^2(k_y b/2)\, e^{-jk_y y}\, dk_y$$

$$= \begin{cases} \frac{1}{4}(b - y) & |y| \leqslant b \\ 0 & |y| > b \end{cases} \tag{4.55}$$

Using Parseval's theorem, equation (4.51) becomes

$$Y_n = \frac{8\pi}{b\lambda} \frac{[\hat{\varepsilon}_r - (f_c/f)^2]}{[\ 1 - (f_c/f)^2]^{1/2}} \int_{-\infty}^{\infty} F_1(y)\ F_2(y)\ dy \tag{4.56}$$

Substitution of equations (4.54) and (4.55) in (4.56) gives

$$Y_n = \frac{2\pi}{b\lambda_g} \frac{[\hat{\varepsilon}_r - (f_c/f)^2]}{[\ 1 - (f_c/f)^2]} \int_0^b (b-y)\ H_0^{(2)}\ (\hat{k}\ y)\ dy \tag{4.57}$$

which agrees with equation (4.27) as expected.

The reflection coefficient of the waveguide system at plane $z=0$ can be expressed in terms of Y_n.

$$R = \frac{1 - Y_n}{1 + Y_n} \tag{4.58}$$

4.4 THE REFLECTION COEFFICIENT OF A SEMI-INFINITE BLOCK OF SEMICONDUCTOR AT THE END OF A PARALLEL-PLATE WAVEGUIDE OPENING ONTO BOUNDED GROUND PLANES

When 'a' in Figure 4.1a approaches infinity, the rectangular waveguide degenerates into a parallel-plate system with infinite flanges (Fig.4.3).With $f_c = 0$ and $\lambda_g = \lambda$, for this configuration, the admittance can be written from equation (4.27) as

$$Y_n = \frac{2\pi}{b\lambda}\ \hat{\varepsilon}_r \int_0^b (b-v)\ H_o^{(2)}\ (\hat{k}v)\ dv \tag{4.59}$$

To check the validity of this equation, the admittance can be calculated for air at the end of a parallel-plate system for which case $\hat{\varepsilon}_r = 1$, $\hat{k} = k_o$ so that

$$Y_n = \frac{2\pi}{b\lambda} \int_o^b (b-v)\, H_o^{(2)}\, (k_o v)\, dv \tag{4.60}$$

a result that agrees with Lewin[43] as expected.

An alternative solution to this problem is also possible in the same manner as in Section 4.3.1.

4.5 Numerical Calculations

Equations (4.22) and (4.23) have been evaluated numerically on a CDC 6400 Digital Computer, to calculate the normalized waveguide admittance and the reflection coefficient at the z=0 plane of the structure of Figure 4.1a. The numerical integration of equation (4.22) was performed by Simpson's rule[46]. For higher accuracy, small increments (value of h in Simpson's rule) were used near the regions of the singularities ($u = 0$, $v = 0$) where the integral changes very rapidly to infinity.

Numerical calculations were made for the following two cases:

(a) $a = 2.286$ cm, $b = 1.016$ cm, $f = 9.522$ GHz

(b) $a = 0.712$ cm, $b = 0.356$ cm, $f = 34.5$ GHz

The results of these calculations are given in Figures 4.4 through 4.7 and in Tables 4.1 through 4.4. The structure of Figure 4.1a can be represented by an equivalent circuit consisting of a conductance and a susceptance as shown in Figure 4.1b. Figures 4.4 and 4.5 show the changes in such parameters as functions of resistivity and dielectric constant. Figures 4.6 and 4.7 show the plots of the reflection coefficients as functions of resistivity and dielectric constant for 34.5 and 9.522 GHz, respectively.

Finally, as a check on numerical results, the integral Y_n in equation (4.21) has been evaluated approximately, for the case where $\hat{k}$ has a large complex value. If $\hat{k}$ has a large negative imaginary part (i.e. in low resistivity materials), the contribution to the integral in equation (4.21) is significant only near the region u = 0 and v = 0. Thus for a>>u and b>>u, the equation (4.21) becomes:

$$Y_n = \frac{[\hat{\varepsilon}_r - (f_c/f)^2]}{[\ 1 - (f_c/f)^2]} \frac{4j}{ab\lambda_g} \int_{u=0}^{a} \int_{v=0}^{b} ab \frac{e^{-j\hat{k}\sqrt{u^2+v^2}}}{\sqrt{u^2+v^2}} du\,dv \tag{4.61}$$

The limits of integration can be extended to infinity without changing the value of the integral significantly. Thus

$$Y_n = \frac{[\hat{\varepsilon}_r - (f_c/f)^2]}{[\ 1 - (f_c/f)^2]} \frac{4j}{\lambda_g} \int_{v=0}^{\infty} [\int_{u=0}^{\infty} \frac{e^{-j\hat{k}\sqrt{u^2+v^2}}}{\sqrt{u^2+v^2}} du] dv \tag{4.62}$$

The integral in the parenthesis is given by[45] $\frac{\pi}{2j} H_o^{(2)}(\hat{k}v)$ and the resulting integral is given by†

---

† In formula (143) of Reference 45, when b→0, $\int_o^{\infty} H_o^{(2)}(zx)\,dx = 1/z$

$$\frac{\pi}{2j} \int_{v=0}^{\infty} H_0^{(2)}(\hat{k}v)\, dv = \frac{\pi}{2j} \frac{1}{\hat{k}} \tag{4.63}$$

where $H_o^{(2)}$ is the Hankel function of the second order.
Thus

$$Y_n \doteq \left[\frac{\hat{\varepsilon}_r}{1 - (f_c/f)^2}\right]^{1/2} \tag{4.64}$$

on the reasonable assumption that Re $[\hat{\varepsilon}_r] >> (f_c/f)^2$ for G_e.

$$\therefore R = \frac{1 - \left[\dfrac{\hat{\varepsilon}_r}{1 - (f_c/f)^2}\right]^{1/2}}{1 + \left[\dfrac{\hat{\varepsilon}_r}{1 - (f_c/f)^2}\right]^{1/2}} \tag{4.65}$$

which agrees with the approximate equation (3.12).

Equation (4.46) was also evaluated numerically in the case of germanium filled half-space for a rectangular waveguide with a=2.286 cm, b=1,016 cm and f=9.522 GHz. The results of these calculations were found to be similar to those of Figure 4.4.

4.6 Experimental Techniques

The principal objective of the experimental programme was to obtain data on the behaviour of the reflection coefficient of a semi-infinite medium, in order to confirm the theoretical predictions of Section 4.2.

(A) SAMPLE PREPARATION:

Large blocks of n-type germanium samples were obtained to cover the cross-sections of X- and Q-band waveguides. The reflecting surfaces were prepared by lapping with a very fine silicon carbide paper. The lengths of the samples were large compared to the skin depth δ, which is found to be given by

$$\delta = \left[\left\{ (\omega^2\mu\varepsilon)^2 + (\omega\mu\sigma)^2 \right\}^{1/4} \cos \frac{\pi - \tan^{-1}\frac{\sigma}{\omega\varepsilon}}{2} \right]^{-1} \qquad (4.66)$$

This equation was evaluated numerically for germanium at 9.522 and 34.5 GHz. The results are shown in Figure 4.8.

"Selectron" which is a trade name for a particular kind of lossless plastic (ε_r = 2.85), was also used for measurement. The dimensions of the piece, in the form of a triangular prism, were: sides: 13" x 13" x 18.5"; height: 19.5".

(B) MICROWAVE MEASUREMENTS

Measurements of the reflection coefficients were made using the microwave bridge circuit of Figure 2.7. The theory of operation and the practical setting-up procedure of such a bridge circuit have been discussed in detail in Chapter II. Photographs of the experimental set-up at 34.5 and 9.522 GHz are as shown in Figures 2.9 and 2.10.

The sample holder as shown in Figure 2.9 is a

D1007 waveguide section with a high-precision 90° flange. This section was connected to one side arm of the reflection bridge. The semiconductor sample is allowed to rest on the flange. In the measurement with selectron and air, the horizontal configuration of Figure 2.10 was used.

Measurements were made with n-type germanium of various resisitivity (0.1, 1, 5, 10, 25, 50 ohm cm), selectron and air at the end of a rectangular waveguide opening onto a metal flange at 9.522 and 34.5 GHz. Equation (2.12) was used to calculate the reflection coefficients.

(c) D.C. MEASUREMENTS:

Measurements were also made of the d.c. resistivity of each sample of semiconductor with a high quality 4-probe tester.

4.7 Results

The results of the reflection coefficient measurements for the case of n-type germanium, selectron, and air are given in Figures 4.6 and 4.7. The microwave resistivity and dielectric constant were determined from these figures by comparing the magnitude and phase of the reflection coefficient with those obtained from calculations. The values of the resistivity and dielectric constant determined in this way are shown in Tables 4.2 and 4.3 together with the values obtained from d.c. measurements. The measured values of the reflection coefficient are also shown in the above-mentioned tables.

4.8 Discussion

Table 4.1 which shows a comparison of the approximate and exact solutions of the reflection coefficients for Ge indicates that the approximate equation (3.12) gives an error in the phase of the calculated reflection coefficient for the condition $\sigma<2\omega\varepsilon_o\varepsilon_r$, as pointed out in Section 3.5.

The theoretical values of the reflection coefficients as shown in Tables 4.2 and 4.3 are calculated from equation (4.23) using the nominal resistivities of Ge. A comparison of the tables shows that over the resistivity range $5<\rho<25$ Ωcm and dielectric constant range $1<\varepsilon_r<2.85$, the calculated values of the reflection coefficient are in good agreement with the measured values at 34.5 GHz, compared to the corresponding values at 9.522 GHz. Since 0.1, 1 and 50 Ωcm samples had resistivities significantly different from their nominal values (cf. D.C. Measurements in Table 4.2), the calculated reflection coefficients of these samples at 9.522 GHz did not agree well with the measured values . This necessitated the reflection coefficients to be computed on the resistivities obtained by d.c. measurements and the results are given in Table 4.4.

Inspection of this table shows that over the range $0.26<\rho<45.76$ Ωcm, the calculated reflection coefficients agree with the measured values at 34.5 GHz. However at 9.522 GHz, these values and in particular, the phases of R, did not agree well. The possible reason for this is the small size of the samples used, particularly the 0.26 and 45.76 Ωcm ones which were inadequate to satisfy the condition of a semi-infinite medium assumed in the theory. This was detected by introducing a metal plate in the half-space around the sample and observing the change in the detector reading of the microwave bridge circuit. The minimum size of a sample should be equal to or greater than $(a+10\delta) \times (b+10\delta) \times 5\delta$ to satisfy the condition of a semi-infinite medium where δ = skin depth and a, b = dimensions of the guide. The other reasons for disagreement at both X- and Q-band are the finite size of the flange and the approximation made in equation (4.23) by neglecting higher order modes.

The reflection coefficient measured on selectron is found to be in good agreement with the calculated value at 34.5 GHz compared to those at 9.522 GHz. This is expected since at X-band, a larger size of selectron is required to approximate the semi-infinite medium assumed in the theory. With air, however, the agreement is good at both these frequencies, because air in the half-space fulfils the condition of a semi-infinite medium in both these cases. The experimental set-up with the sample holder in the vertical position (Figure 2.9) was found to give better results than the horizontal set-up (Figure 2.10) in the case of measurement of air.

A comparison of the microwave and d.c. measurements of resistivity in Tables 4.2 and 4.3 indicates that the microwave measurements at 34.5 GHz give the correct values of resistivity and dielectric constant. However at 9.522 GHz measurements, the dielectric constants for 0.26 and 0.76 ohm cm samples and resistivity for 45.76 ohm cm sample are found to be in error. This is due to the disagreement of the measured and calculated values of the reflection coefficients of these samples as mentioned earlier. Also since the phase variations of the reflection coefficient with ε_r and ρ at the low and high ends of the resistivity range are small, a small error in the phase measurement of R can cause a large error in the ε_r and ρ measurement. The phase error is largely caused by the finite size of the sample and the flange and also by the unmatched condition of the tee of the microwave bridge.

Numerical calculations with experimental verifications have not been carried out for the parallel-plate waveguide system. For future work it would be interesting to see how the reflection coefficient of this structure behaves as a function of the electrical constants of the medium.

FIGURE 4.4: Theoretically Predicted Variations of the Conductance and Susceptance of the Germanium-filled waveguide Structure of Figure 4.1(a) with Resistivity.

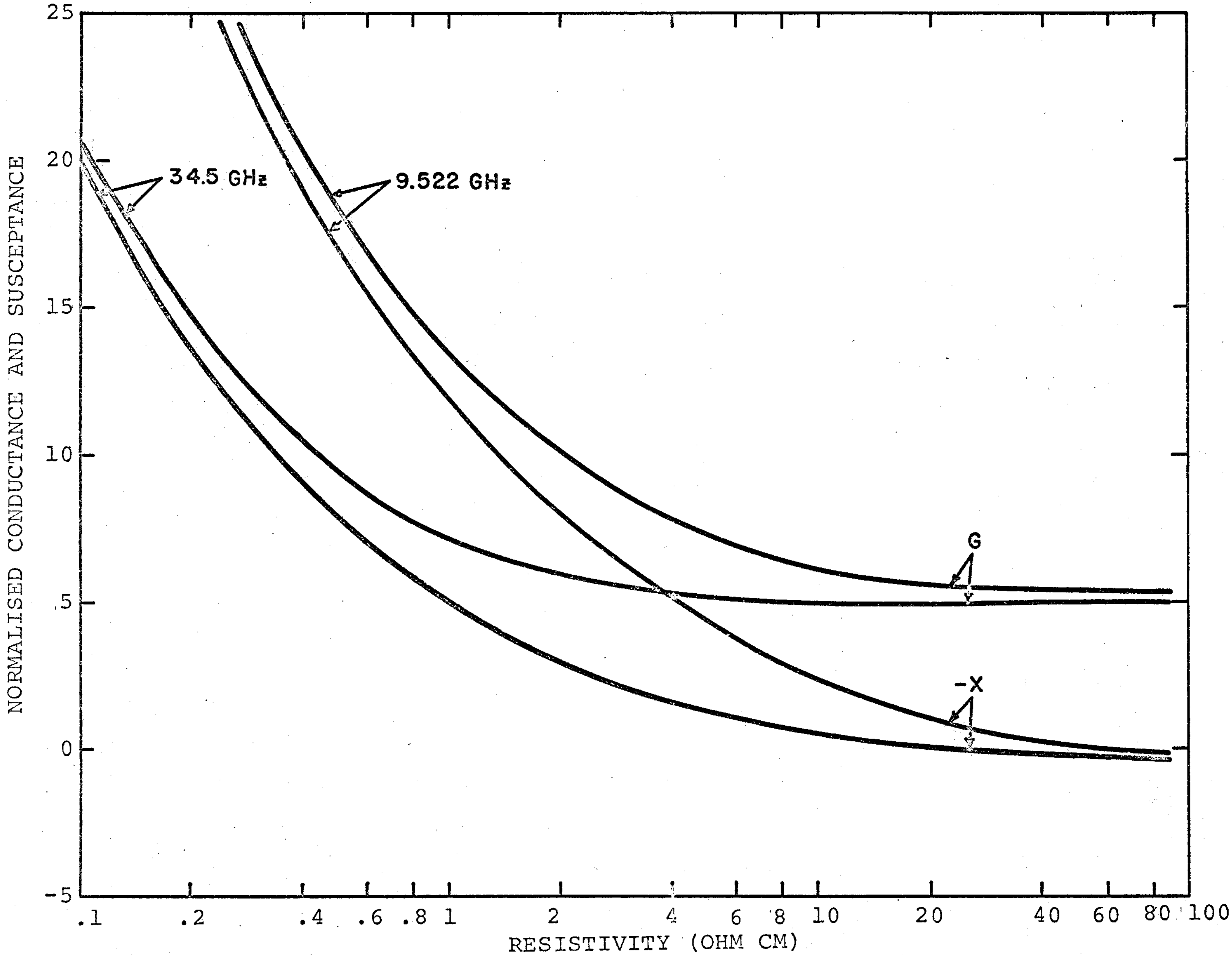

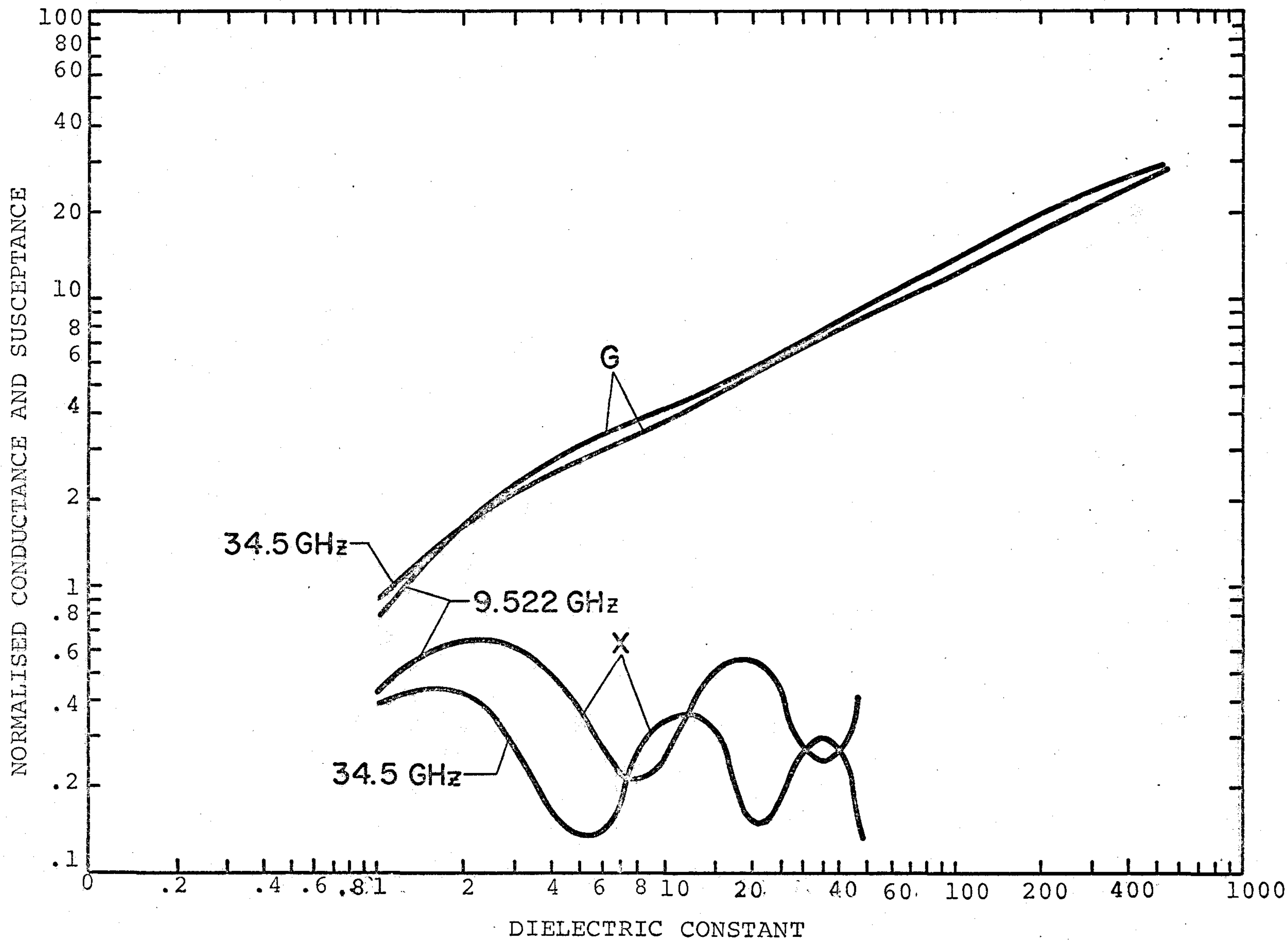

FIGURE 4.5: Theoretically Predicted Variations of the Conductance and Susceptance of the Waveguide Structure of Figure 4.1(a) with Dielectric Constant.

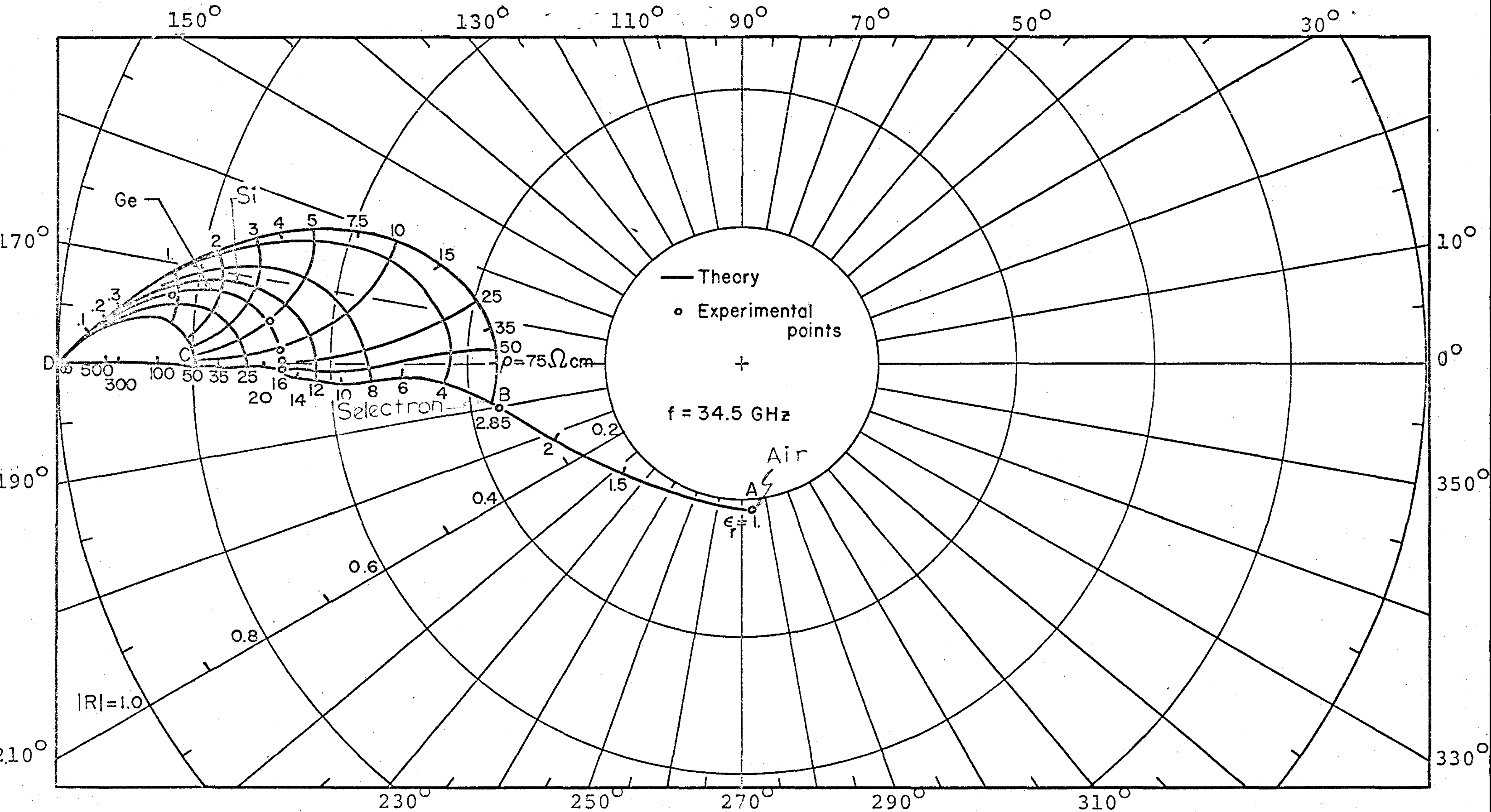

FIGURE 4.6: Polar plots of the reflection coefficients at the plane z=0 of the waveguide structure shown in Figure 4.1(a) as functions of the resistivity and dielectric constant of the medium in the half-space at 34.5 GHz. The circles represent the measured values for n-type germanium, selectron and air.

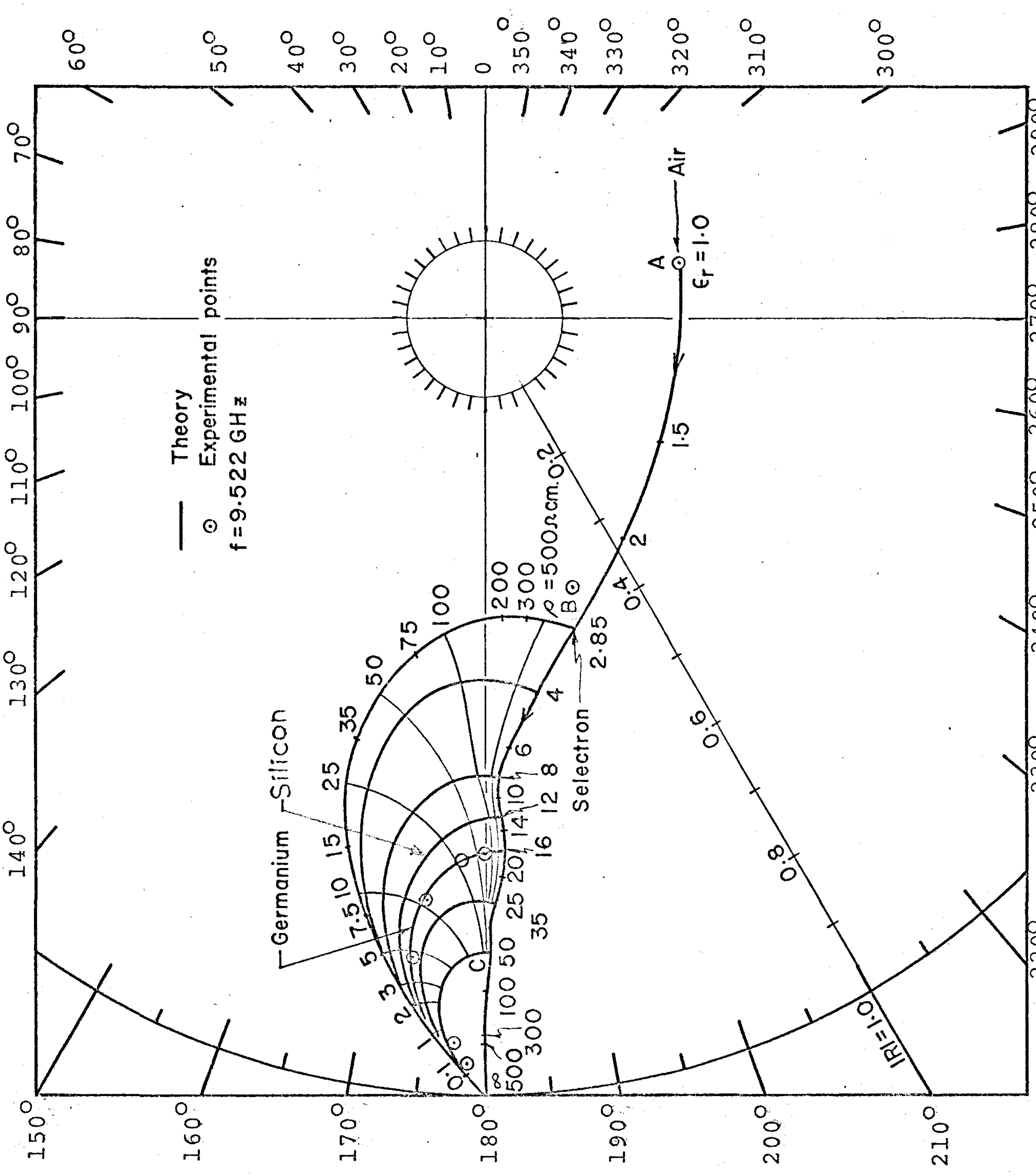

FIGURE 4.7: Polar Plots of the Reflection Coefficients at plane z=0 of the waveguide Structure shown in Figure 4.1(a) as functions of Resistivity and Dielectric constant of the Medium in the half-space for 9.522 GHz. The circles represent the measured Values for n-type Germanium, Selectron and Air.

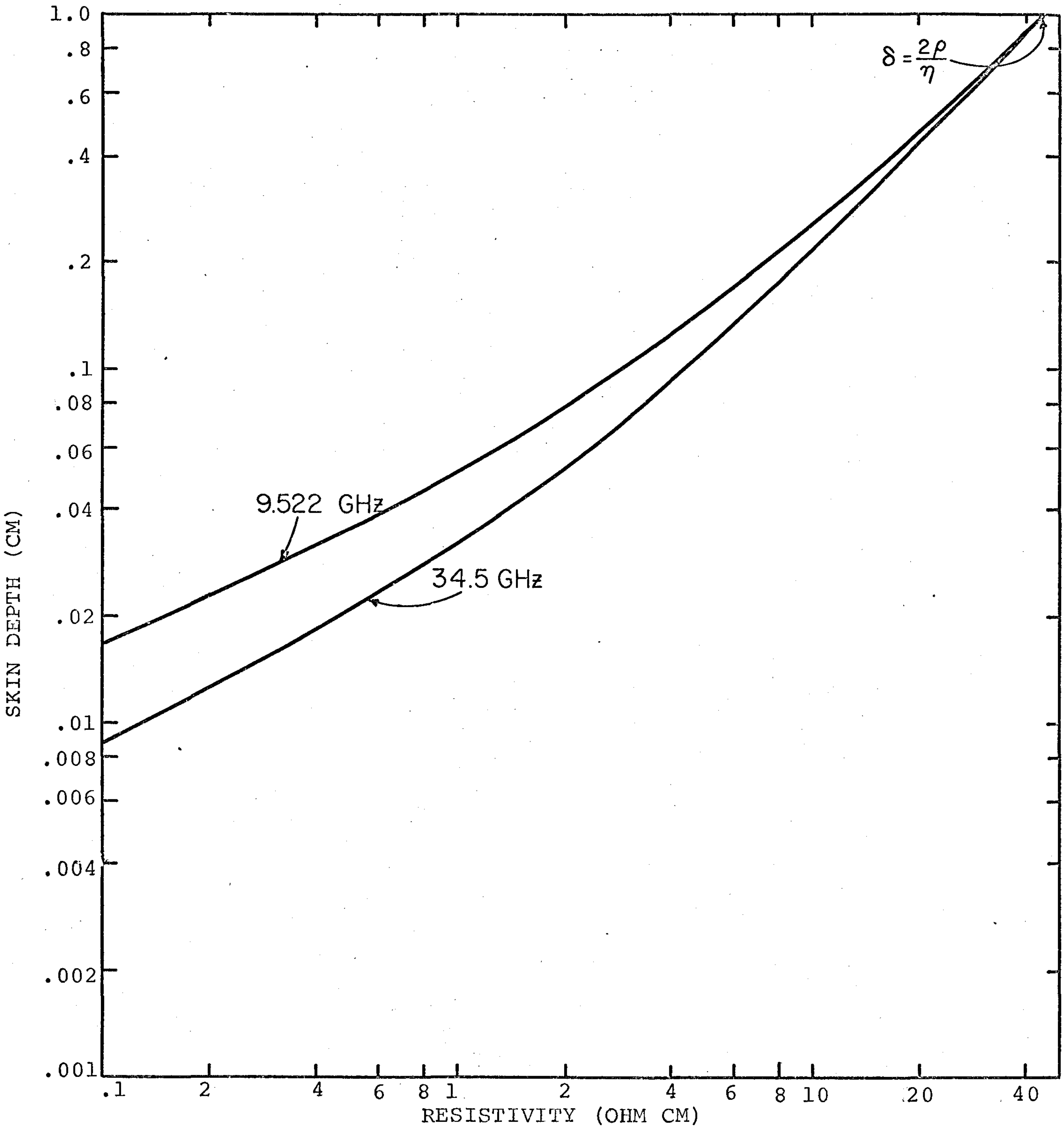

FIGURE 4.8: The Skin Depth of Germanium as a Function of Resistivity.

TABLE 4.1

COMPARISON OF THE APPROXIMATE AND EXACT SOLUTIONS OF THE REFLECTION COEFFICIENTS FOR Ge

Resistivity (nominal) Ωcm	R (9.522 GHz)		R (34.5 GHz)	
	Approx. Eq. (3.12)	Exact Eq. (4.23)	Approx. Eq. (3.12)	Exact Eq. (4.23)
0.1	0.977 $\angle 178.7$	0.976 $\angle 178.7$	0.951 $\angle 177.3$	0.950 $\angle 177.2$
1.0	0.922 $\angle 175.7$	0.919 $\angle 175.9$	0.834 $\angle 172.5$	0.827 $\angle 172.5$
5.0	0.826 $\angle 172.8$	0.818 $\angle 173.0$	0.704 $\angle 174.0$	0.694 $\angle 174.8$
10.0	0.766 $\angle 172.9$	0.755 $\angle 173.5$	0.680 $\angle 176.4$	0.673 $\angle 177.8$
25.0	0.712 $\angle 175.6$	0.702 $\angle 176.9$	0.671 $\angle 178.5$	0.669 $\angle 179.8$
50.0	0.699 $\angle 177.6$	0.690 $\angle 179.3$	0.670 $\angle 179.2$	0.670 $\angle 180.6$

TABLE 4.2

COMPARISON OF THE MICROWAVE AND D.C. MEASUREMENTS OF THE RESISTIVITY AND DIELECTRIC CONSTANT TOGETHER WITH THE CALCULATED AND MEASURED VALUES OF THE REFLECTION COEFFICIENT AT THE AIR-SAMPLE INTERFACE OF FIGURE 4.1a FOR 34.5 GHz

Samples	Resistivity (nominal)	Calculated R Equation (4.23)	Measured R	Microwave Measurements		D.C. Measurements
				ρ	ε_r	
	Ω cm			Ω cm		Ω cm
Germanium (n-type)	0.1	$0.950 \angle 177.2$	$0.916 \angle 175.7$	0.27	18	0.26
	1.0	$0.827 \angle 172.5$	$0.838 \angle 173.5$	0.9	16.5	0.76
	5.0	$0.694 \angle 174.8$	$0.691 \angle 175.0$	5.1	16	4.96
	10.0	$0.673 \angle 177.8$	$0.678 \angle 178.0$	11.0	16	10.3
	25.0	$0.669 \angle 179.8$	$0.6775 \angle 179.7$	24.0	16	24.3
	50.0	$0.670 \angle 180.6$	$0.678 \angle 180.7$	51.0	16	45.8
	Dielectric constant (nominal)					
Air	1.0	$0.214 \angle -86.2$	$0.214 \angle -85.9$	-	1.0	-
Selectron	2.85	$0.372 \angle 189.3$	$0.360 \angle 190.5$	-	2.8	-

TABLE 4.3

COMPARISON OF THE MICROWAVE AND D.C. MEASUREMENTS OF THE RESISTIVITY AND DIELECTRIC CONSTANT TOGETHER WITH THE CALCULATED AND MEASURED VALUES OF THE REFLECTION COEFFICIENT AT THE AIR-SAMPLE INTERFACE OF FIGURE 4.1a FOR 9.522 GHz

Samples	Resistivity (nominal)	Calculated R Equation (4.23)	Measured R	Microwave Measurements ρ	Microwave Measurements ε_r	D.C. Measurements
	Ω cm			Ω cm		Ω cm
Germanium (n-type)	0.1	$0.976\ \underline{\vert 178.7}$	$0.960\ \underline{\vert 178.9}$	0.25	100	0.26
	1.0	$0.919\ \underline{\vert 175.9}$	$0.930\ \underline{\vert 177.8}$	0.75	55	0.76
	5.0	$0.818\ \underline{\vert 173.0}$	$0.831\ \underline{\vert 173.8}$	4.8	17	4.96
	10.0	$0.755\ \underline{\vert 173.5}$	$0.748\ \underline{\vert 174.5}$	11.5	16.5	10.3
	25.0	$0.702\ \underline{\vert 176.9}$	$0.697\ \underline{\vert 177.8}$	27.0	16	24.3
	50.0	$0.690\ \underline{\vert 179.3}$	$0.693\ \underline{\vert 180.6}$	65.0	16	45.8
	Dielectric constant (nominal)					
Air	1.0	$0.263\ \underline{\vert -74.5}$	$0.260\ \underline{\vert -74.3}$	-	1.0	-
Selectron	2.85	$0.417\ \underline{\vert 196.4}$	$0.364\ \underline{\vert 198.01}$	-	2.6	-

TABLE 4.4

COMPARISON OF THE CALCULATED AND MEASURED VALUES OF THE REFLECTION COEFFICIENTS FOR Ge IN THE STRUCTURE OF FIGURE 4.1(a)

D.C. Resistivity (Ωcm)	9.522 GHz		34.5 GHz	
	Calculated R Equation (4.23)	Measured R	Calculated R Equation (4.23)	Measured R
0.26	$0.962 \angle 177.8$	$0.960 \angle 178.9$	$0.918 \angle 175.6$	$0.916 \angle 175.7$
0.76	$0.933 \angle 176.4$	$0.930 \angle 177.8$	$0.858 \angle 173.2$	$0.838 \angle 173.5$
4.96	$0.821 \angle 173.1$	$0.831 \angle 173.8$	$0.695 \angle 174.7$	$0.691 \angle 175.0$
10.3	$0.753 \angle 173.5$	$0.748 \angle 174.5$	$0.673 \angle 177.7$	$0.678 \angle 178.0$
24.30	$0.702 \angle 176.8$	$0.697 \angle 177.8$	$0.669 \angle 179.8$	$0.6775 \angle 179.7$
45.8	$0.690 \angle 179.0$	$0.693 \angle 180.6$	$0.670 \angle 180.5$	$0.678 \angle 180.7$

CHAPTER V

MICROWAVE REFLECTIONS FROM THE SURFACE OF A FINITE MEDIUM (EXACT SOLUTIONS)

5.1 Introduction

The admittance of a rectangular waveguide system radiating into a finite medium, followed by free space can be calculated exactly. The appropriate equations are derived in Section 5.2. The reflection coefficient of a rectangular waveguide system radiating into a semiconductor slab followed by a conducting plate is also derived. The solution is presented in Section 5.3. The admittance of a rectangular waveguide system radiating into a lossless plasma layer is formulated in Section 5.4.

Finally, numerical computations are made. The results of calculations are given for Ge and plasma cases and have been compared with those given by previous authors. Measurements which confirm the theory are made on germanium at 9.35 GHz.

5.2 The Admittance of a Rectangular Waveguide System Radiating Into a Finite Medium Followed by Free Space

The exact solutions for an infinite medium as developed in the last chapter are useful for the determination of semiconductor properties such as σ and ε_r. Unless a semiconductor sample has a length $\ell \geqslant 5\delta$, it cannot be assumed to represent a semi-infinite medium (Section 4.8). Since δ increases with resistivity, an increasingly large sample length (for example, $\ell = 6$ cm for a 50Ω cm sample) is required for high resistivity semiconductors to achieve agreement between theory and experiment. The availability of such large and costly semiconductor samples is a practical problem. Thus the development of the exact solutions for a finite semiconductor slab is desirable.

The expression for the admittance of a rectangular waveguide radiating into a finite slab of semiconductor is derived in this section. The technique is the same as used by Compton(47) and Crosswell, et al(48).

The geometry of the problem is given in Figure 5.1. It is to be noted that the system of coordinates is different from those used previously. The theory of the fields present in such a system may be obtained from the solutions of the equations 4.2a and 4.2b. Unlike the previous case for an infinite medium, the electric vector potential is assumed to have two components. One possible choice for $\vec{F}$ is

$$\vec{F} = \vec{a}_x\phi + \vec{a}_y\psi \tag{5.1}$$

Thus the field components are †

$$Ex = \frac{\partial\psi}{\partial z} \quad \text{(a)} \qquad Hx = \frac{1}{j\omega\mu}\left[\left\{\frac{\partial^2\phi}{\partial x^2} + \frac{\partial^2\psi}{\partial x\partial y}\right\} + k^2\phi\right] \quad \text{(d)}$$

$$Ey = -\frac{\partial\phi}{\partial z} \quad \text{(b)} \qquad Hy = \frac{1}{j\omega\mu}\left[\left\{\frac{\partial^2\phi}{\partial x\partial y} + \frac{\partial^2\psi}{\partial y^2}\right\} + k^2\psi\right] \quad \text{(e)} \qquad (5.2)$$

$$Ez = -\left[\frac{\partial\psi}{\partial x} - \frac{\partial\phi}{\partial y}\right] \quad \text{(c)} \qquad Hz = \frac{1}{j\omega\mu}\left[\frac{\partial^2\phi}{\partial x\partial z} + \frac{\partial^2\psi}{\partial y\partial z}\right] \quad \text{(f)}$$

In region 2, the solutions for ψ and ϕ may be constructed with an 'incident' and a 'reflected' component:

$$\psi_2(x,y,z) = \frac{1}{(2\pi)^2}\int_{-\infty}^{\infty}\int_{-\infty}^{\infty}[I_\psi\, e^{-jk_z z} + R_\psi\, e^{jk_z z}]e^{-jk_x x}e^{-jk_y y}\,dk_x dk_y \tag{5.3}$$

† x, y and z shall be read as the subscripts of E and H in Chapter V.

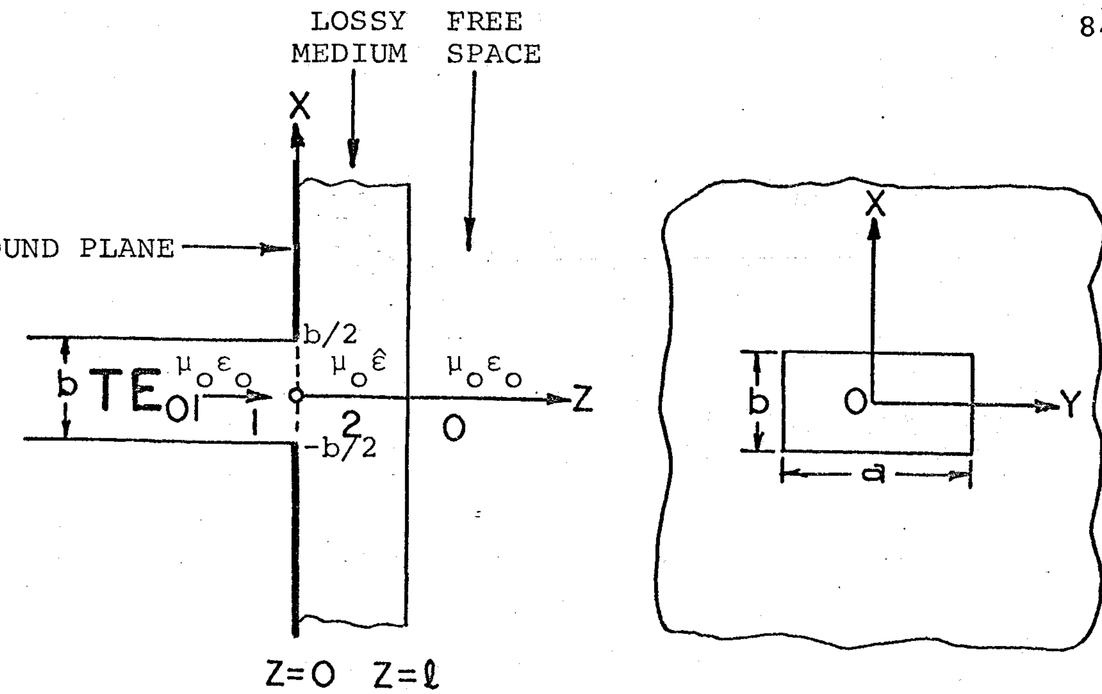

FIGURE 5.1: A Rectangular Waveguide in a Ground Plane Covered by a Lossy Medium.

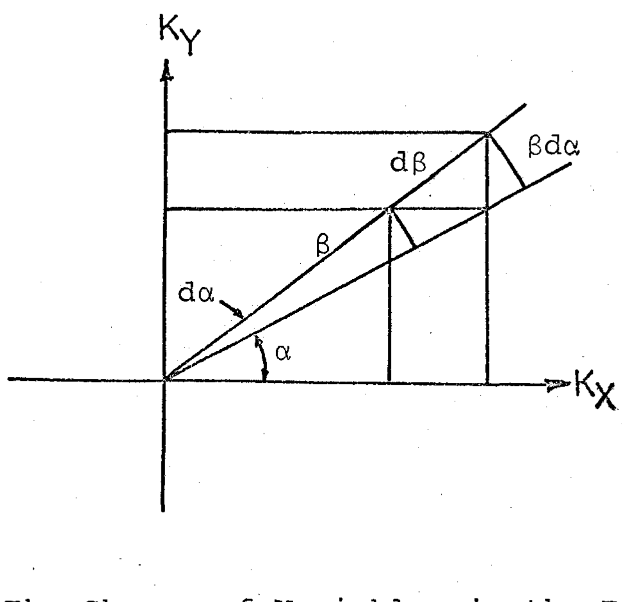

FIGURE 5.2: The Change of Variables in the Equation 5.41.

$$\phi_2(x,y,z) = \frac{1}{(2\pi)^2}\int_{-\infty}^{\infty}\int_{-\infty}^{\infty}[I_\phi e^{-jk_z z}+R_\phi e^{jk_z z}]\, e^{-jk_x x}\, e^{-jk_y y}\, dk_x dk_y \qquad (5.4)$$

and in region 0 with a 'transmitted' component only,

$$\psi_o(x,y,z) = \frac{1}{(2\pi)^2}\int_{-\infty}^{\infty}\int_{-\infty}^{\infty}T_\psi e^{-jk_{zo}z}\, e^{-jk_x x}\, e^{-jk_y y}\, dk_x dk_y \qquad (5.5)$$

$$\phi_o(x,y,z) = \frac{1}{(2\pi)^2}\int_{-\infty}^{\infty}\int_{-\infty}^{\infty}T_\phi e^{-jk_{zo}z}\, e^{-jk_x x}\, e^{-jk_y y}\, dk_x dk_y \qquad (5.6)$$

where the z-direction propagation constants,

$$k_z = \sqrt{\hat{k}^2 - k_x{}^2 - k_y{}^2} \qquad (5.7)$$

$$k_{zo} = \sqrt{k_o{}^2 - k_x{}^2 - k_y{}^2} \qquad (5.8)$$

are chosen so that

$$\mathrm{Re}(k_z),\ \mathrm{Re}(k_{zo}) \geq 0 \qquad (5.9)$$

$$\mathrm{Im}(k_z),\ \mathrm{Im}(k_{zo}) \leq 0\ . \qquad (5.10)$$

The electric and magnetic fields in region 2 can be found from equation 5.2.

$$Ex_2(x,y,z) = \frac{1}{(2\pi)^2}\int_{-\infty}^{\infty}\int_{-\infty}^{\infty} jk_z[-I_\psi e^{-jk_z z}+R_\psi e^{jk_z z}]e^{-jk_x x}e^{-jk_y y}dk_x dk_y$$

---------- (5.11)

$$Ey_2(x,y,z) = \frac{1}{(2\pi)^2}\int_{-\infty}^{\infty}\int_{-\infty}^{\infty} jk_z\left[I_\phi e^{-jk_z z}-R_\phi e^{jk_z z}\right]e^{-jk_x x}e^{-jk_y y}dk_x dk_y$$

---------- (5.12)

$$Hx_2(x,y,z) = \frac{1}{(2\pi)^2}\int_{-\infty}^{\infty}\int_{-\infty}^{\infty}\left[\frac{\hat{k}^2-k_x{}^2}{j\omega\mu}(I_\phi e^{-jk_z z}+R_\phi e^{jk_z z}) - \frac{k_x k_y}{j\omega\mu}(I_\psi e^{-jk_z z}+R_\psi e^{jk_z z})\right] e^{-jk_x x}e^{-jk_y y}dk_x dk_y \qquad (5.13)$$

$$Hy_2(x,y,z) = \frac{1}{(2\pi)^2}\int_{-\infty}^{\infty}\int_{-\infty}^{\infty}\left[\frac{\hat{k}^2-k_y^2}{j\omega\mu}(I_\psi e^{-jk_z z}+R_\psi e^{-jk_z z})\right.$$

$$\left. - \frac{k_x k_y}{j\omega\mu}(I_\phi e^{-jk_z z}+R_\phi e^{jk_z z})\right] e^{-jk_x x} e^{-jk_y y} dk_x dk_y \tag{5.14}$$

and in region 0,

$$Ex_o(x,y,z) = \frac{1}{(2\pi)^2}\int_{-\infty}^{\infty}\int_{-\infty}^{\infty} -jk_{zo}\, T_\psi e^{-jk_{zo}z} e^{-jk_x x} e^{-jk_y y} dk_x dk_y \tag{5.15}$$

$$Ey_o(x,y,z) = \frac{1}{(2\pi)^2}\int_{-\infty}^{\infty}\int_{-\infty}^{\infty} jk_{zo}\, T_\phi e^{-jk_{zo}z} e^{-jk_x x} e^{-jk_y y} dk_x dk_y \tag{5.16}$$

$$Hx_o(x,y,z) = \frac{1}{(2\pi)^2}\int_{-\infty}^{\infty}\int_{-\infty}^{\infty}\left[\frac{k_o^2-k_x^2}{j\omega\mu}T_\phi - \frac{k_x k_y}{j\omega\mu}T_\psi\right] e^{-jk_{zo}z} e^{-jk_x x} e^{-jk_y y} dk_x dk_y \tag{5.17}$$

$$Hy_o(x,y,z) = \frac{1}{(2\pi)^2}\int_{-\infty}^{\infty}\int_{-\infty}^{\infty}\left[\frac{k_o^2-k_x^2}{j\omega\mu}T_\psi - \frac{k_x k_y}{j\omega\mu}T_\phi\right] e^{-jk_{zo}z} e^{-jk_x x} e^{-jk_y y} dk_x dk_y \tag{5.18}$$

where k_o, $\hat{k}$ are wave numbers of 'free space' and 'the complex medium', respectively. Assuming that the total electric field in the aperture is that of the dominant TE_{01} mode, the inverse transform of equations 5.11 and 5.12 at z = 0 plane gives,

$$jk_z(-I_\psi + R_\psi) = \int_{-\infty}^{\infty}\int_{-\infty}^{\infty} Ex(x,y,0) e^{jk_x x} e^{jk_y y}\, dxdy$$

$$= \sqrt{\frac{2}{ab}}\int_{y=-a/2}^{a/2}\int_{x=-b/2}^{b/2} \cos\frac{\pi y}{a}\, e^{jk_x x} e^{jk_y y} dxdy$$

$$= 4\pi\sqrt{\frac{2a}{b}}\ \frac{\sin(k_x b/2)\ \cos(k_y a/2)}{k_x[\pi^2 - (k_y a)^2]} = F \tag{5.19}$$

and $jk_z(I_\phi - R_\phi) = 0$ (5.20)

Equating the electric and magnetic fields at $z = \ell$,

$$-jk_z I_\psi e^{-jk_z \ell} + jk_z R_\psi e^{jk_z \ell} = -jk_{zo} T_\psi e^{-jk_{zo}\ell} \tag{5.21}$$

$$-jk_z I_\phi e^{-jk_z \ell} - jk_z R_\phi e^{jk_z \ell} = +jk_{zo} T_\phi e^{-jk_{zo}\ell} \tag{5.22}$$

$$(\hat{k}^2 - k_x^2)\,[I_\phi e^{-jk_z\ell} + R_\phi e^{jk_z\ell}] - k_x k_y\,[I_\psi e^{-jk_z\ell} + R_\psi e^{jk_z\ell}]$$

$$= (k_o^2 - k_x^2) T_\phi e^{-jk_{zo}\ell} - k_x k_y T_\psi e^{-jk_{zo}\ell} \tag{5.23}$$

$$(\hat{k}^2 - k_y^2)\,[I_\psi e^{-jk_z\ell} + R_\psi e^{jk_z\ell}] - k_x k_y\,[I_\phi e^{-jk_z\ell} + R_\phi e^{jk_z\ell}]$$

$$= (k_o^2 - k_y^2) T_\psi e^{-jk_{zo}\ell} - k_x k_y T_\phi e^{-jk_{zo}\ell} \tag{5.24}$$

Equations 5.19 and 5.21 give,

$$T_\psi = \frac{2k_z I_\psi \sin k_z\ell - Fe^{jk_z\ell}}{jk_{zo}\, e^{-jk_{zo}\ell}} \tag{5.25}$$

and from equations 5.20 and 5.22,

$$T_\phi = \frac{2k_z I_\phi \sin k_z\,\ell}{jk_{zo}\, e^{jk_{zo}\ell}} \tag{5.26}$$

Finally, the solution of equations 5.23 through 5.26 gives two equations involving I_ϕ and I_ψ.

$$I_\phi[(\hat{k}^2 - k_x^2)k_{zo} \cos k_z\ell + j(k_o^2 - k_x^2)k_z \sin k_z\ell\,]$$
$$+ I_\psi[-jk_xk_yk_z \sin k_z\ell - k_xk_yk_{zo} \cos k_z\ell] = -k_xk_y e^{+jk_z\ell}\left[\frac{k_z+k_{zo}}{2k_z}\right] jF \tag{5.27}$$

$$I_\phi[-jk_xk_yk_z \sin k_z\ell - k_xk_yk_{zo} \cos k_z\ell]$$
$$+ I_\psi\,[(\hat{k}^2 - k_y^2)k_{zo} \cos k_z\ell + j(k_o^2 - k_y^2)k_z \sin k_z\ell]$$
$$= \frac{1}{2} e^{jk_z\ell}\left[(k_o^2 - k_y^2) + (\hat{k}^2 - k_y^2)\frac{k_{zo}}{k_z}\right] jF \tag{5.28}$$

In determinant form, I_ψ and I_ϕ are found to be given by,

$$I_\psi = \frac{\begin{vmatrix} A_{11} & B_1 \\ A_{12} & B_2 \end{vmatrix}}{\begin{vmatrix} A_{11} & A_{12} \\ A_{12} & A_{22} \end{vmatrix}} \tag{5.29}$$

$$I_\phi = \frac{\begin{vmatrix} B_1 & A_{12} \\ B_2 & A_{22} \end{vmatrix}}{\begin{vmatrix} A_{11} & A_{12} \\ A_{12} & A_{22} \end{vmatrix}} \tag{5.30}$$

where
$$\begin{aligned}
A_{11} &= (\hat{k}^2 - k_x^2)k_{zo} \cos k_z\ell + j(k_o^2 - k_x^2)k_z \sin k_z\ell \\
A_{12} &= -k_xk_y\,[k_{zo} \cos k_z\ell + jk_z \sin k_z\ell] \\
A_{22} &= (\hat{k}^2 - k_y^2)k_{zo} \cos k_z\ell + j(k_o^2 - k_y^2)k_z \sin k_z\ell \\
B_1 &= -k_xk_y\, e^{jk_z\ell}\left[\frac{k_z + k_{zo}}{2k_z}\right] jF \\
B_2 &= \frac{1}{2} e^{jk_z\ell}\left[(k_o^2 - k_y^2) + (\hat{k}^2 - k_y^2)\frac{k_{zo}}{k_z}\right] jF
\end{aligned} \tag{5.31}$$

Also, from equations 5.19 and 5.20 R_ψ and R_ϕ are given by,

$$R_\psi = \frac{F}{jk_z} + I_\psi \tag{5.32}$$

$$R_\phi = I_\phi \tag{5.33}$$

The equations 5.11 and 5.14 may be rewritten as,

$$Ex_2(x,y,0) = \frac{1}{(2\pi)^2} \int_{-\infty}^{\infty} \int_{-\infty}^{\infty} G_1(k_x,k_y)\bigg|_{z=0} e^{-jk_x x} e^{-jk_y y} dk_x dk_y \tag{5.34}$$

$$Hy_2(x,y,0) = \frac{1}{(2\pi)^2} \int_{-\infty}^{\infty} \int_{-\infty}^{\infty} G_2(k_x,k_y)\bigg|_{z=0} e^{-jk_x x} e^{-jk_y y} dk_x dk_y \tag{5.35}$$

where

$$G_1(k_x,k_y)\bigg|_{z=0} = jk_z[-I_\psi + R_\psi] \tag{5.36}$$

$$G_2(k_x,k_y)\bigg|_{z=0} = \frac{\hat{k}^2 - k_y^{\ 2}}{j\omega\mu_o}[I_\psi + R_\psi] - \frac{k_x k_y}{j\omega\mu_o}[I_\phi + R_\phi]\,. \tag{5.37}$$

The aperture admittance may now be calculated as

$$Y = \int_{x=-b/2}^{b/2} \int_{y=-a/2}^{a/2} \vec{E}^*(x,y,0) \times \vec{H}(x,y,0)\,dxdy$$

$$= \int_{x=-b/2}^{b/2} \int_{y=-a/2}^{a/2} Ex_2^*(x,y,0)\ Hy_2(x,y,0)\,dxdy\ . \tag{5.38}$$

Applying Parseval's theorem to equation 5.38 (the limits of integration may be extended to infinity because E(x,y,0) is zero outside the aperture) and substituting equations 5.36 and 5.37, we obtain

$$Y = \frac{1}{(2\pi)^2} \int_{-\infty}^{\infty} \int_{-\infty}^{\infty} G_1^*(k_x,k_y)\; G_2(k_x,k_y) dk_x dk_y \quad \dagger$$

$$= \frac{1}{(2\pi)^2} \int_{-\infty}^{\infty} \int_{-\infty}^{\infty} \{jk_z[-I_\psi + R_\psi]\}^* \; \frac{1}{j\omega\mu_o} [(\hat{k}^2 - k_y^2)(I_\psi + R_\psi)$$

$$- k_x k_y (I_\phi + R_\phi)]\} \; dk_x dk_y \; . \tag{5.39}$$

With equations 5.32 and 5.33, this may be written as,

$$Y = \frac{1}{(2\pi)^2} \int_{-\infty}^{\infty} \int_{-\infty}^{\infty} \frac{F^*}{j\omega\mu_o} \; [(\hat{k}^2 - k_y{}^2)(2I_\psi - \frac{jF}{k_z}) - k_x k_y \; 2I_\phi] dk_x dk_y \tag{5.40}$$

Normalising this admittance with respect to the characteristic admittance of the waveguide $Y_o = [1 - (f_c/f)]^{1/2} / \sqrt{\mu_o/\varepsilon_o}$, we obtain

$$Y_n = -j \; \frac{\lambda_g}{(2\pi)^3} \int_{-\infty}^{\infty} \int_{-\infty}^{\infty} F[(\hat{k}^2 - k_y{}^2)(2I_\psi - \frac{jF}{k_z}) - k_x k_y \; 2I_\phi] dk_x dk_y \; . \tag{5.41}$$

To facilitate numerical evaluation of the admittance, the following change of variable is made:

---

† For the Fourier transform pair,

$$g(x,y) = \frac{1}{(2\pi)^2} \int_{-\infty}^{\infty} \int_{-\infty}^{\infty} G(k_x,k_y) e^{-jk_x x} e^{-jk_y y} \; dk_x dk_y$$

$$G(k_x,k_y) = \int_{-\infty}^{\infty} \int_{-\infty}^{\infty} g(x,y) e^{jk_x x} e^{jk_y y} \; dxdy$$

Parseval's theorem is:

$$\int_{-\infty}^{\infty} \int_{-\infty}^{\infty} g_1(x,y) \; g_2^*(x,y) dxdy = \frac{1}{(2\pi)^2} \int_{-\infty}^{\infty} \int_{-\infty}^{\infty} G_1(k_x,k_y) G_2^*(k_x,k_y) dk_x dk_y$$

$$k_x = \beta \cos \alpha \tag{5.42}$$

$$k_y = \beta \sin \alpha \tag{5.43}$$

$$dk_x dk_y = d\beta \times (\beta d\alpha) \tag{5.44}$$

so that

$$Y_n = \int_{\beta=0}^{\infty} \int_{\alpha=0}^{2\pi} - \frac{j\lambda_g}{(2\pi)^3} F'[(\hat{k}^2 - \beta^2 \sin^2\alpha)(2I_\psi - j\frac{F'}{k_z\beta})$$

$$- 2\beta^2 \cos\alpha \sin\alpha I_\phi]d\beta d\alpha \tag{5.45}$$

when

$$F' = 4\pi \sqrt{\frac{2a}{b}} \frac{\sin(\beta \frac{b}{2} \cos\alpha) \cos(\beta \frac{a}{2} \sin\alpha)}{\cos\alpha[\pi^2 - (\beta a \sin \alpha)^2]} \tag{5.46}$$

and I_ψ, I_ϕ are redefined in equation 5.31 with $k_x = \beta \cos \alpha$ and $k_y = \beta \sin \alpha$.

Also, $$k_z = \sqrt{\hat{k}^2 - \beta^2} \tag{5.47}$$

$$k_{zo} = \sqrt{k_o^2 - \beta^2} \tag{5.48}$$

are chosen so that equations 5.9 and 5.10 are satisfied.

Choosing proper roots of k_z and k_{zo}, the admittance can be rewritten as,

$$Y_n = \int_{\alpha=0}^{2\pi} \{\int_{\beta=0}^{k_o} - \frac{j\lambda_g}{(2\pi)^3} F'[(\hat{k}^2 - \beta^2\sin^2\alpha)(2I_\psi - \frac{jF'}{k_z\beta})$$

$$- 2\beta^2 \cos\alpha \sin\alpha I_\phi]d\beta\} d\alpha + \int_{\alpha=0}^{2\pi} \{\int_{\beta=k_o}^{\alpha} - \frac{j\lambda_g}{(2\pi)^3} \times$$

$$F'[(\hat{k}^2 - \beta^2\sin^2\alpha)(2I_\psi - \frac{jF'}{k_z\beta}) - 2\beta^2 \cos\alpha \sin\alpha I_\phi]d\beta\} d\alpha$$

$$= \int_{\alpha=0}^{2\pi} I_1(\alpha)d\alpha + \int_{\alpha=0}^{2\pi} I_2(\alpha)d\alpha \tag{5.48a}$$

$$\left.\begin{aligned} k_z &= \sqrt{\hat{k}^2 - \beta^2} \\ k_{zo} &= \sqrt{k_o^2 - \beta^2} \end{aligned}\right\} \text{ in the integral } I_1(\alpha)$$

where

and

$$\left.\begin{aligned} k_z &= \sqrt{\hat{k}^2 - \beta^2} \\ k_{zo} &= -j\sqrt{\beta^2 - k_o^2} \end{aligned}\right\} \text{ in the integral } I_2(\alpha).$$

The reflection coefficient at plane $z = 0$ is given by,

$$R = \frac{1 - Y_n}{1 + Y_n} \tag{5.48b}$$

The derivation up to this point is similar to that of Compton[47] and Crosswell et.al.[48].

5.3 The Admittance of a Rectangular Waveguide System Radiating into a Semiconducting Slab Followed by a Conducting Plate

Heaton and Pal[16], in one of their recent publications, derived an expression for the reflection coefficient of a semiconductor slab placed across the open end of a rectangular waveguide. Their theory, which is not essentially different from that of Lindmayer and Kutsko[7], is based on an unbounded wave propagating in an axial direction. They assume that the z-directed propagation constant in the semiconductor region is of the form $\gamma_z = jk_z = j\omega\sqrt{\mu\hat{\varepsilon}}$. This is not fully justified, and in particular for semiconductor samples having low $\hat{\varepsilon}_r$, when the wave may propagate in the transverse directions as well.

A more general expression for the reflection coefficient of a semiconductor slab with complex permittivity held against the waveguide flange and followed by a short circuit, is derived in this section. The solution is based on the assumption of a TE_{01} field incident at the aperture and is obtained by extending the results derived in the last section. Numerical computations are presented for Ge slab case for varying values of resistivity and thickness. A comparison shows that the results given by the cited authors[16] are justified for low resistivity samples and are approximate for high resistivity ones (Fig. 5.5).

The geometry of the problem is described in Figure 5.3. A rectangular waveguide excited by the dominant TE_{01} mode opening onto an infinite metal flange which is covered by a semiconductor slab of thickness ℓ and complex relative permittivity $\hat{\varepsilon}_r$. It is assumed that no higher order modes are excited at the aperture and the fields everywhere vary in time as $e^{j\omega t}$. For the structure of Figure 5.3, the electric fields in equations 5.11 and 5.12 disappear at the semiconductor-metal boundary ($z = \ell$), which give the following equations:

$$I_\psi = R_\psi e^{j2k_z \ell} \tag{5.49}$$

$$I_\phi = R_\phi e^{j2k_z \ell} \tag{5.50}$$

Equations 5.50 and 5.33 give,

$$I_\phi = R_\phi = 0 \tag{5.51}$$

Equations 5.49 and 5.32 give,

$$I_\psi = \frac{jF}{k_z} \frac{1}{[1 - e^{j2k_z \ell}]} \tag{5.52}$$

With equations 5.51 and 5.52 in 5.39,

$$Y = \frac{1}{(2\pi)^2} \int_{-\infty}^{\infty} \int_{-\infty}^{\infty} F^* \frac{\hat{k}^2 - k_y^{\,2}}{j\omega\mu_o} I_\psi (1 + e^{-j2k_z \ell}) dk_x dk_y$$

$$= \frac{1}{(2\pi)^2} \int_{-\infty}^{\infty} \int_{-\infty}^{\infty} \frac{F^2 (\hat{k}^2 - k_y^{\,2})}{\omega\mu_o \, k_z \tanh(jk_z \ell)} dk_x dk_y \tag{5.53}$$

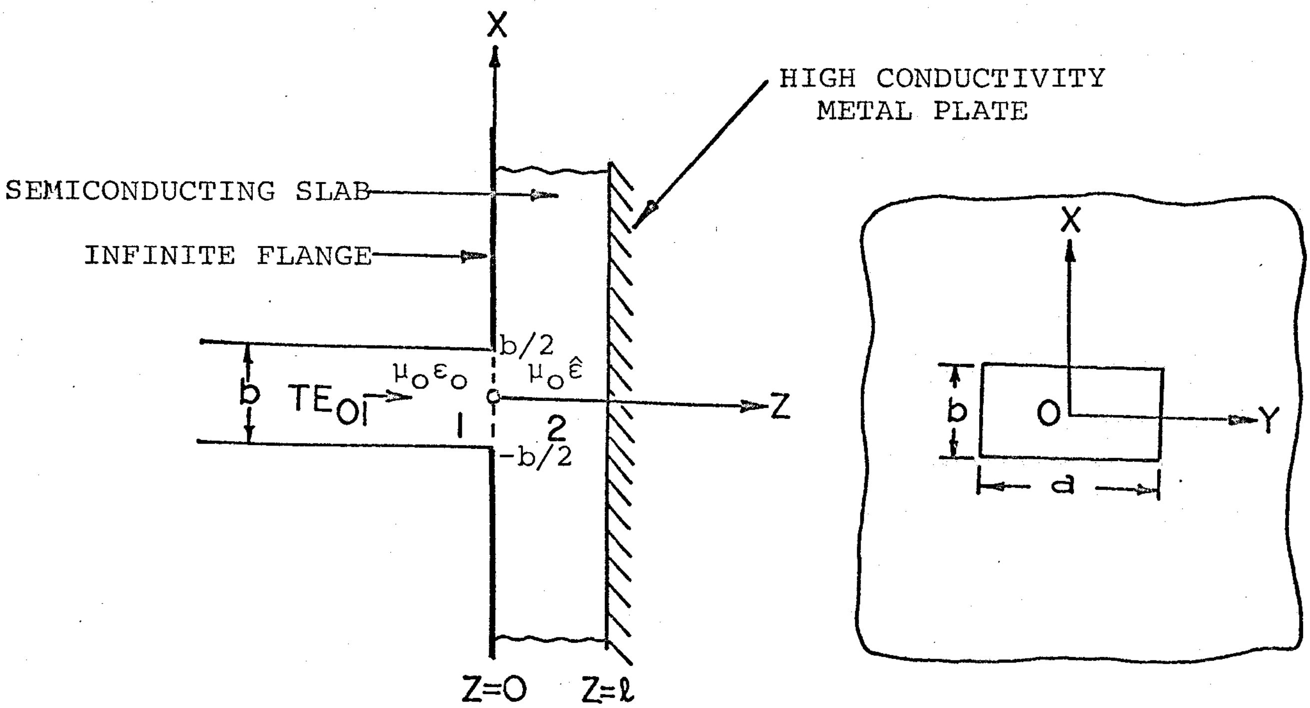

FIGURE 5.3: A Rectangular Waveguide in a Ground Plane Covered by a Semiconductor-Metal Sandwich.

which becomes after normalisation,

$$Y_n = \frac{\lambda_g}{(2\pi)^3} \int_{-\infty}^{\infty} \int_{-\infty}^{\infty} \frac{F^2 (\hat{k}^2 - k_y^2)}{k_z \tanh(jk_z \ell)} \, dk_x dk_y \tag{5.54}$$

In order to facilitate the numerical evaluation of the admittance, the following change of variables is made,

$$k_x = \beta \cos \alpha$$

$$k_y = \beta \sin \alpha \quad \text{, so that}$$

$$Y_n = \int_{\beta=0}^{\infty} \left[\int_{\alpha=0}^{2\pi} \frac{\lambda_g}{(2\pi)^3} \frac{F'^2 (\hat{k}^2 - \beta^2 \sin^2 \alpha)}{\beta k_z \tanh(jk_z \ell)} \, d\alpha \right] d\beta \tag{5.55}$$

where

$$F' = 4\pi \sqrt{\frac{2a}{b}} \; \frac{\sin(\beta \frac{b}{2} \cos \alpha) \cos(\beta \frac{a}{2} \sin \alpha)}{\cos \alpha [\pi^2 - \beta^2 a^2 \sin^2 \alpha]} \tag{5.56}$$

and

$$k_z = \sqrt{\hat{k}^2 - \beta^2} \, . \tag{5.57}$$

The reflection coefficient at the plane z = 0 is given by,

$$R = \frac{1 - Y_n}{1 + Y_n} \tag{5.58}$$

5.4 The Admittance of a Rectangular Waveguide System Radiating Into a Plasma Layer

The admittance of a waveguide system radiating into a homogeneous medium has become a matter of some concern to microwave antenna engineers in recent years[49-53]. The presence of a medium at the aperture of a waveguide determines the input admittance of the waveguide. Knowledge of the variation of the input admittance and the changes in radiated signal level with electrical constants of the medium, is important for the design of microwave antennas, such as the rectangular or parallel-plate aperture types, in a ground plane. Besides the change in radiated signal level, the reflected wave which results from antenna mismatch, may adversely affect the operation of the transmitter. The re-entry of high speed space vehicles into earth's atmosphere, which consists of plasma layers, creates problems in maintaining radio communications between the space ships and the ground[49]. The measurement of the admittance of a waveguide may also be employed to infer plasma properties. The dielectric constant of a plasma layer can be expressed as $\varepsilon_r = 1 - \frac{ne^2}{m\varepsilon_o\omega^2}$ and ranges from zero to unity. For zero dielectric constant, $\omega_p = \sqrt{\frac{ne^2}{m\varepsilon_o}}$, which is known as the plasma frequency.

The solutions to the admittance of a waveguide under a plasma slab require extensive computer programmes for the numerical calculations due to the two dimensional nature of the integral and its infinite limit. The solution to the same problem under a lossy medium by Compton[47] has some computational advantages over the previous solutions, since it contains only one infinite integral, instead of two. In this Section, the original formulation by Compton for the rectangular waveguide under a lossy slab is modified for the case of a lossless plasma layer. Computations utilizing the new formulation are presented for varying values of thickness and dielectric constant of the plasma layer. The results obtained are found to agree with those given by the other authors[49-51].

The geometry of the problem is given in Figure 5.1 except that the slab is replaced by a lossless plasma layer ($\varepsilon_r < 1$). The admittance is similar to equation 5.45 in which k_z and k_{zo} assume different roots with increasing β. Choosing proper roots of k_z and k_{zo}, the admittance may be written as,

$$Y_n = \int_{\alpha=0}^{2\pi}\{\int_{\beta=0}^{k} - \frac{j\lambda_g}{(2\pi)^3} F' \; [(k^2 - \beta^2 \sin^2 \alpha)(2I_\psi - \frac{jF'}{k_z\beta})-2\beta^2\cos \alpha\sin \alpha I_\phi]d\beta\}d\alpha$$

$$+ \int_{\alpha=0}^{2\pi} \{\int_{k}^{k_o} - \frac{j\lambda_g}{(2\pi)^3} F'[(k^2 - \beta^2 \sin^2 \alpha)(2I_\psi - \frac{jF'}{k_z\beta})-2\beta^2\cos \alpha\sin \alpha I_\phi]d\beta\}d\alpha$$

$$+ \int_{\alpha=0}^{2\pi} \{ \int_{k_o}^{\infty} - \frac{j\lambda_g}{(2\pi)^3} F'[(k^2 - \beta^2 \sin^2\alpha)(2I_\psi - \frac{jF'}{k_z\beta})-2\beta^2\cos \alpha\sin \alpha I_\phi]d\beta\}d\alpha$$

$$= \int_{\alpha=0}^{2\pi} I_1(\alpha)d\alpha + \int_{\alpha=0}^{2\pi} I_2(\alpha)d\alpha + \int_{\alpha=0}^{2\pi} I_3(\alpha)d\alpha \tag{5.59}$$

where

$$\left.\begin{aligned} k_z &= \sqrt{k^2 - \beta^2} \\ k_{zo} &= \sqrt{k_o^2 - \beta^2} \end{aligned}\right\} \tag{5.60}$$

in the first integral $I_1(\alpha)$,

$$\left.\begin{aligned} k_z &= -j\sqrt{\beta^2 - k^2} \\ k_{zo} &= \sqrt{k_o^2 - \beta^2} \end{aligned}\right\} \tag{5.61}$$

in the second integral $I_2(\alpha)$ and

$$\left.\begin{aligned} k_z &= -j\sqrt{\beta^2 - k^2} \\ k_{zo} &= -j\sqrt{\beta^2 - k_o^2} \end{aligned}\right\} \tag{5.62}$$

in the third integral $I_3(\alpha)$.

To facilitate numerical calculations, the integrals $I_1(\alpha)$, $I_2(\alpha)$, and $I_3(\alpha)$ are simplified with the change of variables $\omega = \frac{\beta}{k}$, $\omega = \frac{\beta}{k_o}$, $\omega^2 = \beta^2 - k_o{}^2$, respectively.

$$I_1(\alpha) = \int_0^1 - \frac{j\lambda_g}{(2\pi)^3} F'k^2[(1 - \omega^2\sin^2\alpha)(2I_\psi - \frac{jF'}{k_z\omega k}) - 2\omega^2\cos\alpha\sin\alpha I_\phi]kd\omega \tag{5.63}$$

where
$$k_z = k\sqrt{1 - \omega^2} \tag{5.64}$$

$$k_{zo} = k_o\sqrt{1 - \omega^2\varepsilon_r} \tag{5.65}$$

and F', I_ψ and I_ϕ are redefined with $\beta = \omega k$ in equations 5.46, 5.29, and 5.30 respectively.

$$I_2(\alpha) = \int_{\sqrt{\varepsilon_r}}^1 - \frac{j\lambda_g}{(2\pi)^3} F'k_o{}^2[(\varepsilon_r - \omega^2\sin^2\alpha)(2I_\psi - \frac{jF'}{k_z\omega k_o})-2\omega^2\cos\alpha\sin\alpha I_\phi]k_o d\omega \tag{5.66}$$

where
$$k_z = -jk_o\sqrt{\omega^2 - \varepsilon_r} \tag{5.67}$$

$$k_{zo} = k_o\sqrt{1 - \omega^2} \tag{5.68}$$

and F', I_ψ and I_ϕ are redefined with $\beta = \omega k_o$ in equations 5.46, 5.29, and 5.30 respectively.

$$I_3(\alpha) = \int_0^\infty - \frac{j\lambda_g}{(2\pi)^3} F'[\{k^2 - (\omega^2 + k_o^2)\sin^2\alpha\}\{2I_\psi - \frac{jF'}{k_z(\omega^2 + k_o{}^2)^{1/2}}\}$$

$$- 2(\omega^2 + k_o{}^2)\cos\alpha\sin\alpha I_\phi] \frac{\omega d\omega}{[\omega^2 + k_o^2]^{1/2}} \tag{5.69}$$

where
$$k_z = -j\sqrt{\omega^2 + k_o{}^2 - k^2} \tag{5.70}$$

$$k_{zo} = -j\omega \tag{5.71}$$

and F', I_ψ and I_ϕ are redefined with $\beta = [\omega^2 + k_o^2]^{1/2}$ in equations 5.46, 5.29 and 5.30 respectively.

5.4.1 The Admittance of a Waveguide System Radiating Into a Semi-Infinite Medium

Equation 5.39 can be simplified to the admittance of a semi-infinite medium as obtained in Section 4.2. When the length of the slab in Figure 5.1 becomes infinite, R_ψ and R_ϕ are zero. Thus equation 5.39 becomes after normalisation,

$$Y_n = \frac{\lambda_g}{(2\pi)^3} \int_{-\infty}^{\infty} \int_{-\infty}^{\infty} -k_z(\hat{k}^2 - k_y^2) I_\psi^2 \, dk_x dk_y \, . \tag{5.72}$$

Using the relation $I_\psi = -\dfrac{F}{jk_z}$, this becomes

$$Y_n = \frac{\lambda_g}{(2\pi)^3} \int_{-\infty}^{\infty} \int_{-\infty}^{\infty} \frac{F^2(\hat{k}^2 - k_y^2)}{k_z} \, dk_x dk_y$$

$$= \int_{\alpha=0}^{2\pi} \int_{\beta=0}^{\infty} \frac{\lambda_g}{(2\pi)^3} \frac{F'^2(\hat{k}^2 - \beta^2 \sin^2\alpha)}{\beta\sqrt{\hat{k}^2 - \beta^2}} \, d\alpha d\beta \tag{5.73}$$

where the following change of variables has been made:

$$k_x = \beta \cos \alpha$$

$$k_y = \beta \sin \alpha \, .$$

It is noted that equation 5.73 is equivalent to equation 4.21 . For a lossless plasma medium $\hat{k} = k$ so that

$$Y_n = \int_{\alpha=0}^{2\pi} \left[\int_{\beta=0}^{k} \frac{\lambda_g}{(2\pi)^3} \frac{F'^2 (k^2 - \beta^2 \sin^2 \alpha)}{\beta \sqrt{k^2 - \beta^2}} \, d\beta \right] d\alpha$$

$$+ j\int_{\alpha=0}^{2\pi} \left[\int_{k}^{k_o} \frac{\lambda_g}{(2\pi)^3} \frac{F'^2 (k^2 - \beta^2 \sin^2 \alpha)}{\beta \sqrt{\beta^2 - k^2}} \, d\beta \right] d\alpha$$

$$+ j\int_{\alpha=0}^{2\pi} \left[\int_{k_o}^{\infty} \frac{\lambda_g}{(2\pi)^3} \frac{F'^2 (k^2 - \beta^2 \sin^2 \alpha)}{\beta \sqrt{\beta^2 - k^2}} \, d\beta \right] d\alpha$$

$$= \int_{\alpha=0}^{2\pi} I_1(\alpha) d\alpha + j \int_{\alpha=0}^{2\pi} I_2(\alpha) d\alpha + j \int_{\alpha=0}^{2\pi} I_3(\alpha) d\alpha \,. \tag{5.74}$$

The integrals I_1, I_2, I_3 are transformed with the following change of variables,

$$\omega = \frac{\beta}{k} \quad , \quad \omega = \frac{\beta}{k} \quad , \quad \omega^2 = \beta^2 - k_o^2 \qquad \text{respectively.}$$

Thus,

$$I_1(\alpha) = \int_0^1 \frac{\lambda_g}{(2\pi)^3} \frac{F'^2 k(1 - \omega^2 \sin^2 \alpha)}{\omega\sqrt{1 - \omega^2}} \, d\omega \tag{5.75}$$

where F' is redefined with $\beta = \omega k$ in equation 5.46.

$$I_2(\alpha) = \int_1^{\frac{1}{\sqrt{\varepsilon_r}}} \frac{\lambda_g}{(2\pi)^3} \frac{F'^2 k(1 - \omega^2 \sin^2 \alpha)}{\omega\sqrt{\omega^2 - 1}} \, d\omega \tag{5.76}$$

where F' is same as in equation 5.75.

$$I_3(\alpha) = \int_0^{\infty} \frac{\lambda_g}{(2\pi)^3} \frac{F'^2 [k^2 - (\omega^2 + k_o^2)\sin^2 \alpha]}{[\omega^2 + k_o^2][\omega^2 + k_o^2 - k^2]^{\frac{1}{2}}} \, \omega d\omega \tag{5.77}$$

where F' is redefined with $\beta = [\omega^2 + k_o^2]^{1/2}$ in equation 5.46.

McMASTER UNIVERSITY LIBRARY

5.5 Numerical Results and Their Interpretations

(a) The approximate equation 3.17 has been evaluated numerically on a CDC 6400 Digital Computer to determine roughly the effect of the slab thickness on the reflection coefficients. The exact solution is represented by equation 5.48b, which requires extensive computer programming for evaluation. Figure 5.4 exhibits such effects in Ge for the case $a = 0.712$ cm, $b = 0.356$ cm, and $f = 34.5$ GHz.

(b) Equation 5.55 has been evaluated numerically on a CDC 6400 Digital Computer by Simpson's rule. The integration on α is carried out first while that on β is carried out over a finite range. The upper limit of β is chosen in such a way that the range of integration includes all the values of β for which the integrand has a significant value. To reduce the computation time, the integration on α from 0 to 2π may be computed by means of Gauss' quadrature formula[54]. The range of integration can be taken as 0 to $\pi/2$ for accuracy and the integrand is multiplied by four to obtain the final value.

Numerical calculations were obtained for the following two cases:

(a) $a = 2.286$ cm , $b = 1.016$ cm , $f = 9.35$ GHz

(b) $a = 0.712$ cm , $b = 0.356$ cm , $f = 34.5$ GHz

The results of this calculation are shown in Figures 5.5 through 5.8. Figures 5.5 and 5.6 show the VSWR and the reflection coefficient as functions of resistivity and thickness of semiconductor slabs for the case $a = 2.286$ cm, $b = 1.016$ cm and $f = 9.35$ GHz. Figures 5.7 and 5.8 show the VSWR and reflection coefficient as functions of resistivity and thickness, for the case $a = 0.712$ cm, $b = 0.356$ and $f = 34.5$ GHz.

Finally, as a check on numerical results, the integral Y_n may be evaluated approximately for the case where $\hat{k}$ has a large (complex) value. When $\hat{k}$ is large in equation 5.54,

$$k_z = \sqrt{\hat{k}^2 - k_x^{\,2} - k_y^{\,2}} \simeq \hat{k} \quad \text{and} \quad \hat{k}^2 - k_y^{\,2} \simeq \hat{k}^2 .$$

With these simplifications, equation 5.54 becomes

$$Y_n = \left[\frac{\hat{\varepsilon}_r}{1 - (f_c/f)^2}\right]^{1/2} \frac{1}{\tanh(\gamma_2 \ell)} \quad \frac{1}{(2\pi)^2} \int_{-\infty}^{\infty} \int_{-\infty}^{\infty} F^2 dk_x dk_y \tag{5.78}$$

where

$$F = 4\pi\sqrt{\frac{2a}{b}} \quad \frac{\sin(k_x\, b/2)\ \cos(k_y\, a/2)}{k_x[\pi^2 - (k_y\, a)^2]} \tag{5.79}$$

$$\gamma_2 = j\hat{k} \tag{5.80}$$

Also,

$$\frac{1}{(2\pi)^2} \int_{-\infty}^{\infty} \int_{-\infty}^{\infty} F^2 dk_x dk_y$$

$$= \frac{8a}{b} \int_{-\infty}^{\infty} \frac{\sin^2(k_x\, b/2)}{k_x^{\,2}}\, dk_x \int_{-\infty}^{\infty} \frac{\cos^2(k_y\, a/2)}{[\pi^2 - (k_y\, a)^2]^2}\, dk_y \tag{5.81}$$

With the change of variable $k_x\, b/2 = x$, the first integral is reduced to,

$$2 \int_0^{\infty} \frac{\sin^2 x\, dx}{x^2} \frac{b}{2} = b\,\frac{\pi}{2} \tag{5.82}$$

and with $k_y\, a/2 = \omega$, the second integral is reduced to †

$$\int_{-\infty}^{\infty} \frac{\cos^2 \omega}{[\pi^2 - (2\omega)^2]^2} \frac{2}{a}\, d\omega = \frac{1}{4a} \int_0^{\infty} \frac{\cos^2 \omega}{[(\pi/2)^2 - \omega^2]^2}\, d\omega = \frac{1}{4a}\,\frac{1}{\pi} \tag{5.83}$$

† Problem 4-39, Reference 44.

$$\mathrm{Re} \int_0^{\infty} \frac{1 + e^{j2\omega}}{[(\pi/2)^2 - \omega^2]^2}\, d\omega = \int_0^{\infty} \frac{2\cos^2 \omega}{[(\pi/2)^2 - \omega^2]^2}\, d\omega = \frac{2}{\pi}$$

With these simplifications, equation 5.81 becomes unity so that equation 5.78 may be written as

$$Y_n = \left[\frac{\hat{\varepsilon}_r}{1 - (f_c/f)^2}\right]^{1/2} \frac{1}{\tanh(\gamma_2 \ell)} \tag{5.84}$$

The reflection coefficient at the z = 0 plane is therefore given by

$$R = \frac{1 - \left[\dfrac{\hat{\varepsilon}_r}{1 - (f_c/f)^2}\right]^{1/2} \coth \gamma_2 \ell}{1 + \left[\dfrac{\hat{\varepsilon}_r}{1 - (f_c/f)^2}\right]^{1/2} \coth \gamma_2 \ell}, \tag{5.85}$$

a simplified result that agrees with the approximate equation 3.11 as expected.

(c) Equation 5.59 has also been evaluated numerically for a rectangular waveguide system with a = 2.286, b = 1.016 and f = 10.524 GHz, for several values of ε_r and ℓ. The computation of the integrals I_1, I_2, I_3 was done first with the aid of the Gaussian Quadrature Formula, with α held constant at a number of equidistant points in the range $0 - 2\pi$, at an interval of 0.105. These values, which form the integrand for the α-integral, are then summed by Simpson's rule to evaluate the α-integral.

The results of this calculation are shown in Figures 5.9 through 5.13. Figures 5.9, 5.10 and 5.11 show the normalised conductance and susceptance as functions of dielectric constant and layer thickness. Figures 5.12 and 5.13 show the magnitude and phase of the reflection coefficient as functions of dielectric constant and layer thickness. The results are found to agree with those given by other authors[49-51].

In future work, the waveguide admittance of the structure of Figure 4.2 under a plasma layer can be obtained. This structure will have some computational advantages over the previous solutions as it provides only one integral instead of two.

5.6 Experimental Confirmation

The principal objective of the experimental programme was to obtain data on the behaviour of the reflection coefficients of finite germanium slabs in order to confirm the theoretical predictions of Section 5.3.

The samples of germanium with the dimensions 3 x 2.5 x 0.1 cm and 3 x 2.5 x 0.2 cm were cut from a large block of 10 and 50 ohm cm n-type germanium crystals by means of a 20-mil diamond-head wheel cutter. Reflecting surfaces were polished with a fine emery paper.

Measurements of the reflection coefficients were made on these samples at 9.35 GHz. The slabs were backed by a high conductivity short-circuit plate and the measuring procedure was the same as described in Section 4.6. The photograph of the sample holder is shown in Figure 2.11.

Measurements were also made of the d.c. resistivity of each sample of semiconductor with a high quality 4-probe tester.

5.7 Results and Discussion

The results of the reflection coefficient measurements on samples of n-type germanium are given in Figures 5.5 and 5.6. The measured values of the reflection coefficient and VSWR were found to agree with the calculated values. The VSWR values calculated from the theory of Heaton and Pal[16] are found to disagree with the measured values as shown in Figure 5.5. A comparison of the microwave measurements with d.c. measurements of the resistivity, which is shown in Table 5.1, indicates that the microwave measurements agree reasonably with d.c. measurements. Since this method of measurement involves the placement of a slab of semiconductor at the open end of a waveguide, it has been termed the "open-end-waveguide measuring technique".

Table 5.1

A Comparison of the Microwave and D.C. Measurements of the Resistivity of n-type Ge Samples

Nominal Resistivity Ge (ohm cm)	Slab Thickness (cm)	Microwave Measurements (ohm cm)	D.C. Measurements (ohm cm)
10	0.1	11.4	11.0
10	0.2	11.7	11.6
50	0.1	35.0	45.6
50	0.2	40.0	46.0

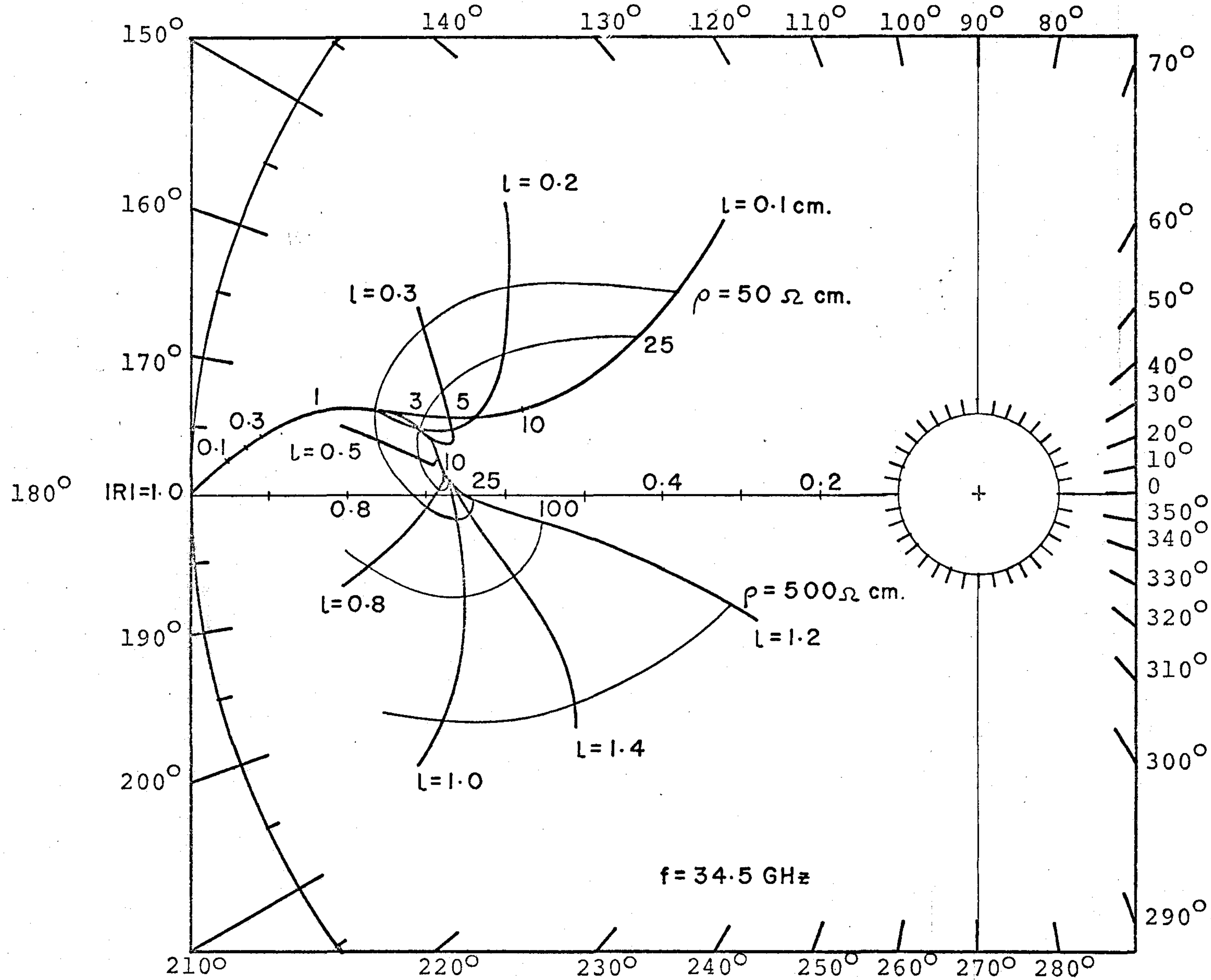

FIGURE 5.4: Theoretically predicted Effects of the Slab Thickness on the Reflection Coefficients of Germanium in the Waveguide Structure of Figure 1.3.

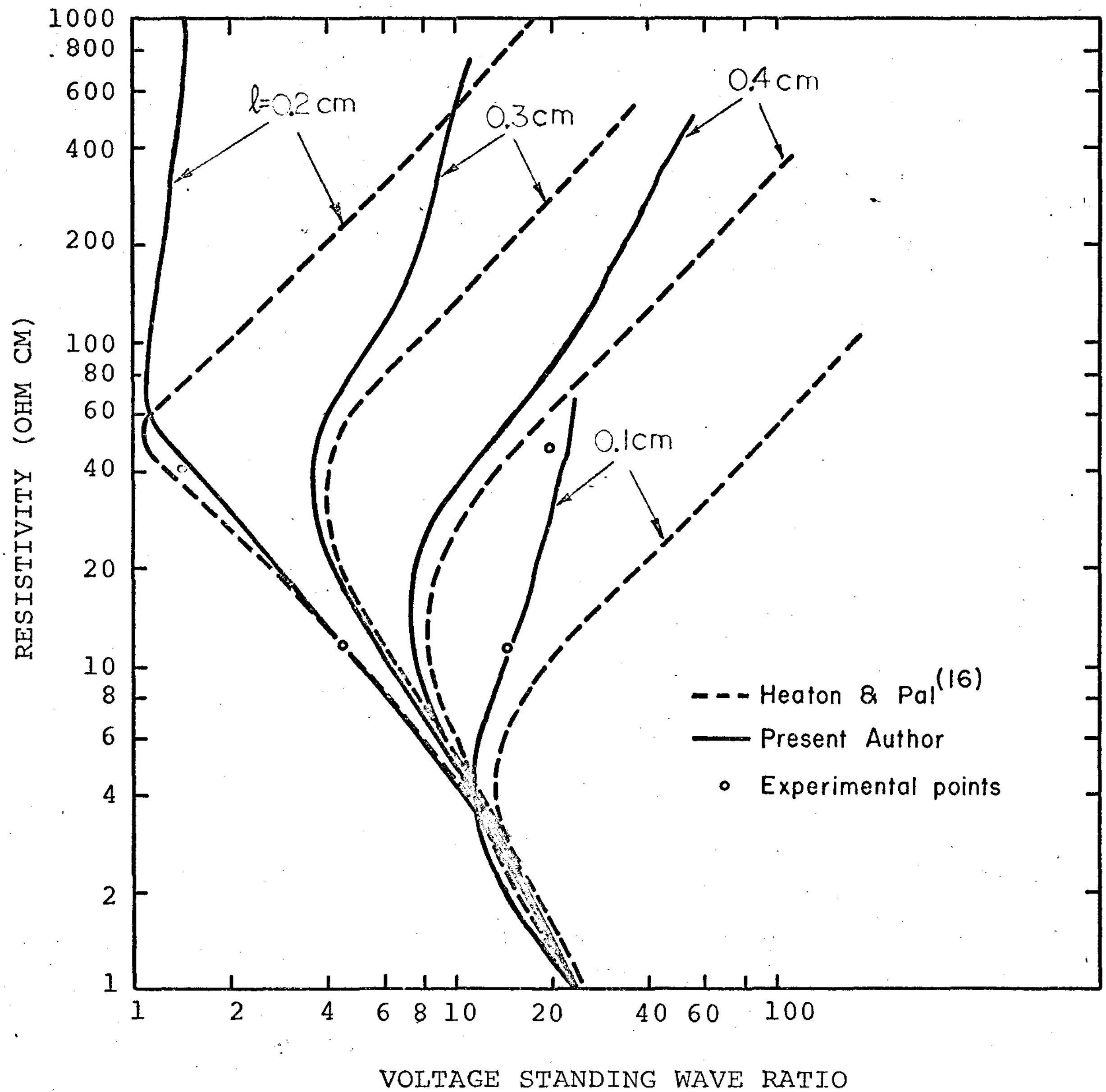

FIGURE 5.5: Resistivity versus Voltage Standing Wave Ratio for Various Values of Slab Thickness of Germanium in the Waveguide Structure of Figure 5.3 at 9.35 GHz.

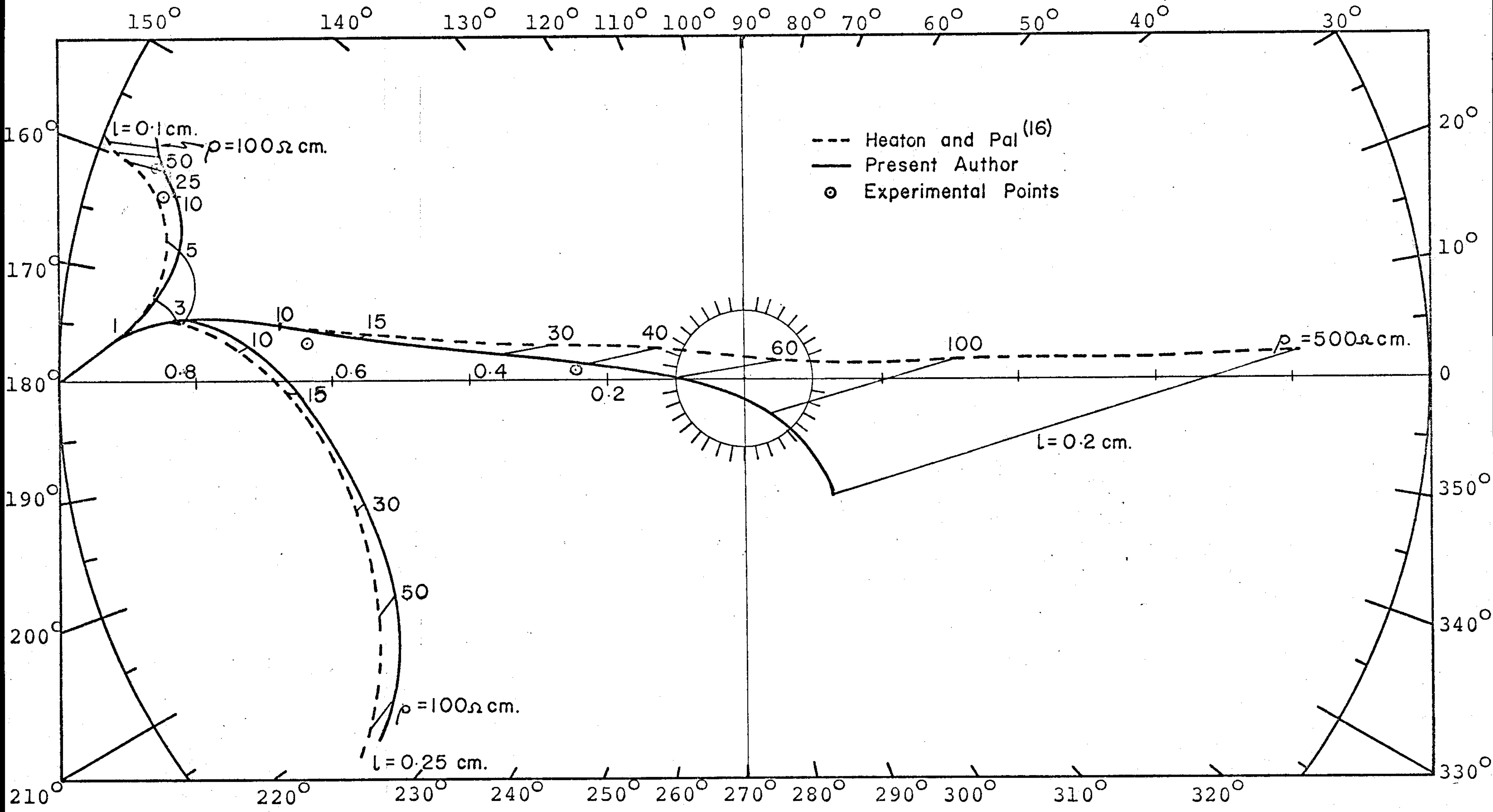

FIGURE 5.6: Polar Plots of the Reflection Coefficients as Functions of Resistivity and Slab Thickness of Germanium in the Waveguide Structure of Figure 5.3 for 9.35 GHz.

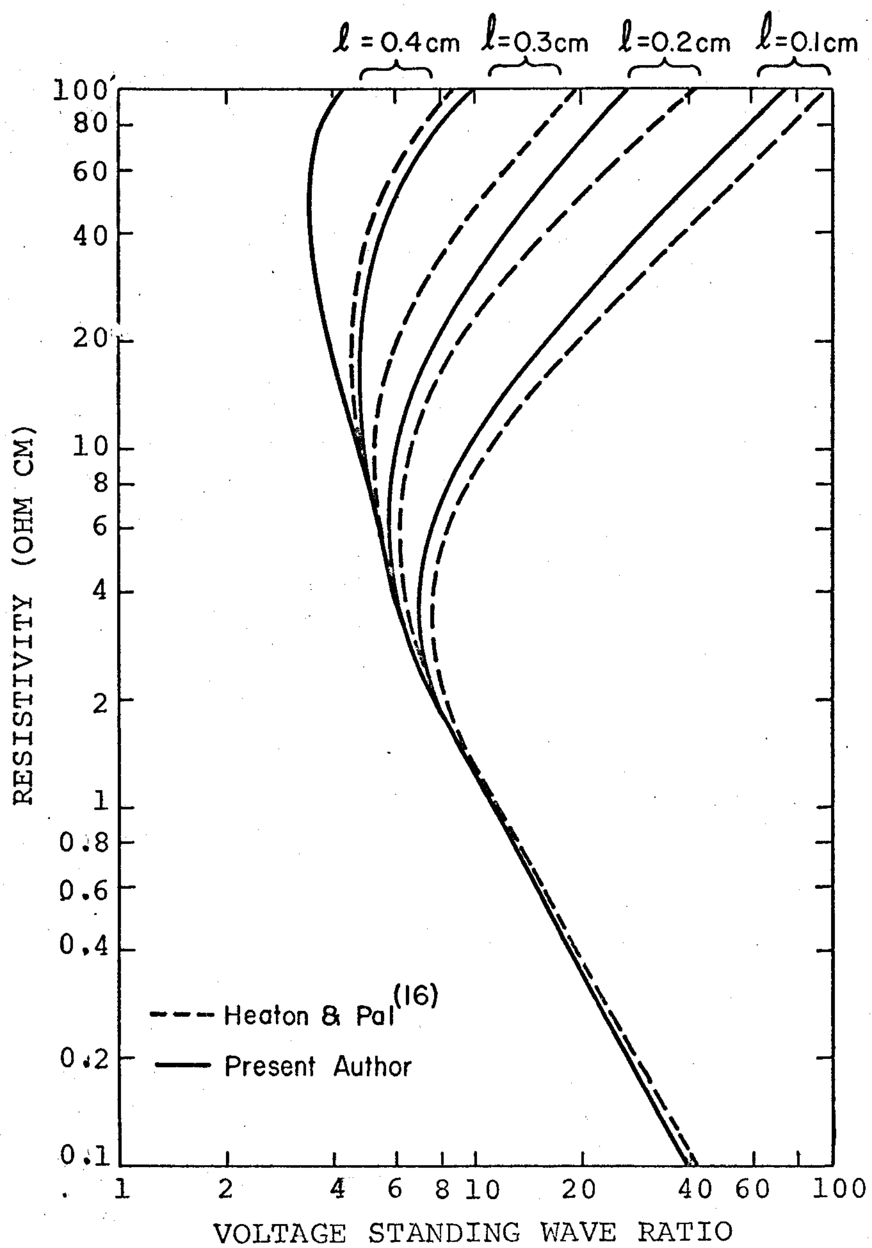

FIGURE 5.7: Resistivity versus Voltage Standing Wave Ratio for Germanium in the Waveguide System of Figure 5.3 at 34.5 GHz.

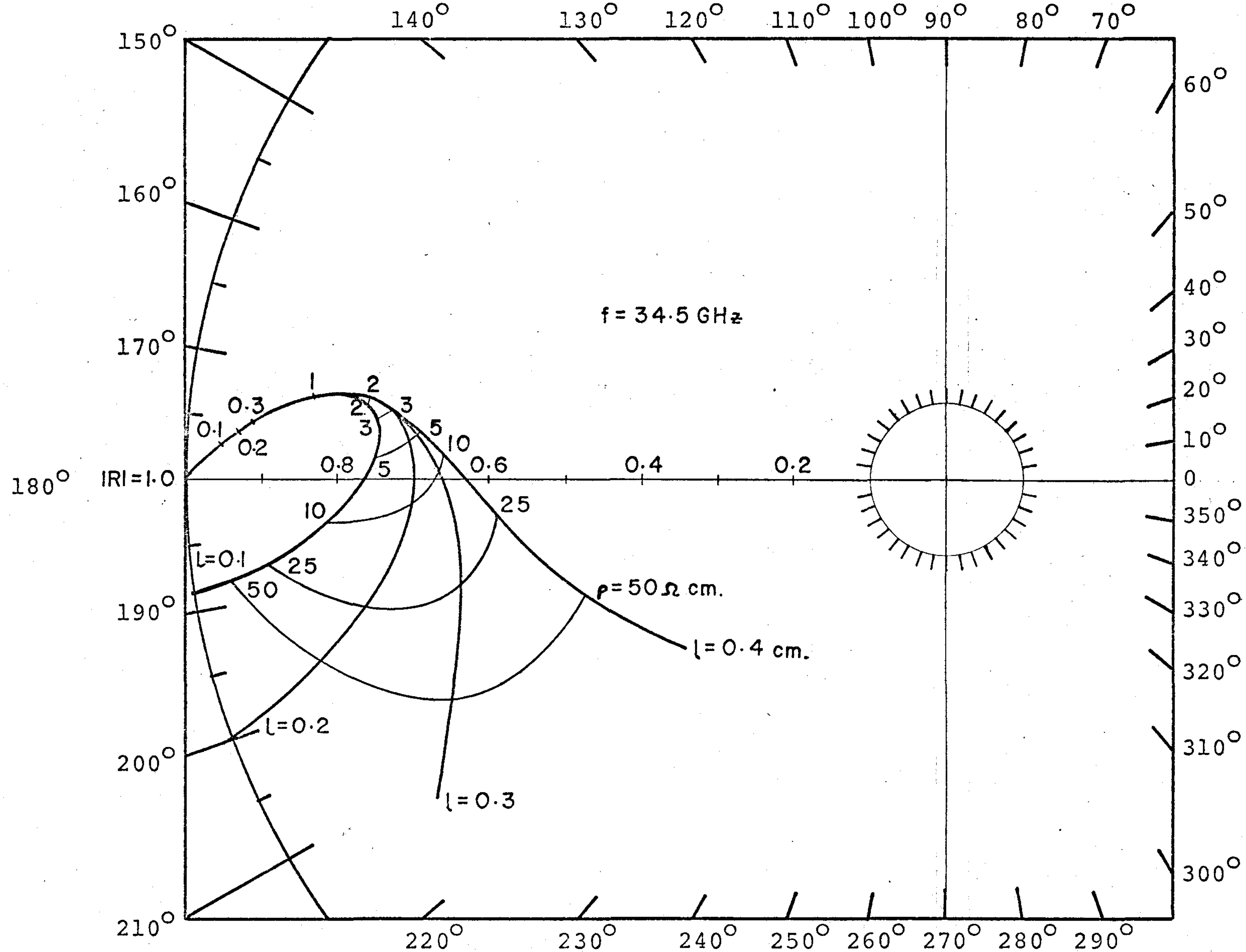

FIGURE 5.8: Polar Plots of the Computed Reflection Coefficients as Functions of Resistivity and Slab Thickness of Germanium in the Waveguide System of Figure 5.3 for 34.5 GHz.

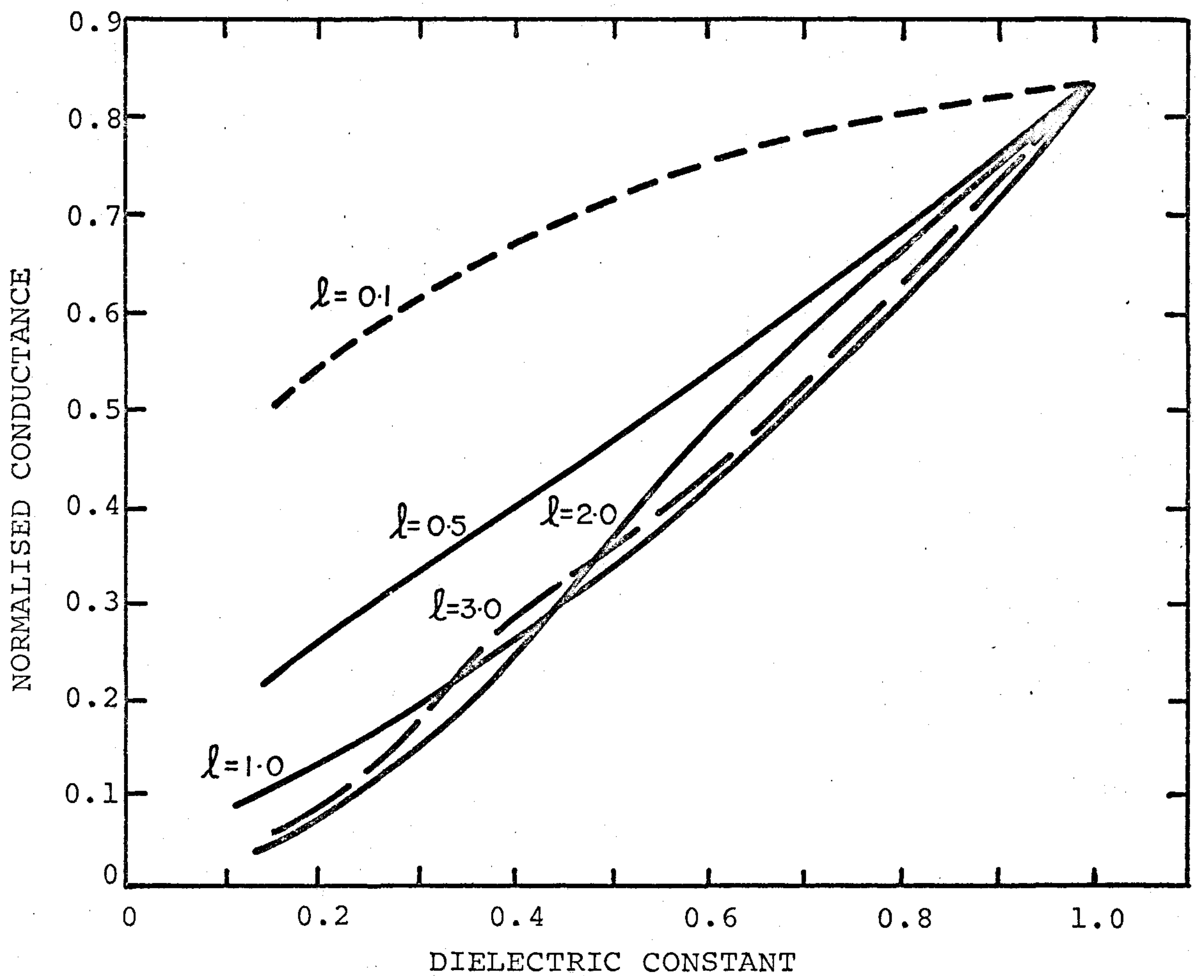

FIGURE 5.9: Calculated Values of the Conductance of a Rectangular Waveguide System Radiating into a Plasma Layer as a Function of Dielectric Constant at 10.524 GHz for Various Values of Layer Thickness shown.

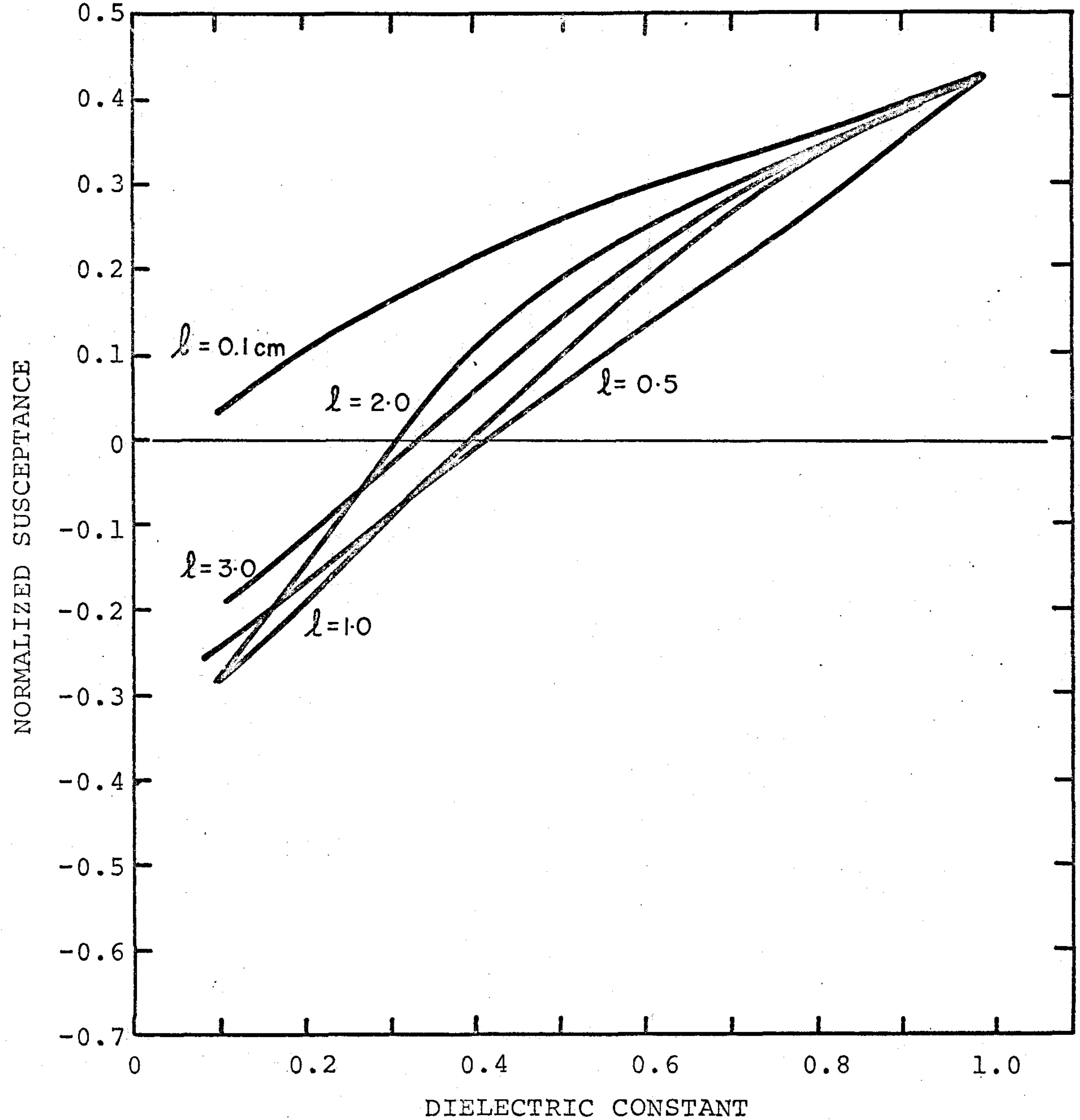

FIGURE 5.10: Calculated Values of the Susceptance of a Rectangular Waveguide System Radiating into a Plasma Layer as a Function of Dielectric Constant for Various Values of Layer Thickness at 10.524 GHz.

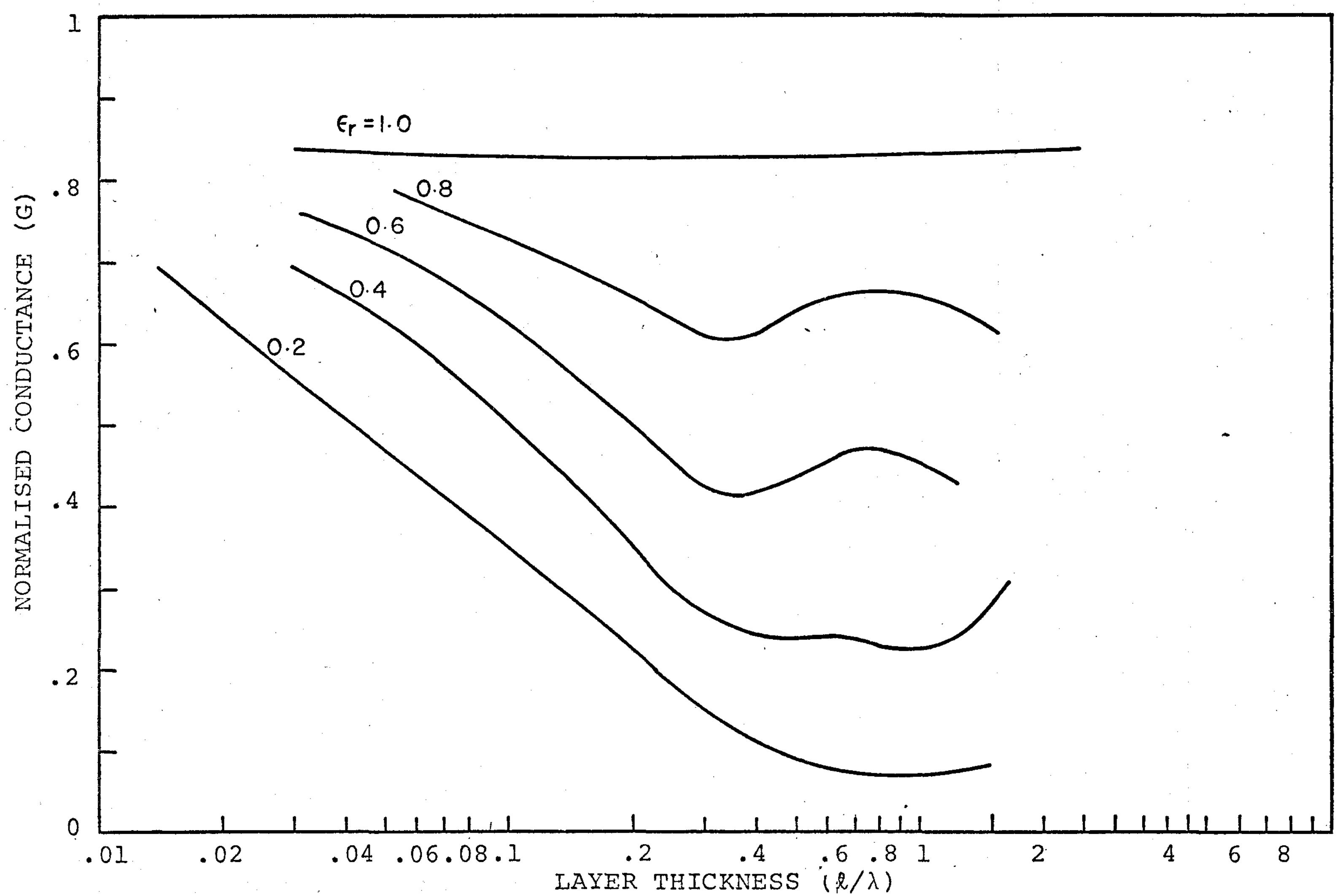

FIGURE 5.11: Calculated Values of the Conductance of a Rectangular Waveguide System Radiating in a Plasma Layer as a Function of Layer Thickness at 10.524 GHz.

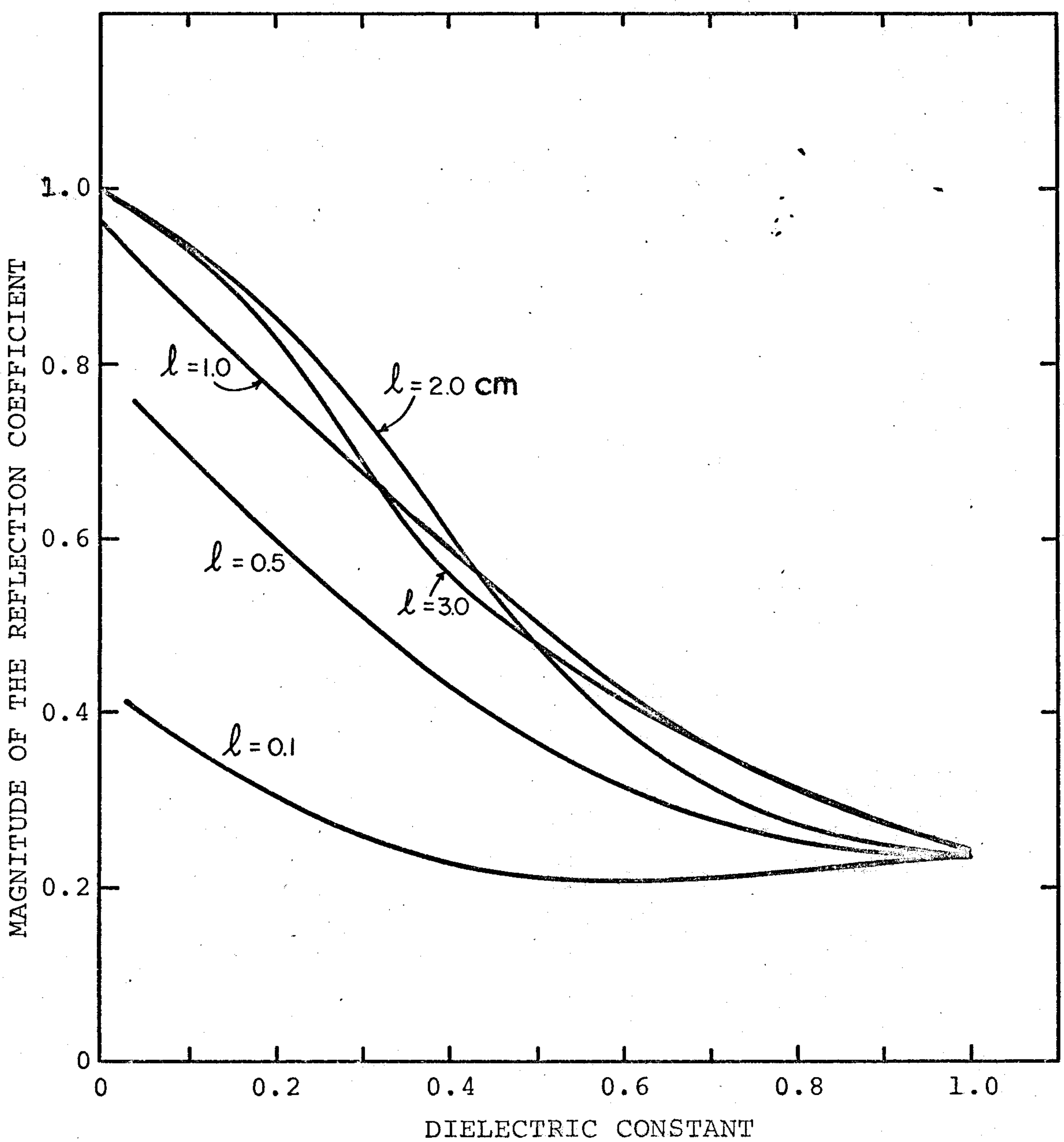

FIGURE 5.12: Computed Values of the Magnitude of the Reflection Coefficient of a Rectangular Waveguide System Radiating into a Plasma Layer as a Function of Dielectric Constant for Various Values of Layer Thickness at 10.524 GHz.

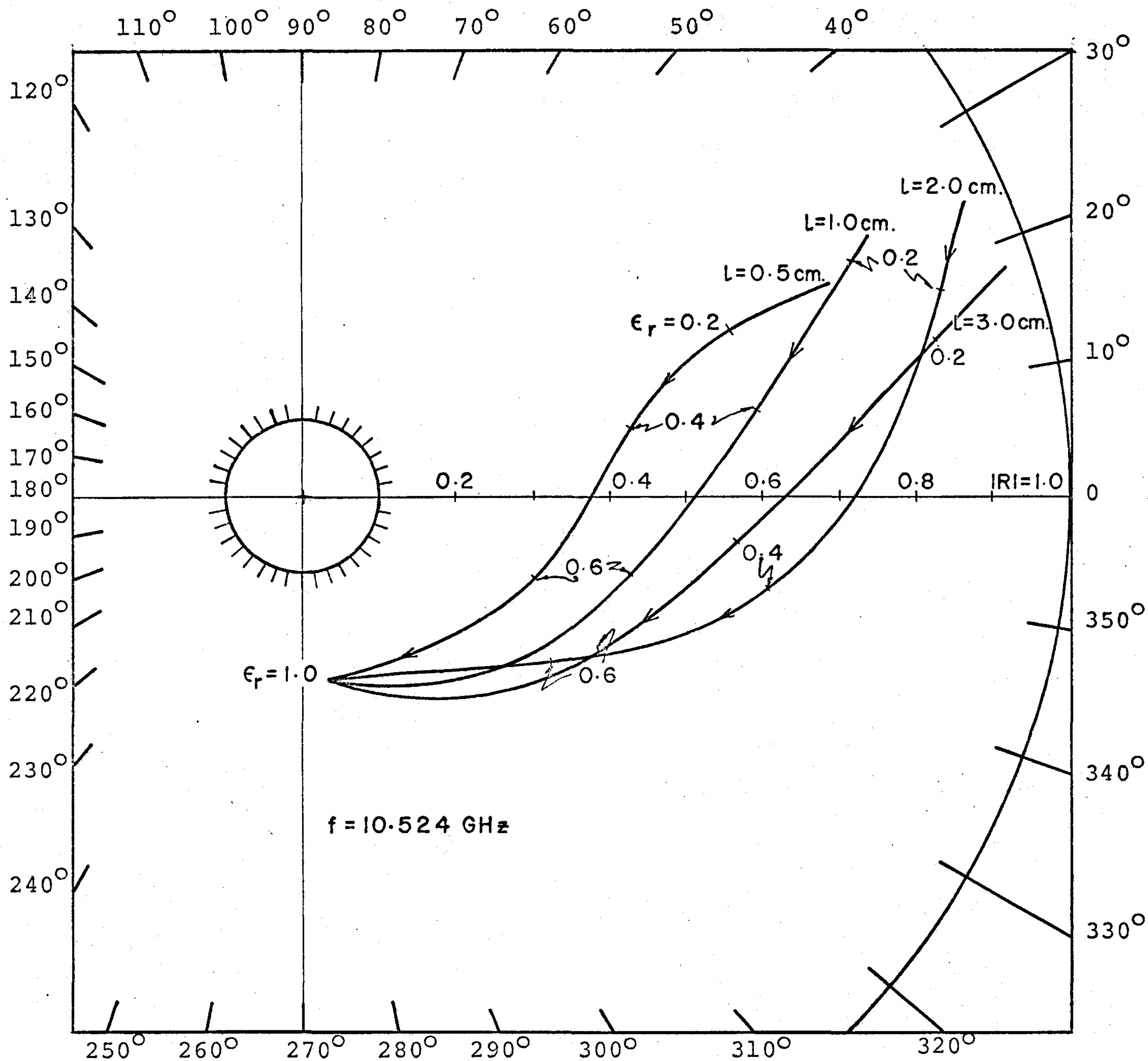

FIGURE 5.13: Polar Plots of the Calculated Reflection Coefficients of a Rectangular Waveguide System Radiating into a Plasma Layer as Functions of Layer Thickness and Dielectric Constant at 10.524 GHz.

CHAPTER VI

ANISOTROPY OF THE MICROWAVE CONDUCTIVITY OF SEMICONDUCTORS IN THE PRESENCE OF A HIGH ELECTRIC FIELD

6.1 Introduction

It has been known for some time that the application of a pulsed d.c. electric field to a semiconductor sample causes a considerable reduction in the conductivity of the sample. This effect, as first pointed out by Shockley[55], arises from an increase in the average energy or the temperature of the carriers. During the application of the field the lattice temperature is kept constant by making the pulses short and of low repetition rate. Thus the d.c. conductivity of semiconductors depends on the intensity of the electric field, the lattice temperature, the carrier concentration, and the direction of the d.c. field with respect to the crystal orientation.

When a small-signal microwave field is superimposed on the d.c. field, there are other effects of interest. In addition to the above mentioned parameters, the small-signal microwave conductivity depends on (a) the orientation of the microwave field with respect to the d.c. field[25, 26], and (b) the frequency of the microwave signal[20].

The microwave conductivity for parallel orientation has been studied theoretically by a number of authors[20-23, 27, 29]. For germanium, the theoretical calculation agrees with experimental results[20, 24, 28]. For the perpendicular conductivity case, however, a satisfactory theory has not been reported, but some preliminary measurements have been made by Gunn[25] which indicate that the perpendicular conductivity is nearly the same as the d.c. conductivity. Greshenzen, et.al.[28], also reported similar measurements on p-type germanium in the 8mm band and found the expected anisotropy between the microwave conductivities for fields parallel and perpendicular to the d.c. field. The existence of this anisotropic conductivity in parallel and perpendicular directions led to the prospect of a new microwave device, namely, the "hot electron rotator"[25-26, 56-57]. However, a definite theory with experimental confirmation of this anisotropic effect, which would confirm the feasibility of operation of such a device, has remained an unsolved problem.

This Chapter deals with the investigation of the anisotropy of the small-signal microwave conductivity of n-type germanium in the presence of a high electric field directed at an angle to the microwave field. In Section 6.2, an expression for the microwave conductivity of a semiconductor sample is derived in terms of the parallel and perpendicular conductivities and the angle between the microwave and d.c. field vectors. A theory of the parallel and perpendicular conductivity is presented in Section 6.3. The angular and frequency dependence of the microwave conductivity is also developed from the hot electron theory and the solution is presented in Section 6.4. Finally, measurements which confirm the theory have been carried out on an 11.4 ohm cm, n-type germanium sample at 9.381 GHz.

6.2 The Small-Signal Microwave Conductivity of Semiconductors in the Presence of a High D.C. Electric Field Directed at an Angle to the Microwave Field

From physical reasoning Gunn[25] has argued that the small-signal microwave conductivity of an isotropic semiconductor sample in the presence of a strong d.c. field becomes anisotropic in the sense that it depends on the mutual orientation of the d.c. and microwave field vectors. He states that the parallel microwave conductivity (σ_{11}) of a semiconductor sample, when subjected to a large d.c. electric field and a small parallel microwave field, is given by the incremental conductivity $\frac{\partial J}{\partial F}$, whereas the conductivity of the same sample ($\sigma_{\perp}$) subjected to the same fields, this time in a mutually perpendicular direction, is given by the d.c. conductivity $\frac{J}{F}$. Thus referring to Figure 6.1,

$$\sigma_{11} = \sigma_i = \left.\frac{\partial J}{\partial F}\right|_{F=F_o} \tag{6.1}$$

$$\sigma_{\perp} = \sigma_d = \left.\frac{J}{F}\right|_{F=F_o} \tag{6.2}$$

where σ_i is the incremental conductivity and σ_d is the d.c. conductivity.

Consider an electromagnetic wave F_1 incident on a semiconductor sample, which is subjected to a very strong d.c. field F_o in the x-direction at an angle Θ between the

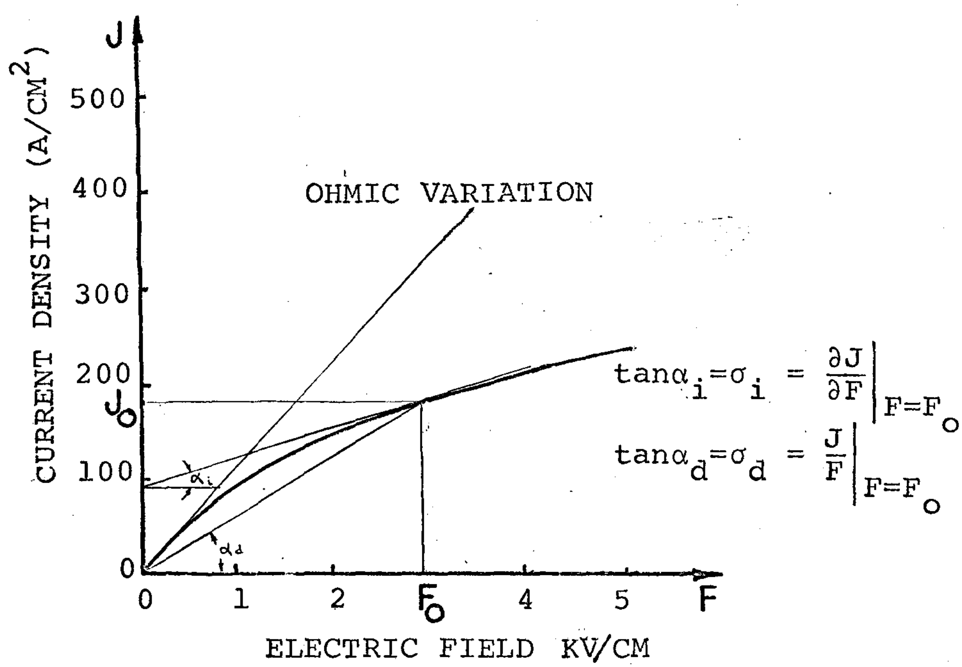

FIGURE 6.1: Current Density versus D.C. Field Strength in a Semiconductor Sample. σ_i is the Incremental Conductivity and σ_d is the D.C. Conductivity. The Scale is taken Arbitrarily.

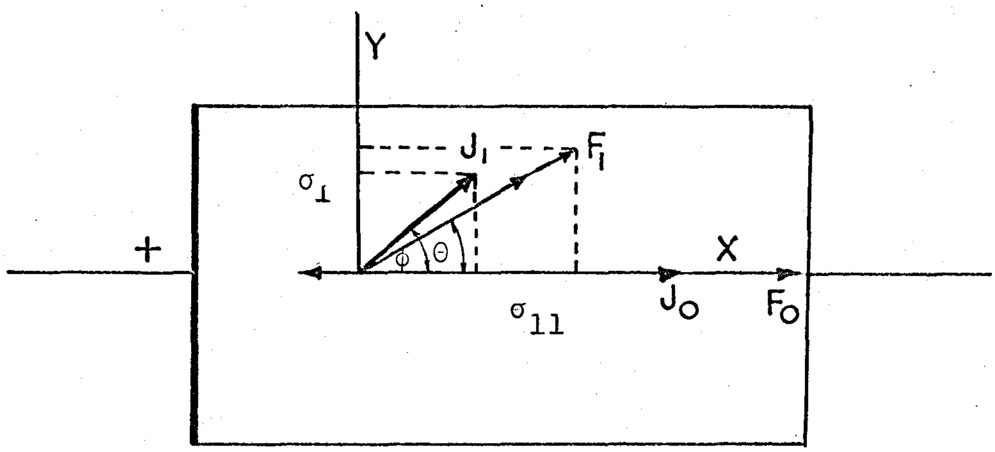

(a)

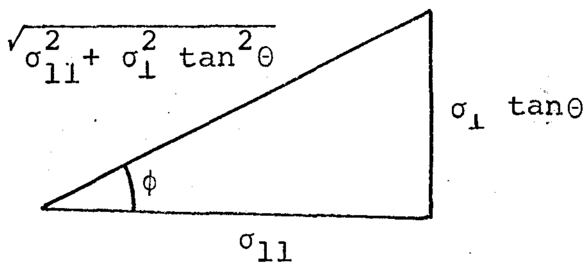

(b)

FIGURE 6.2: (a) A Semiconductor Sample with a Microwave Field F_1, directed at an angle Θ to the D.C. Field F_o.

FIGURE 6.2: (b) Relationship between the Angles Θ and ϕ.

d.c. and microwave field vectors(Figure 6.2a). We assume that

$$\omega\tau << 1 \tag{6.3}$$

which removes the frequency dependence of the conductivity and ensures $\sigma_{11} = \sigma_i$ (Since in the limit of very high frequencies when $\omega\tau >> 1$, the anisotropy[20] vanishes and $\sigma_{11} = \sigma_\perp$). Under this assumption, it is appropriate to apply Gunn's model for the calculation of the microwave conductivity.

In the semiconductor sample, a microwave current $\vec{J}_1$ flows in addition to the d.c. current J_o. Due to the anisotropic conductivity, $\vec{J}_1$ will not be parallel to the microwave field $\vec{F}_1$. This has been proved in Section 6.4.. Let us assume that $\vec{J}_1$ makes an angle ϕ with the x-axis. The x- and y- components of the microwave current are,

$$J_1 \cos\phi = \sigma_{11} F_1 \cos\Theta \tag{6.4a}$$

$$J_1 \sin\phi = \sigma_\perp F_1 \sin\Theta \tag{6.4b}$$

which give $\tan\phi = \dfrac{\sigma_\perp}{\sigma_{11}} \tan\Theta$. (6.5)

The angle of rotation of the microwave current vector from the microwave field vector is defined as

$$\begin{aligned}\psi &= \phi - \Theta \\ &= \tan^{-1}\left[\frac{\sigma_\perp}{\sigma_{11}} \tan\Theta\right] - \Theta\end{aligned} \tag{6.6}$$

which shows that, for isotropic effect, $\phi = \Theta$. The components of the microwave field from equations (6.4a) and (6.4b) may be written as

$$F_{1x} = \frac{J_1 \cos\phi}{\sigma_{11}} \tag{6.7}$$

$$F_{1y} = \frac{J_1 \sin\phi}{\sigma_{\perp}} \tag{6.8}$$

which may be added along $\vec{J}_1$ direction,

$$F_{1J} = \frac{J_1 \cos^2\phi}{\sigma_{11}} + \frac{J_1 \sin^2\phi}{\sigma_{\perp}} \; . \tag{6.9}$$

Denoting a microwave conductivity† $\sigma_\phi = \frac{J_1}{F_{1J}}$ to be measured along $\vec{J}_1$, we obtain

$$\frac{1}{\sigma_\phi} = \frac{\cos^2\phi}{\sigma_{11}} + \frac{\sin^2\phi}{\sigma_{\perp}} \; . \tag{6.10}$$

Equation (6.5) gives the relationship between ϕ and Θ from Figure 6.2(b). Thus

$$\cos\phi = \frac{\sigma_{11}}{\sqrt{\sigma_{11}^{\,2} + \sigma_{\perp}^{\,2} \tan^2\Theta}} \tag{6.11}$$

$$\sin\phi = \frac{\sigma_{\perp} \tan\Theta}{\sqrt{\sigma_{11}^{\,2} + \sigma_{\perp}^{\,2} \tan^2\Theta}} \tag{6.12}$$

so that

$$\sigma_\phi = \frac{\sigma_{11}^{\,2} \cos^2\Theta + \sigma_{\perp}^{\,2} \sin^2\Theta}{\sigma_{11} \cos^2\Theta + \sigma_{\perp} \sin^2\Theta} \; . \tag{6.13}$$

† Page 98, Reference 42

Thus a knowledge of σ_{11} and $\sigma_{\perp}$ enables one to calculate the microwave conductivity at an angle.

The equation (6.13) may also be obtained from the consideration of the absorption of microwave power by the "hot" carriers in parallel and perpendicular directions. The microwave power absorbed by a semiconductor sample is given by[58]

$$P_{sample} = \int \sigma \, (F_1/\sqrt{2})^2 \, dV \tag{6.14}$$

where σ is the microwave conductivity and V is the volume of the sample. Assuming an uniform field in the sample, this may be written as[59]

$$P_{sample} = \sigma \frac{F_1^2}{2} V. \tag{6.15}$$

The power absorption by the components of the microwave field as given by equations (6.7) and (6.8) may be written respectively as

$$\begin{aligned} P_{11} &= \sigma_{11} \frac{F_{1x}^2 V}{2} \\ &= \frac{J_1^2}{2} \frac{\cos^2\phi}{\sigma_{11}} V \end{aligned} \tag{6.16}$$

and

$$P_{\perp} = \frac{J_1^2}{2} \frac{\sin^2\phi}{\sigma_{\perp}} V. \tag{6.17}$$

The total power absorbed is therefore given by

$$P = P_{11} + P_{\perp}$$

$$= [\frac{\cos^2\phi}{\sigma_{11}} + \frac{\sin^2\phi}{\sigma_{\perp}}] \frac{J_1{}^2 V}{2} . \qquad (6.18)$$

Denoting a conductivity σ_ϕ again in the direction of J_1, we obtain

$$\frac{1}{\sigma_\phi} = \frac{\cos^2\phi}{\sigma_{11}} + \frac{\sin^2\phi}{\sigma_{\perp}} \qquad (6.19)$$

which agrees with the equation (6.10) and may be simplified to the equation (6.13).

To check the validity of the equation (6.13), we calculate σ_ϕ for special cases of Θ. Thus for $\Theta = 0^o$ and 90^o respectively,

$$\sigma_\phi = \sigma_{11} \qquad (6.20)$$

$$\sigma_\phi = \sigma_{\perp} \qquad (6.21)$$

as expected.

6.3 Theory of the Microwave Conductivity of N-type Germanium for Parallel and Perpendicular Field Orientations

This section contains the development of the theoretical expressions for the parallel and perpendicular conductivity of n-type germanium. The technique is similar to that of Nag and Das[23] for the calculation of the parallel conductivity. An approximate solution of the problem may be obtained by solving the appropriate Boltzmann equation, taking into account the effect of acoustic and optical phonon scattering and assuming isotropic effective mass. The effect of the e-e scattering has been neglected as in the method of Yamashita, et.al.[60], and Stratton[61].

6.3.1 The Energy Distribution Function for the Carriers and the Boltzmann Equation

To determine the approximate energy distribution function for the electrons in n-type germanium, we assume a model with spherical engery surfaces† as in the methods of Nag and Das[23].

The occupancy function for the carriers, under the influence of an electric field, is disturbed from its equilibrium. Such a non-equilibrium distribution function for the carriers having the wave vector $\vec{k}$ for the case of n-type germanium may be written as (Appendix D)

$$f(\vec{k}) = f(E) + k_x\, g(E) + k_y\, h(E) \qquad (6.22)$$

where k_x and k_y are the components of the wave vectors in the x and y directions, respectively; g(E) and h(E) are the perturbed values of the distribution function in the x-and y-directions, respectively; f(E) is the isotropic part and k_x g(E) and k_y h(E) are the anisotropic parts of the distribution function; E represents the energy of the carrier.

The total rate of change of the distribution function may be written in the form‡

$$\frac{Df(\vec{k})}{Dt} = \frac{\partial f(\vec{k})}{\partial t} + \frac{\partial f(\vec{k})}{\partial k_x}\frac{dk_x}{dt} + \frac{\partial f(\vec{k})}{\partial k_y}\frac{dk_y}{dt} + \frac{\partial f(\vec{k})}{\partial k_z}\frac{dk_z}{dt} \qquad (6.23)$$

Writing $\frac{dk_x}{dt} = -\frac{eF_x}{\hbar}$, we may rewrite this equation as

$$\frac{Df(\vec{k})}{Dt} = \frac{\partial f(\vec{k})}{\partial t} - \frac{e}{\hbar}\left[\frac{\partial f(\vec{k})}{\partial k_x} F_x + \frac{\partial f(\vec{k})}{\partial k_y} F_y + \frac{\partial f(\vec{k})}{\partial k_z} F_z\right]$$

---

† Page 153, This Thesis.

‡ Page 109, Reference 42.

where F_x, F_y, and F_z are the applied electric fields in the x-, y-, and z-directions, respectively. Since $F_z = 0$ (Figure 6.2), we may write this as

$$\frac{Df(\vec{k})}{Dt} = \frac{\partial f(\vec{k})}{\partial t} - \frac{e}{\hbar}\left[\frac{\partial f(\vec{k})}{\partial k_x} F_x + \frac{\partial f(\vec{k})}{\partial k_y} F_y\right]. \qquad (6.24)$$

This equation gives the variation of $f(\vec{k})$ caused by the fields. There is also in operation a mechanism which tends to restore $f(\vec{k})$ to its equilibrium value, namely the collisions of electrons with imperfections. The rate of change of $f(\vec{k})$ due to collisions is denoted by $\left.\frac{\partial f(\vec{k})}{\partial t}\right|_{coll}$. Thus we write the Boltzmann equation as

$$\left.\frac{\partial f(\vec{k})}{\partial t}\right|_{Field} - \frac{e}{\hbar}\left[\frac{\partial f(\vec{k})}{\partial k_x} F_x + \frac{\partial f(\vec{k})}{\partial k_y} F_y\right]_{Field} = \left.\frac{\partial f(\vec{k})}{\partial t}\right|_{Coll} \qquad (6.25)$$

Since the applied electric field varies as a function of time, we write the following equations using equation (6.22),

$$\left.\frac{\partial f(\vec{k})}{\partial t}\right|_{Field} = \frac{\partial f(E)}{\partial t} + k_x \frac{\partial g(E)}{\partial t} + k_y \frac{\partial h(E)}{\partial t} \qquad (6.26)$$

$$\frac{\partial f(\vec{k})}{\partial k_x} = \frac{\partial f(E)}{\partial k_x} + \frac{\partial}{\partial k_x}\{k_x g(E)\} + \frac{\partial}{\partial k_x}\{k_y h(E)\}$$

$$= \frac{\partial f(E)}{\partial E}\frac{dE}{dk_x} + g(E) + k_x \frac{\partial g(E)}{\partial E}\frac{dE}{dk_x} + h(E)\frac{\partial k_y}{\partial k_x} + k_y \frac{\partial h(E)}{\partial E}\frac{dE}{dk_x} \qquad (6.27)$$

Choosing one of the energy minima of the conduction band in germanium which are located at the zone edge along [111] axes as the origin, we obtain

$$\frac{dE}{dk_x} = \frac{d}{dk_x}\left\{\frac{\hbar^2}{2m^*}(k_x^2 + k_y^2 + k_z^2)\right\}$$

$$= \frac{\hbar^2}{m^*} k_x \qquad (6.28)$$

where m* is the effective mass of electrons and $\hbar$ is the reduced Plank's constant. Thus

$$\frac{\partial f(\vec{k})}{\partial k_x} = \frac{\hbar^2 k_x}{m^*}\frac{\partial f(E)}{\partial E} + g(E) + \frac{\hbar^2 k_x^{\,2}}{m^*}\frac{\partial g(E)}{\partial E} + h(E)\frac{\partial k_y}{\partial k_x}$$
$$+\frac{\hbar^2 k_y k_x}{m^*}\frac{\partial h(E)}{\partial E}. \tag{6.29}$$

For spherical energy surfaces ($k_x = k_y = k_z$), $\frac{\hbar^2 k_x^{\,2}}{m^*}$ may be shown to be equal to $\frac{2}{3}E$. Thus, with $h(E) = 0$, as in the case of parallel fields, equation (6.27) gives equation (6) of Nag and Das[23], as expected. Similarly,

$$\frac{\partial f(k)}{\partial k_y} = \frac{\hbar^2 k_y}{m^*}\frac{\partial f(E)}{\partial E} + h(E) + \frac{\hbar^2 k_y^{\,2}}{m^*}\frac{\partial h(E)}{\partial E} + g(E)\frac{\partial k_x}{\partial k_y}$$
$$+\frac{\hbar^2}{m^*} k_x k_y \frac{\partial g(E)}{\partial E}. \tag{6.30}$$

Neglecting the impurity and e-e scattering, the collision term may be written as

$$\left.\frac{\partial f(\vec{k})}{\partial t}\right|_{coll} = \left.\frac{\partial f(\vec{k})}{\partial t}\right|_{ac} + \left.\frac{\partial f(\vec{k})}{\partial t}\right|_{op} \tag{6.31}$$

where the first and the second terms on the right represent the change in the distribution function due to the interaction of electrons with acoustic and optical modes of lattice vibrations, respectively. The rate of change of the distribution function due to the acoustic and optical phonon scattering has been studied extensively by Yamashita,et.al.[60].

A careful analysis of their results has shown, in the present case, that the acoustic term is given by

$$\left.\frac{\partial f(\vec{k})}{\partial t}\right|_{ac} = \frac{A}{E^{1/2}} \Big[E^2 \frac{\partial^2 f(E)}{\partial E^2} + \left(\frac{E^2}{kT} + 2E\right) \frac{\partial f(E)}{\partial E} + \frac{2Ef(E)}{kT}$$

$$- k_x \frac{E}{2m^*c^2} g(E) - k_y \frac{E}{2m^*c^2} h(E)\Big] \tag{6.32}$$

where the first four terms on the right are contributed by the symmetric part of the distribution function and the remaining quantities are due to the asymmetric (or directional) parts of the distribution function. Similarly, the optical term may be written as

$$\left.\frac{\partial f(\vec{k})}{\partial t}\right|_{op} = \frac{B}{\hbar\omega_{oE}{}^{1/2}} \Big[\hbar\omega \; (e^s+1) \left(E\frac{\partial^2 f(E)}{\partial E^2} + \frac{\partial f(E)}{\partial E}\right)$$

$$+ 2(e^s+1) \left(E\frac{\partial f(E)}{\partial E} + f(E)\right) - k_x \frac{E}{\hbar\omega_o} (e^s+1)\; g(E)$$

$$- k_y \frac{E}{\hbar\omega_o} (e^s+1)\; h(E)\Big] \tag{6.33}$$

where[23] $A = 8ec^2/3(\pi kT)^{1/2} \mu_a$, $s = \hbar\omega_o/kT$,

$B = 9/16\ (AD^2/c^2)\ (\hbar^2 \zeta^2/2m^*kT)\ (1/e^s-1)$, c= velocity of sound in the semiconductor. Inserting equations (6.26), (6.29), (6.30), (6.32) and (6.33) in (6.25) and equating the terms of the same angular dependence (i.e. k_x and k_y terms), we obtain the pair of equations:

$$\frac{\partial g(E)}{\partial t} - \frac{e\hbar}{m^*}\frac{\partial f(E)}{\partial E} F_x = - \frac{A}{E^{1/2}} \frac{E}{2m^*c^2} g(E) - \frac{B}{(\hbar\omega_o)^2} E^{1/2}(e^s+1)\ g(E) \tag{6.34}$$

$$\frac{\partial h(E)}{\partial t} - \frac{e\hbar}{m^*}\frac{\partial f(E)}{\partial E} F_y = - \frac{A}{E^{1/2}} \frac{E}{2m^*c^2} h(E) - \frac{B}{(\hbar\omega_o)^2} E^{1/2}(e^s+1)\ h(E) \tag{6.35}$$

which become after some rearrangement,

$$g(E) = \frac{2m^*c^2}{A\Omega} \frac{1}{E^{1/2}} \left[\frac{e\hbar}{m^*} F_x \frac{\partial f(E)}{\partial E} - \frac{\partial g(E)}{\partial t}\right] \tag{6.36}$$

$$h(E) = \frac{2m^*c^2}{A\Omega} \frac{1}{E^{1/2}} \left[\frac{e\hbar}{m^*} F_y \frac{\partial f(E)}{\partial E} - \frac{\partial h(E)}{\partial t}\right] \tag{6.37}$$

$$\text{where } \Omega = 1 + \frac{B}{A} \frac{2m^*c^2}{(\hbar\omega_o)^2} (e^s + 1). \tag{6.38}$$

The components of the total electric field in the x- and y-directions may be written as

$$\begin{aligned} F_x &= F_o + \mathrm{Re}\, F_1 \cos\theta\, e^{j\omega t} \\ &= F_o\, [1 + \mathrm{Re}\, \lambda_x\, e^{j\omega t}] \end{aligned} \tag{6.39}$$

$$\begin{aligned} F_y &= 0 + \mathrm{Re}\, F_1 \sin\theta\, e^{j\omega t} \\ &= F_o\, [0 + \mathrm{Re}\, \lambda_y\, e^{j\omega t}] \end{aligned} \tag{6.40}$$

where the quantities λ_x and λ_y are given by

$$\lambda_x = \frac{F_1 \cos\Theta}{F_o} \ll 1 \tag{6.41}$$

$$\lambda_y = \frac{F_1 \sin\Theta}{F_o} \ll 1. \tag{6.42}$$

The presence of the microwave field will perturb the distribution function (i.e., the quantities f(E), g(E), and h(E)) by a small amount about its equilibrium values. Assuming that the amount of perturbation is proportional to the microwave field strength, the x- and y- directed perturbations may be written as

$$\begin{aligned} f(E) &= f_o(E) + \text{Re}\ \lambda_x\ f_1(E)\ e^{j\omega t} \\ g(E) &= g_o(E) + \text{Re}\ \lambda_x\ g_1(E)\ e^{j\omega t} \end{aligned} \tag{6.43}$$

and

$$\begin{aligned} f(E) &= f_o(E) + \text{Re}\ \lambda_y\ f_1(E)\ e^{j\omega t} \\ h(E) &= h_o(E) + \text{Re}\ \lambda_y\ h_1(E)\ e^{j\omega t}. \end{aligned} \tag{6.44}$$

Since we wish to determine σ_{11} and $\sigma_{\perp}$, the parameters of interest are g_1 and h_1, which give the microwave currents in the x- and y- directions, respectively. For the calculation of g_1 (i.e., parallel current), we substitute equation (6.43) in equation (6.36), which yields

$$g_o(E) + \mathrm{Re}\,\lambda_x\, g_1\, (E)\, e^{j\omega t}$$

$$= \frac{2\overset{*}{m}c^2}{A\Omega E^{1/2}} \left[\frac{e\hbar}{m^*}\, F_o\, (1 + \mathrm{Re}\,\lambda_x\, e^{j\omega t})\right.$$

$$\left. \times \frac{\partial}{\partial E} \{ f_o(E) + \mathrm{Re}\,\lambda_x\, f_1(E)\, e^{j\omega t} \} - \frac{\partial}{\partial t} \{ g_o(E) + \mathrm{Re}\,\lambda_x\, g_1(E)\, e^{j\omega t} \}\right] \tag{6.45}$$

$$\doteqdot \frac{2\overset{*}{m}c^2}{A\Omega E^{1/2}} \left[\frac{e\hbar}{m^*} F_o\, (1 + \mathrm{Re}\,\lambda_x\, e^{j\omega t})\, \frac{\partial f_o(E)}{\partial E}\right.$$

$$\left. + \frac{e\hbar}{m^*} F_o\, \mathrm{Re}\,\lambda_x\, \frac{\partial f_1(E)}{\partial E}\, e^{j\omega t} - \mathrm{Re}\,\lambda_x\, g_1(E)\, j\omega\, e^{j\omega t}\right] \tag{6.46}$$

on negecting higher order terms. Equating the a.c. quantities, we obtain

$$g_1 = \frac{\frac{2m^*c^2}{A\Omega E^{1/2}} \left[\frac{e\hbar}{m^*} F_o \left\{ \frac{\partial f_o(E)}{\partial E} + \frac{\partial f_1(E)}{\partial E} \right\}\right]}{1 + j\omega\, \frac{2\overset{*}{m}c^2}{A\Omega E^{1/2}}} \tag{6.47}$$

which agrees with the corresponding result given by Nag and Das[23] (c.f. Equation 15). Similarly, substituting equation (6.44) in equation (6.37) for the calculations of h_1 (i.e. perpendicular current), we obtain,

$$h(E) + \mathrm{Re}\,\lambda_y\, h_1(E)\, e^{j\omega t}$$

$$\doteqdot \frac{2\overset{*}{m}c^2}{A\Omega E^{1/2}} \left[\frac{e\hbar}{m^*} F_o\, (0 + \mathrm{Re}\,\lambda_y\, e^{j\omega t})\, \frac{\partial f_o(E)}{\partial E} - \mathrm{Re}\,\lambda_y\, h_1(E)\, j\omega e^{j\omega t}\right]. \tag{6.48}$$

Equating the a.c. quantities, we finally obtain,

$$h_1(E) = \frac{\dfrac{2m^*c^2}{A\Omega E^{1/2}} \left[\dfrac{e\hbar}{m^*} F_o \dfrac{\partial f_o(E)}{\partial E} \right]}{1 + j\omega \dfrac{2m^*c^2}{A\Omega E^{1/2}}} . \qquad (6.49)$$

Equations (6.47) and (6.49) do not agree with the results of Staecker and Das[26], who showed that $g_1(E)$ and $h_1(E)$ are functions of Θ. From hot electron theory, it will be shown that the parallel and perpendicular conductivities are independent of Θ.†

6.3.2 The Microwave Conductivity and The Change in Dielectric Constant

It has been shown by Nag and Das[23] that $f_1(E)$ consists of both real and imaginary parts,

$$f_1(E) = f_{1r}(E) + jf_{1i}(E) \qquad (6.50)$$

Expanding the denominator of equation (6.47) in the binomial form and retaining only the first order terms, we may write,

$$g_1(E) = \frac{e\hbar}{m^*} \frac{2m^*F_oc^2}{A\Omega E^{1/2}} \left[\frac{\partial f_o(E)}{\partial E} + \frac{\partial f_{1r}(E)}{\partial E} + j \frac{\partial f_{1i}(E)}{\partial E} \right] \left[1 - j \frac{\omega\tau_m}{(E/kT)^{1/2}} \right]$$

(6.51)

where $\tau_m = \dfrac{2m^*c^2}{A\Omega(kT)^{1/2}}$. Assuming that $\omega\tau_m << 1$, g_1 may be rewritten as

$$g_1(E) \doteqdot \frac{2\hbar c^2F_oe}{A\Omega E^{1/2}} \left[\frac{\partial f_o(E)}{\partial E} + \frac{\partial f_{1r}(E)}{\partial E} + j \frac{\partial f_{1i}(E)}{\partial E} \right]. \qquad (6.52)$$

† Equations 6.78 and 6.79 of This Thesis.

The x- component of the microwave current is given by

$$J_{1x} = F_1 \cos\Theta \; e^{j\omega t} \; N_o \frac{e\hbar}{m^*} \int k_x^2 \, g_1(E) \, dk_x \, dk_y \, dk_z \qquad (6.53)$$

where N_o is the normalisation constant of the distribution function in the absence of a microwave field. Substituting equation (6.52) for $g_1(E)$

$$J_{1x} = F_1 \cos\Theta \; e^{j\omega t} \left(\frac{N_o e\hbar}{m^*}\right) \int \left(\frac{2e\hbar c^2 F_o}{A\Omega E^{1/2}}\right) \frac{\partial f_o(E)}{\partial E} \times$$

$$\left[1 + \frac{\partial f_{1r}(E)}{\partial E} \Big/ \frac{\partial f_o(E)}{\partial E} + j \frac{\partial f_{1i}(E)}{\partial E} \Big/ \frac{\partial f_o(E)}{\partial E} \right] k_x^2 \, dk_x dk_y dk_z \qquad (6.54)$$

which may be written as

$$J_{1x} = F_1 \cos\Theta \; e^{j\omega t} \; \sigma_{dc} \left[1 + \frac{m_r}{m_o} + j \frac{m_i}{m_o} \right] \qquad (6.55)$$

where σ_{dc} is the field dependent d.c. conductivity and the parameters m_o, m_r and m_i are defined by Nag and Das. Similary, $h_1(E)$ from equation (6.49) may be approximately written as

$$h_1(E) \doteqdot \frac{2e\hbar c^2 F_o}{A\Omega E^{1/2}} \left[\frac{\partial f_o(E)}{\partial E}\right]. \qquad (6.56)$$

The y-component of the microwave current may be written as

$$J_{1y} = F_1 \sin\Theta \; e^{j\omega t} \left(\frac{N_o e\hbar}{m^*}\right) \int h_1(E) \, k_y^2 \, dk_x \, dk_y \, dk_z$$

$$= F_1 \sin\Theta \; e^{j\omega t} \left(\frac{N_o e\hbar}{m^*}\right) \int \left(\frac{2e\hbar c^2 F_o}{A\Omega E^{1/2}}\right) \frac{\partial f_o(E)}{\partial E} \, k_y^2 \, dk_x \, dk_y \, dk_z \qquad (6.57)$$

$$= F_1 \sin\Theta \; e^{j\omega t} \; \sigma_{d.c.} \qquad (6.58)$$

Equation (6.55) gives the parallel conductivity and the change in dielectric constant, while equation (6.58) gives the perpendicular conductivity. Thus

$$\sigma_{11} = \sigma_{d.c.} \left[1 + \frac{m_r}{m_o} \right] \tag{6.59}$$

$$\sigma_{\perp} = \sigma_{d.c.} \tag{6.60}$$

$$\Delta\varepsilon = \frac{\sigma_{d.c.}}{\omega\varepsilon_o} \quad \frac{m_i}{m_r} \; . \tag{6.61}$$

where $\sigma_{d.c.}$ may be easily seen in equation (6.57) and

$$m_o = \int \frac{1}{E}1/2 \; \frac{\partial f_o(E)}{\partial E} \quad k_x{}^2 \; dk_x \; dk_y \; dk_z \; ,$$

$$m_r = \int \frac{1}{E}1/2 \; \frac{\partial f_{1r}(E)}{\partial E} \; k_x{}^2 \; dk_x \; dk_y \; dk_z \; ,$$

$$m_i = \int \frac{1}{E}1/2 \; \frac{\partial f_{1i}(E)}{\partial E} \; k_x{}^2 \; dk_x \; dk_y \; dk_z .$$

The ratio of $\frac{m_r}{m_o}$ has been evaluated numerically by Nag and Das. Considering only the optical phonon scattering, the value obtained is -.24 which indicates that $\sigma_{11}<\sigma_{\perp}$. Further, it is seen that the equations (6.59) and (6.60) correspond to the equations (6.1) and (6.2), respectively.

6.4 <u>The Microwave Conductivity of Semiconductors from the Hot Electron Theory</u>

It is known from the hot electron theory that the field dependent current density $\vec{J}_o$ at medium field strengths is described by

$$\vec{J}_o = \sigma_o \; [1 - \beta F_o^2] \; \vec{F}_o \tag{6.62}$$

where σ_o is the low-field ohmic conductivity, F_o is the magnitude of the electric field where the conductivity is measured, and β is a constant which, in general, depends on the carrier temperature T and the crystallographic directions of the applied electric field. It has been shown by Schmidt-Teidmann[21] that

$$\begin{aligned} \beta_{110} &= \beta_{100}(T) - \frac{\gamma(T)}{2} \\ \beta_{111} &= \beta_{100}(T) - \frac{2}{3}\gamma\ (T) \\ \beta_{100} &= \beta_{100}(T) \end{aligned} \tag{6.63}$$

where the subscripts denote the direction of the applied field and γ is another constant, and is given by

$$\gamma = \text{constant} \times \frac{3(k-1)^2}{(2k+1)} \tag{6.64}$$

where $k = \frac{m_\ell}{m_t}$. For isotropic effective mass, $\gamma = 0$.

The d.c. conductivity in different crystallographic directions has been determined experimentally by a number of authors[62], who observed that the anisotropy is small at room temperature. However, at low temperature, this has been found to be quite significant. The crystallographic anisotropy of the microwave conductivity has been studied theoretically by Guha and Nag[29] who indicate that like d.c. conductivity, the anisotropy of microwave conductivity is very small at room temperature. Noting their observation as true, we take the parameter β to be isotropic at room temperature where microwave conductivity is to be determined. We shall write β isotropic as β for the sake of simplicity. When a microwave field is applied at an angle to the d.c. field,

$$\vec{F}_t = \vec{F}_o + \vec{F}_1 \sin\omega t \tag{6.65}$$

a microwave current $\vec{J}_1$ flows in addition to the d.c. current $\vec{J}_o$. We rewrite equation (6.62), in a more general form, as

$$\vec{J}_t = \sigma_o (1 - \beta |F_t|^2) \vec{F}_t \tag{6.66}$$

where $|F_t|$ is the magnitude of the total electric field. Since the electric field is composed of a d.c. component as well as an a.c. component, it is appropriate to write the current density on averaging $|F_t|^2$ over the allowed values of electron energy E. Thus

$$\vec{J}_t = \sigma_o [1 - \beta <|F_t|^2>_E] \vec{F}_t \tag{6.67}$$

Equation (6.65) may be written as

$$\vec{F}_t = \vec{a}_x [F_o + F_1 \cos\Theta \sin\omega t] + \vec{a}_y [F_1 \sin\Theta \sin\omega t] \tag{6.68}$$

whose modulus becomes

$$|F_t|^2 = F_o^2 + 2F_o F_1 \cos\Theta \sin\omega t + F_1^2 \sin^2\omega t \tag{6.69}$$

Substituting this in equation (6.67), we obtain

$$\vec{J}_t = \sigma_o [1 - \beta \{F_o^2 + 2F_o F_1 \cos\Theta < \sin\omega t >_E + F_1^2 <\sin^2\omega t>_E\}]$$

$$\times (\vec{F}_o + \vec{F}_1 \sin\omega t)$$

$$= \sigma_o [1 - \beta \{F_o^2 + 2F_oF_1 \cos\Theta <\sin\omega t >_E + F_1^2 <\sin^2\omega t>_E\}] \vec{F}_o$$

$$+ \sigma_o [1 - \beta \{F_o^2 + 2F_oF_1 \cos\Theta <\sin\omega t >_E + F_1^2 <\sin^2\omega t>_E\}] \vec{F}_1 \sin\omega t \tag{6.70}$$

Considering only the current components which are vibrating at an angular frequency ω, the microwave current can be written as

$$\vec{J}_1 = \sigma_o \, [-2\beta F_o F_1 \cos\Theta \;\; \langle \sin\omega t \rangle_E] \, \vec{F}_o + \sigma_o \, [1-\beta F_o^{\,2}] \, \vec{F}_1 \sin\omega t \tag{6.71}$$

It can be shown that the average value of $\sin\omega t$ over the electron energy E is

$$\langle \sin\omega t \rangle_E = \frac{1}{1+j\omega\tau} \;\; \sin\omega t \tag{6.72}$$

where τ is the relaxation time of carriers. So that equation (6.71) becomes

$$\vec{J}_1 = \sigma_o \, [-2\beta F_o F_1 \cos\Theta \, \frac{\sin\omega t}{1+j\omega\tau}] \, \vec{F}_o + \sigma_o \, [1-\beta F_o^{\,2}] \, \vec{F}_1 \sin\omega t \tag{6.73}$$

where the first term is a component of the microwave current flowing in the opposite direction to the d.c. field and is caused by the cross-modulation due to the microwave field. The second term is the F_1-directed microwave current which has two components:

$\sigma_o \, (1-\beta F_o^{\,2}) F_1 \cos\Theta \;\; \sin\omega t$ in the x-direction and

$\sigma_o \, (1-\beta F_o^{\,2}) F_1 \sin\Theta \;\; \sin\omega t$ in the y-direction.

The x-component of the microwave current is attenuated by the cross-modulation. As a result, $\vec{J}_1$ is not parallel to $\vec{F}_1$. Let J_1 makes an angle ϕ to the x-axis (Figure 6.2). The components of the current in the J_1-direction from equation (6.73) may then be written as

$$\vec{J}_1 = \sigma_o \left[-2\beta F_o F_1 \cos\Theta \; \frac{\sin\omega t}{1+j\omega\tau}\right] F_o \cos\phi + \sigma_o \left[1-\beta F_o^2\right] F_1 \sin\omega t \cos(\phi-\Theta)$$

$$= \sigma_o \left[(1-\beta F_o^2) - \frac{2\beta F_o^2 \cos\Theta\cos\phi}{(1+j\omega\tau)\cos(\phi-\Theta)}\right] F_1 \cos(\phi-\Theta) \sin\omega t$$

$$= \sigma_{dc} \left[1 - \frac{2\beta F_o^2 \cos\Theta\cos\phi}{(1-\beta F_o^2)(1+j\omega\tau)\cos(\phi-\Theta)}\right] F_1 \cos(\phi-\Theta) \sin\omega t \tag{6.74}$$

The microwave conductivity in the direction of J_1 may be written as

$$\sigma_\phi = \sigma_{dc} \left[1 - \frac{2\beta F_o^2 \cos\Theta\cos\phi}{(1-\beta F_o^2)(1+j\omega\tau)\cos(\phi-\Theta)}\right]$$

$$= \sigma_{dc} \left[1 - \frac{2\beta F_o^2}{(1-\beta F_o^2)(1+j\omega\tau)(1 + \frac{\sigma_\perp}{\sigma_{11}} \tan^2\Theta)}\right] \tag{6.75}$$

which shows that the microwave conductivity is dependent on Θ, $\omega\tau$, F_o, σ_{11} and $\sigma_\perp$. It is to be noted that $\omega\tau$ dependence of σ is the result of averaging $|E_t|^2$ over the electron energy. The microwave conductivity may therefore be calculated from the perpendicular and parallel conductivities.

Further, the real part of the microwave conductivity, is given by,

$$\mathrm{Re}[\sigma_\phi] = \sigma_{dc} \left[1 - \frac{2\beta F_o^2}{(1-\beta F_o^2)(1+\omega^2\tau^2)(1+\frac{\sigma_\perp}{\sigma_{11}} \tan^2\Theta)}\right] \tag{6.76}$$

while the change in dielectric constant, is given by

$$\Delta\varepsilon_r = \frac{\sigma_{dc}}{\omega\varepsilon_o} \frac{2\beta F_o^2 \omega\tau}{(1-\beta F_o^2)(1+\omega^2\tau^2)(1+\frac{\sigma_\perp}{\sigma_{11}} \tan^2\Theta)} \qquad (6.77)$$

Specialising for $\Theta=0^o$ and 90^o, we obtain

$$\sigma_{11} = \sigma_{dc} \left[1 - \frac{2\beta F_o^2}{(1-\beta F_o^2)(1+\omega^2\tau^2)} \right] \qquad (6.78)$$

$$\sigma_\perp = \sigma_{d.c.} \qquad (6.79)$$

Equation (6.59) corresponds to equation (6.78) under conditions of medium field strengths.

6.5 Numerical Computations

Equations (6.6) and (6.13) have been evaluated numerically on the CDC 6400 Computer. The microwave conductivity and the angle of rotation of the microwave current vector from the microwave field vector are calculated using the values of σ_{11} and $\sigma_\perp$ deduced graphically from the J_c-F_o curve. The results of these calculations are shown in Figures 6.3 through 6.5.

6.6 Experimental Techniques

The principal objective of the experimental programme was to obtain suitable data on the behaviour of microwave conductivity of an 11.4 ohm cm, n-type germanium in the presence of a high electric field, in order to confirm the theoretical predictions described in Section 6.2. Measurements were made at a frequency of 10 GHz and at room temperature. One of the considerations that led to the

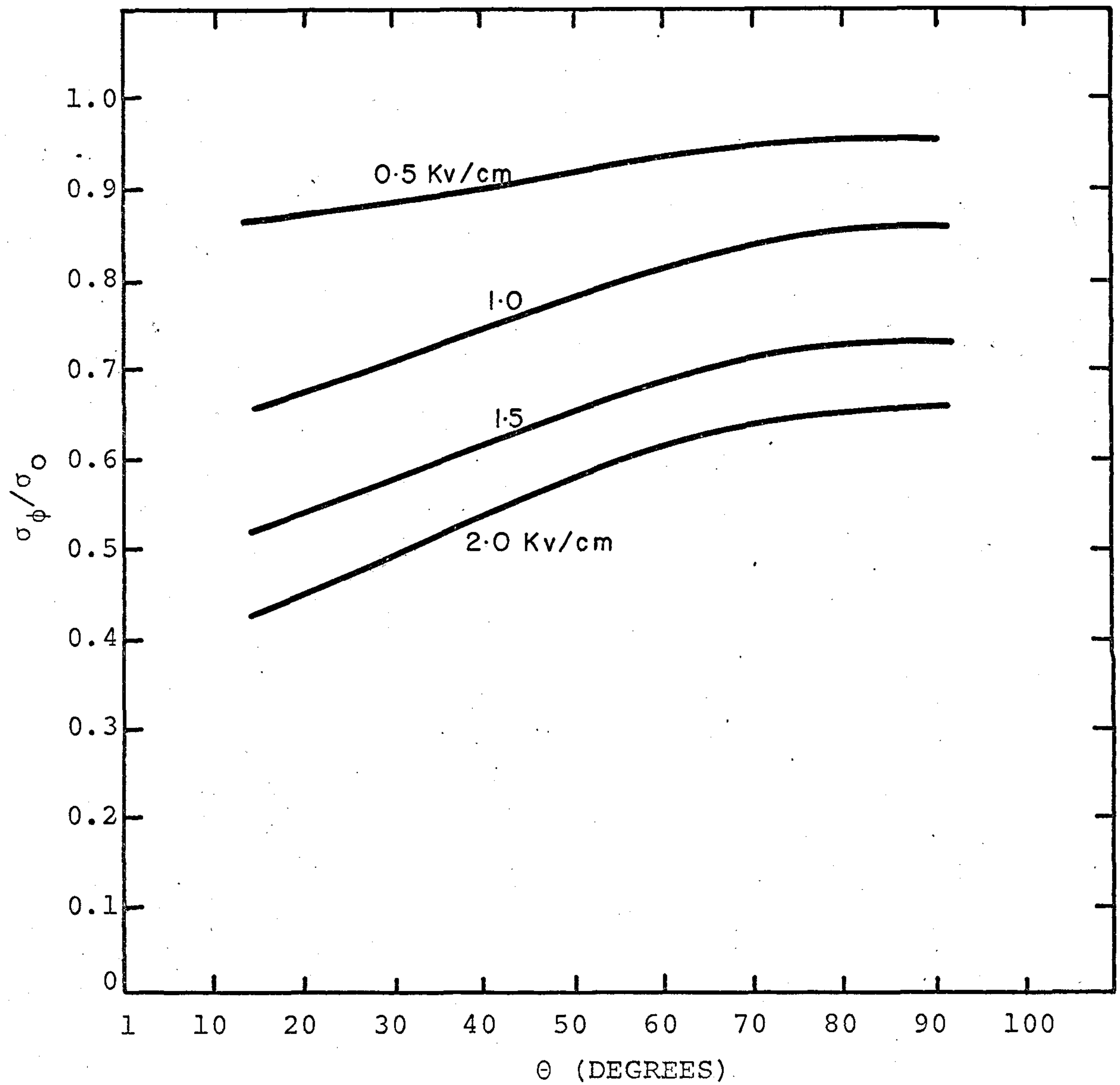

FIGURE 6.3: Computed Curves of the Microwave Conductivity for an 11.4 ohm cm, n-type Germanium as a function of the Angle between the Microwave and D.C. Field Vectors. σ_o is the low field ohmic conductivity.

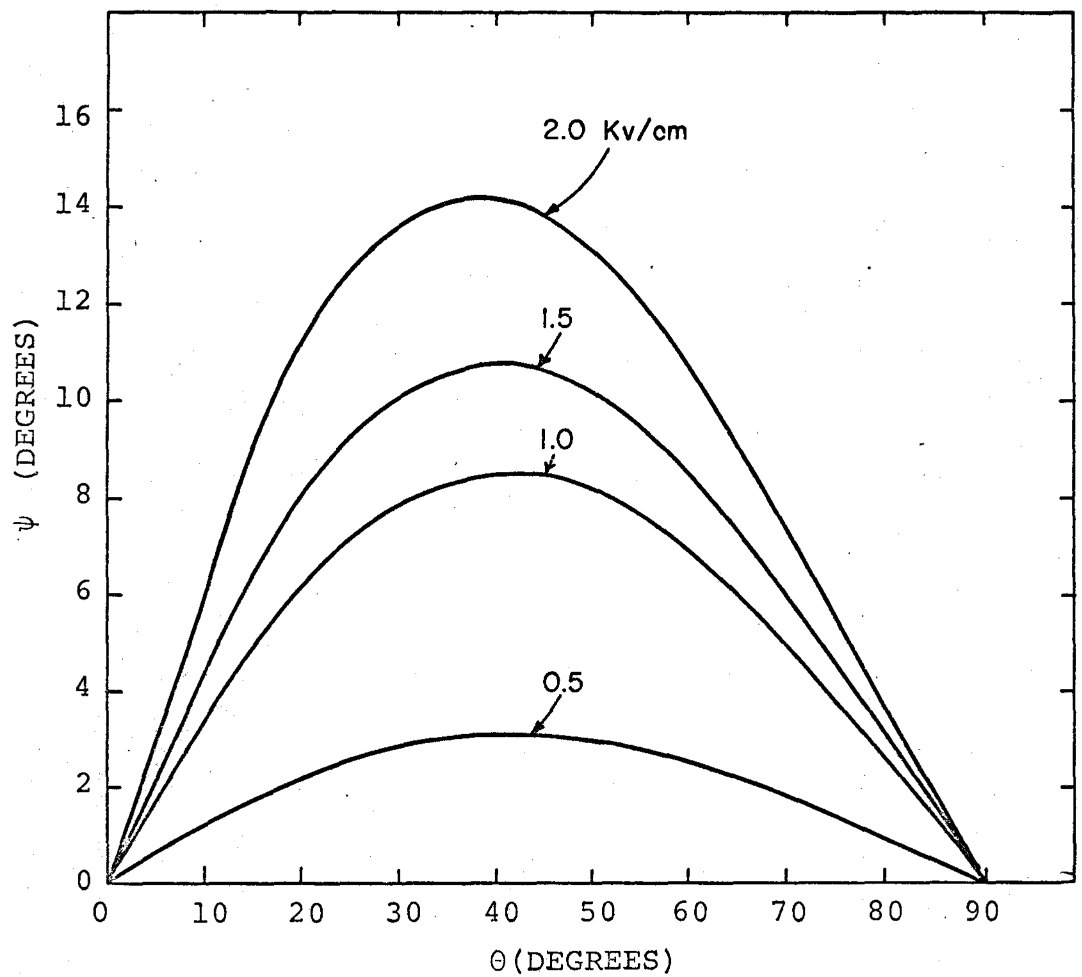

FIGURE 6.4: The Angle of Rotation of the Microwave Current Vector in an 11.4 ohm cm n-type Germanium against Θ for Various Values of the Applied D.C. Field.

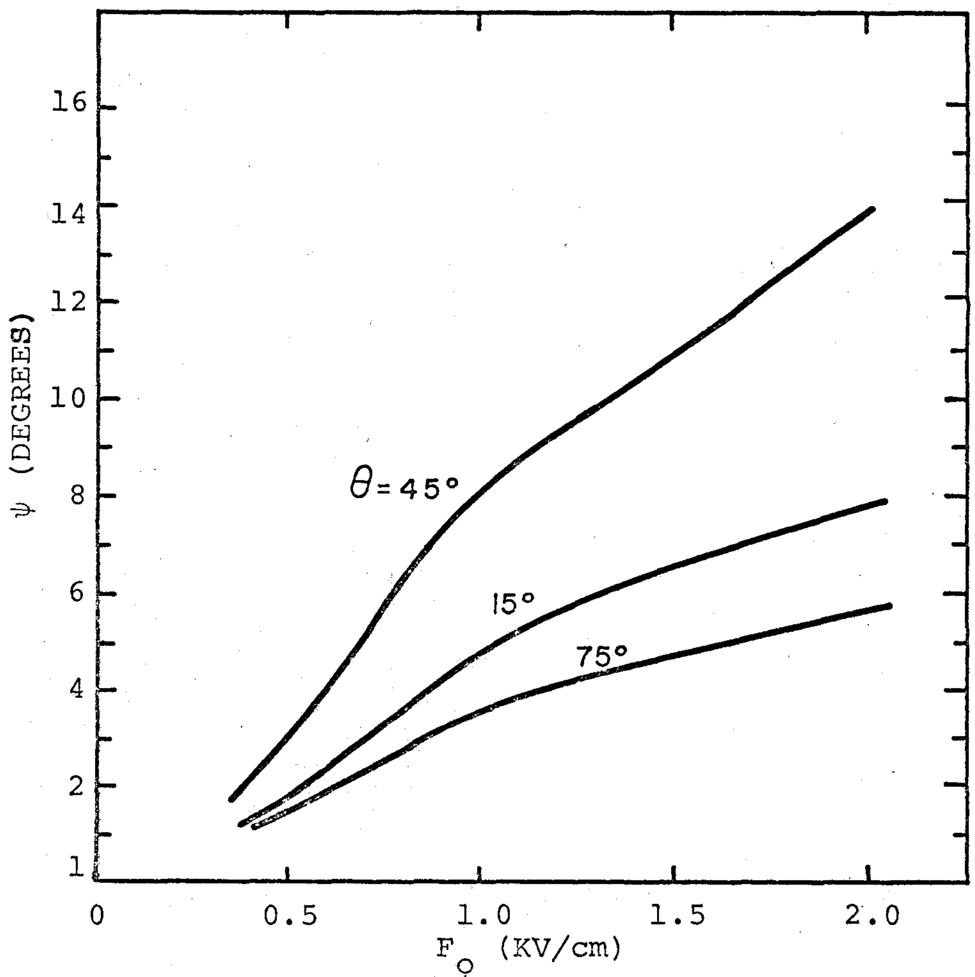

FIGURE 6.5: Computed Curves of the Angle of Rotation of the Microwave Current Vector in an 11.4 ohm cm n-type Germanium as a function of the D.C. Field Strength.

selection of 10 GHz or more precisely 9.381 GHz as the experimental frequency is that the value of $\omega\tau$ is small at this frequency ($\omega\tau \doteq 0.25$). This ensures the observation of only the angular dependence of the real part of the microwave conductivity and allows us to neglect the imaginary part of the microwave conductivity. The reasons for choosing 11.4 ohm-cm, n-type germanium are that it shows hot electron effects and it has low joule heating for the large samples required for 10 GHz measurements. The experimental programme of this section consists of the following jobs:

(a) the construction of non-injecting contacts ;

(b) the measurement of the d.c. current-voltage characteristcs in an 11.4 ohm-cm, n-type germanium sample ;

(c) the measurement of the small-signal microwave conductivity in the same sample as a function of the angle between the microwave and d.c. field vectors.

One of the important considerations in the design of the sample is that the same sample be used for all measurements. This ensures that the sample has the same electrical properties with respect to the crystallographic direction. The samples of Ge with dimensions 3 x 2.5 x 0.2 cm were cut in a plane perpendicular to <111> from a large block of n-type germanium crystal by means of a 20-mil diamond-head wheel cutter. Figure 5.6 was used to determine the thickness of the sample. This figure shows that the deviation of the magnitude of the reflection coefficient by the pulsed field is maximum in

0.2 cm thick sample. The sides of the samples were determined to cover the cross-section of the waveguide at various angles between the d.c. and microwave field vectors.

6.6.1 The Construction of Non-Injecting Contacts

One of the main difficulties in the measurement of the conductivity of semiconductors at high electric fields is the preparation of non-injecting contacts. An injecting contact modulates the conductivity of a semiconductor sample by way of injecting minority carriers and cause a deviation in the high field conductivity effect. Before taking measurements, one should therefore ensure that the contacts are non-injecting.

Injection is usually eliminated by preparing a sample in the dumbbell form so that any minority carriers that may be injected may not reach the main filament during the pulse period. The construction of non-injecting contacts in a rectangular sample, as required in the microwave measurements, has been found to be a major problem.

A number of authors[63-64] described a method of preparing non-injecting contacts by means of electroplating a solution of gold on a Ge-sample (plating solution: 1.2 gm $KAu(CN_2)$, 1 gm k(CN) per 100 ml. distilled water) and soldering to the gold surfaces with a hot soldering iron. A similar but a slightly different technique has been adopted in the present work. The procedure is as follows:

All faces of the samples were polished with a fine SiC emery paper and cleaned for a few seconds in warm chloroform, alcohol, and distilled water, respectively. The edges of the samples were then wetted with HF. Contacts to the Ge-slabs were made by first depositing a few microns (5-6μ) of gold mixed with traces of antimony on the sample edge by the vacuum deposition technique and then soldering tin-antimony solder to the gold surfaces using a polyflux. An Edward's Model 12E3 Vacuum-coating unit was employed for the deposition of gold. The unit has a four-position filament holder to allow successive evaporations without disturbing the vacuum. Molybdenum boats were used as filaments for the evaporation of gold. Ge samples were hung in the vacuum chamber with wires. The surfaces of the samples were covered with a cleaned tape where deposition was not wanted.

Some contacts were also made in an alloying furnace, after the usual cleaning procedure. A 0.010 inch strip of tin-antimony solder was sandwiched between one sample edge and a nickel strip, and the combination was joined in an alloying furnace in the presence of pure hydrogen. Best results were, however, obtained by the vacuum deposition technique.

Gold was chosen because of its high resistance to oxidation and low electrical contact resistance. Care was taken to ensure that the gold did not melt during the soldering operation.

6.6.2 D.C. Measurements of the Current-Voltage Characteristics

The current-voltage characteristics of an n-type germanium sample was measured using the experimental arrangement of Figure 6.6. The room temperature d.c. resistivity of the sample was found to be 11.4 ohm cm by 4-point probe method. To avoid joule heating in the sample, pulsed electric fields of 0.5 μsec. duration were employed, with repetition rates of 1 p/s. The sample was first matched to the pulse generator by means of a parallel chain of resistors, to ensure a single well-shaped rectangular pulse. The current through the specimen was determined by measuring the voltage across a 2 ohm resistor. The voltage across the specimen was measured independently. Both current and voltage measurements were taken with the aid of a Tektronix type 585 oscilloscope.

6.6.3 Microwave Measurements

A photograph of the equipment used for the measurement of the change in the reflection coefficients during the period of the pulse field is as shown in Figure 2.12. The sample holder was connected to one side arm of the reflection bridge in vertical position. The sample was allowed to rest between the flange and a high-precision short-circuit plate (Fig. 6.7). To apply pulsed d.c. fields, the sample was insulated carefully from the waveguide circuits with thin polyethelene films. The big advantage of this holder is the ease of rotation of the sample with respect to the microwave field vectors.

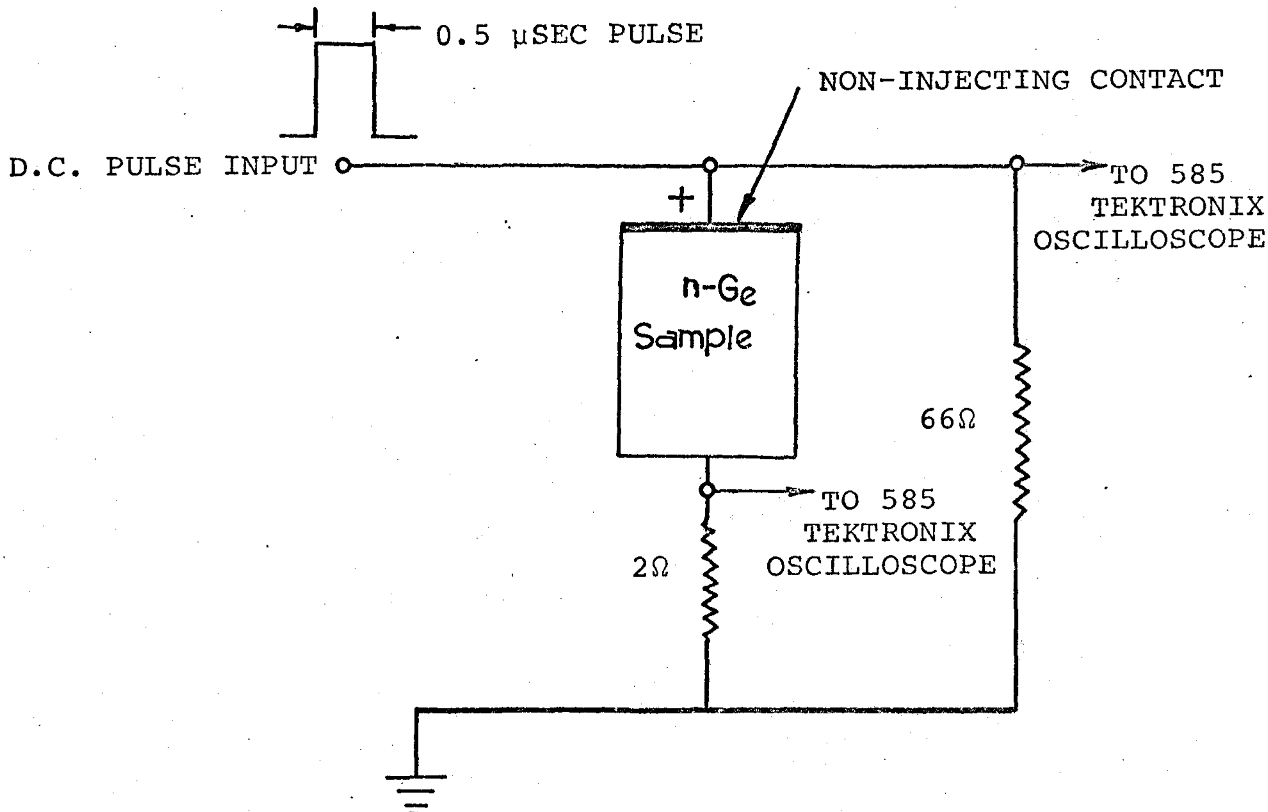

FIGURE 6.6: Network for Measuring Current and Voltage Applied to the Sample.

The I.F. amplifier used was a wide-band amplifier centered at 30 Mc/s. The difference frequency of 30 Mc/s from two X-13 Klystrons was amplified and displayed on a wide-band Tektronix type 585 oscilloscope.

The reflection coefficient of the sample was measured with the microwave bridge discussed in Chapter II. At first, no d.c. pulse was applied and the real part of the microwave conductivity was deduced from the reflection coefficient measured, using Figure 5.5. Then pulses were applied resulting in a change of reflection coefficient that caused an a.c. output in the E-arm of the bridge. A previous adjustment was made in the bridge for a zero output level. The a.c. output was then amplified during the period of the pulse by the I.F. amplifier and was displayed on the oscilloscope. The sketch of such an I.F. amplification system is shown in Figure 6.8. The precision attenuator and the precision short circuit were next adjusted to bring the I.F. output level of the pulse period to the zero position. Initially a 0.5 μsec pulse was found to be inadequate for the response of the I.F. amplifier. Measurements were finally made with 2 μsec. pulse.

The noise pick-up from the discharge of the thyratron as observed on the scope was found to be of constant magnitude at a fixed pulse field level. This constant noise level was made negligible (1-2%) compared to the I.F. output level by maximizing the output of the I.F. amplifier on tuning the local

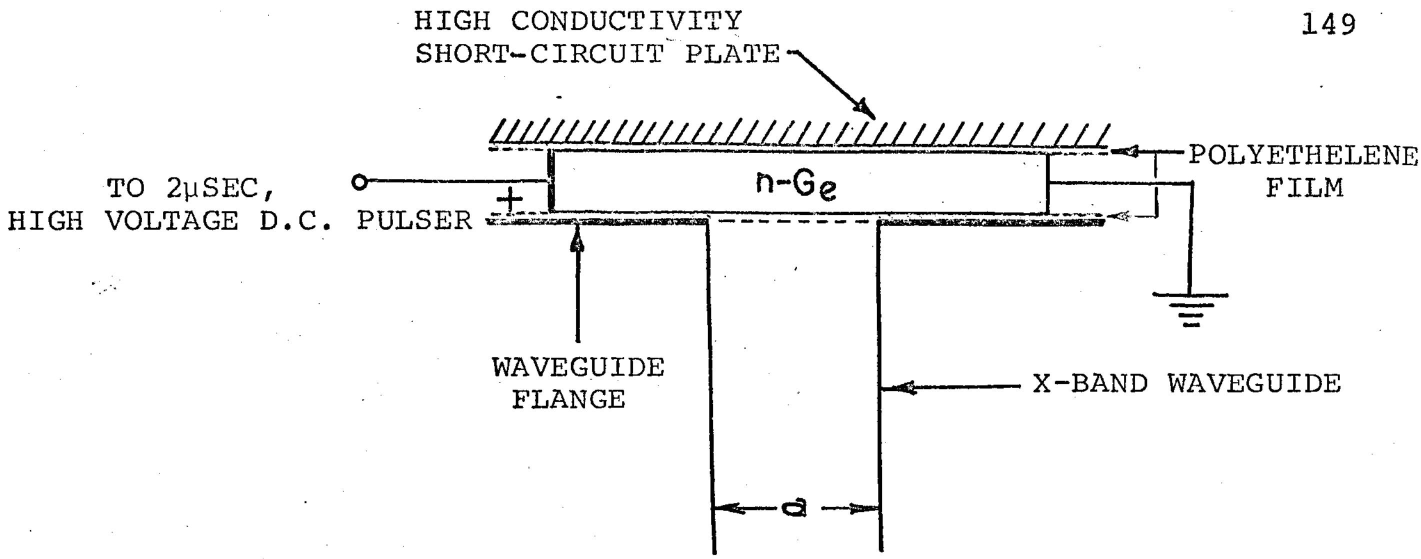

FIGURE 6.7: The Sample Holder for the Microwave Measurements.

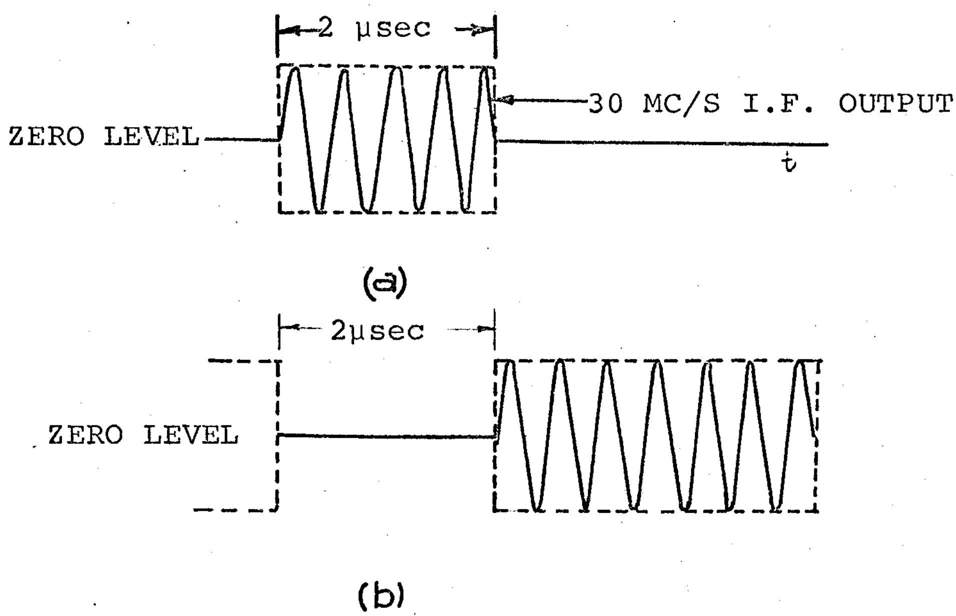

FIGURE 6.8: (a) The 30 MC/S I.F. Output caused by the Pulsed D.C. Field.

(b) The Same I.F. Output after Adjusting the Bridge to a Null Balance.

oscillator. The a.c. output level during the pulse period was found easier to balance than a corresponding d.c. level. A linear gain of the amplifier at input levels, caused by the pulsed field and the absence of the injection of the minority carriers are required for accurate measurements.

Measurements were made for the conditions when $\Theta=0^{\circ}$, 40°, and 90°. The principal consideration of selecting $\Theta=40^{\circ}$ as one experimental angle between the microwave and d.c. field vectors is that the theoretical conductivity at this angle was found intermediate between the parallel and perpendicular conductivity.

It will be noted that the presence of insulation changes the resistivity from the absolute value, 11.4 ohm cm. However, the absolute values of resistivity are not required as the comparison between theory and experiment is made on the basis of relative changes in the sample conductivity.

6.7 Results and Discussion

The results of high field measurements at room temperature are given in Figures 6.9 and 6.10. D.C. data is plotted in Figure 6.9, which shows the current density in an 11.4 ohm cm, n-type Ge sample as a function of electric field intensity. Microwave data (marked 0, x ,●) is presented in Figure 6.10 where all quantities are normalised to their corresponding values at zero d.c. field. The real part of the small-signal microwave conductivity calculated from theory (curves a,b,c) is also presented in Figure 6.10. The curves

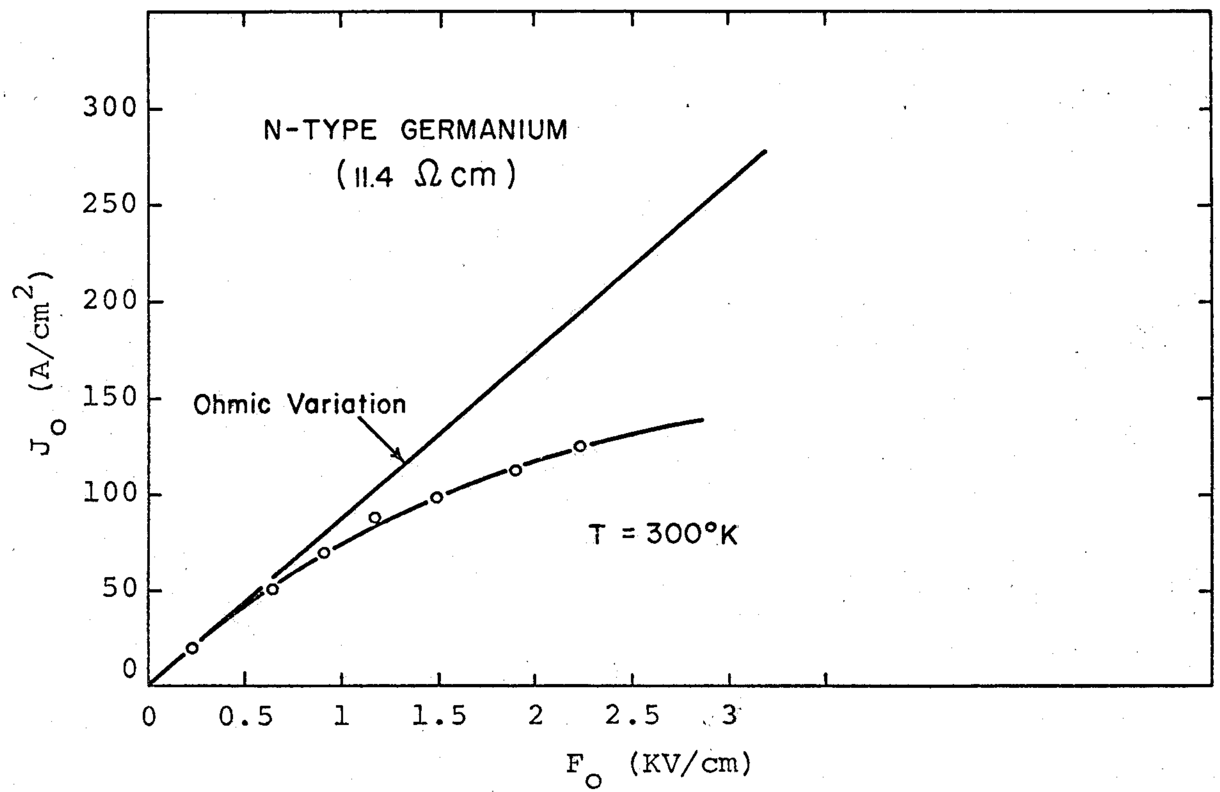

FIGURE 6.9: D.C. Current Density versus Electric Field Strength in an 11.4 ohm cm n-type Germanium Sample.

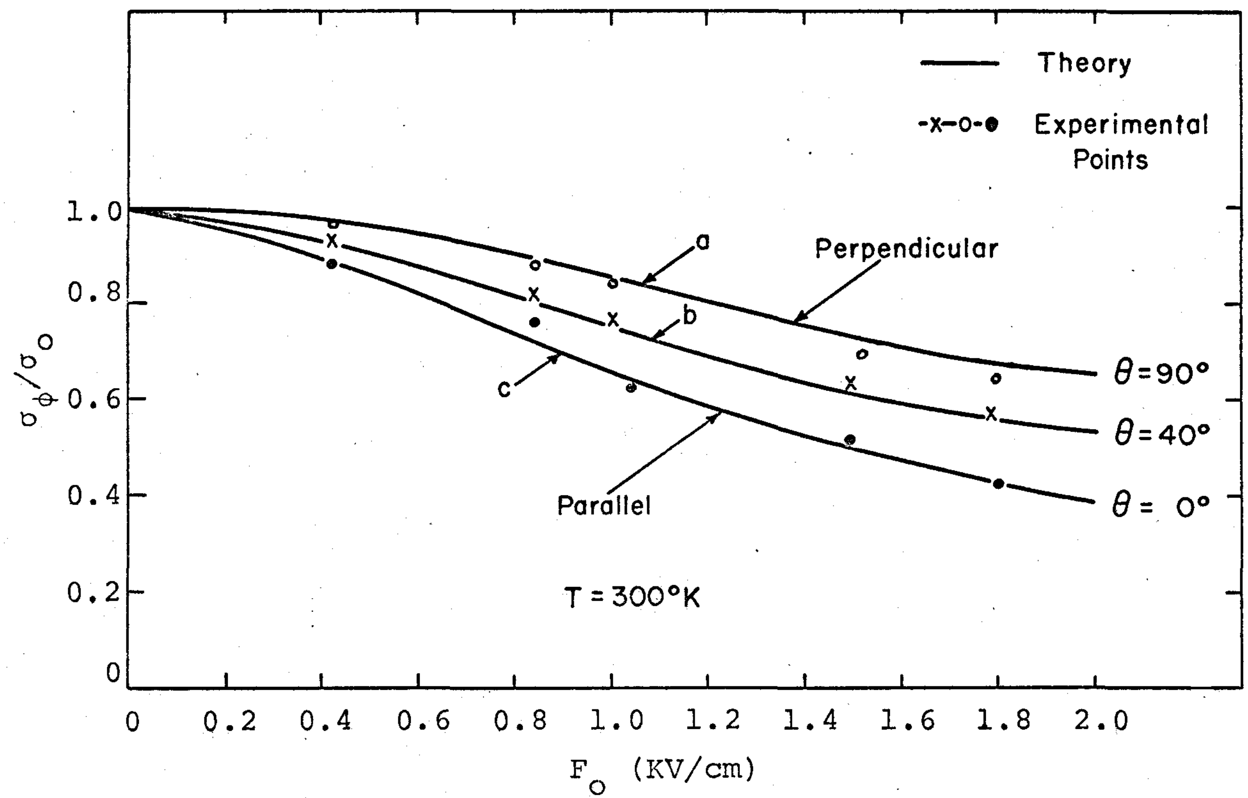

FIGURE 6.10: Microwave Conductivities of an 11.4 ohm cm n-type Germanium Sample at 9.381 GHz for parallel, perpendicular and 40^o Field Orientations.

a $\sigma_\perp/\sigma_o$ deduced from 300^{o}k d.c. data

b $\sigma_{\Theta=40^o}/\sigma_o$ calculated from equation 6.13

c σ_{11}/σ_o deduced from 300^{o}k d.c. data a and c, which represent perpendicular and parallel conductivity, respectively are deduced from room temperature d.c. data (Figure 6.9), while the curve 'c' is calculated from equation 6.13. The experimental results are found to be in fair agreement with the theoretical values.

The measurements of the microwave conductivity were limited to 1.8 kv/cm because of the large sample length required to cover the cross-section of the waveguide, and because of the consequent sparking and surface breakdown problems encountered.

It is to be noted that this measurement for the conditions of the d.c. field vector directed at an angle to the microwave field vector is a unique one. It would be worthwhile also to take measurements in other materials such as InSb, in which the anisotropic effect[33, 34] has been reported to be strong at low fields (120V/cm) at 77°k. Consequently the problem of injection at high fields will be minimised.

---

† The electrons in germanium has four equivalent minima in k space along [111] directions, where the constant energy surfaces are ellipsoids. For the applied electric fields in the [100] direction, the effective mass is the same in each valley. For other directions of the field, the situations is more complicated and particularly at low temperature. However, at room temperature the current densities as a function of electric field for various orientation differ by less than 5% [20,29]. Thus, it appears that the assumption of spherical energy surfaces is a good approximation for electrons. This footnote has been mentioned on page 125.

CHAPTER VII

CONCLUSIONS

7.1 General

A method for the measurement of the microwave conductivity of a semiconductor sample subjected to a high d.c. electric field has been described, which provides for varying the angles between the microwave and applied d.c. electric field vectors. The method depends on the placement of a semiconductor sample at the open end of a rectangular waveguide ; the conductivity of the sample is inferred from the measurements of the reflection coefficient at the air-semiconductor interface. The measuring system developed is not only suitable for high-field measurements, but it is also advantageous for the normal measurements of the conductivity and dielectric constant of semiconductors at microwave frequencies.

The objectives of this thesis were to study and measure the microwave conductivity of semiconductors in the presence of a high electric field and in particular, the dependence of the microwave conductivity on the angle between the microwave and d.c. field vectors. For the parallel field case, a theory, as well as a measuring system, has been reported in the literature[20, 24]. The measuring system consists of a 'transmission bridge' for the measurement of the propagation constant of a rectangular waveguide, partially filled with a semiconductor sample. The principal disadvantages of such a system are:

(a) The propagation constant of the partially filled waveguide does not have a simple relationship with the conductivity of the sample.

(b) The desirable variation of the angle between the microwave and d.c. field vectors cannot be achieved.

(c) The mounting of the sample in the waveguide, as well as insulating the sample from the waveguide circuit, is a difficult process to achieve.

The development of a measuring system that could be suitable for high-field measurements was, therefore, required.

Chapters II to V, which cover a major portion of this thesis, are devoted to the development of such a measuring system, consisting of a microwave reflection-type bridge(13), while Chapter VI is devoted to the investigation of the small-signal anisotropic conductivity of n-type germanium in the presence of a high electric field.

7.2 The Microwave Reflection Bridge

The theory of operation of a reflection-type bridge, together with its practical setting-up procedure, has been presented in Chapter II. A method is also described for the correction of the measurement error, which arises from the scattering coefficients at the input ports of the precision attenuator (one of the standard components of the bridge).

Experiments have been carried out to measure the scattering coefficients of two commercially available rotary-vane precision attenuators. Measured values of the magnitude and phase of these scattering coefficients, which are summarised in Figures 2.5 and 2.6, have been found to be in good agreement with the calculated values. The relative error in the measured magnitudes of the reflection coefficients due to S_{11}, which is indicated in Figure 2.4, is found to be a function of the magnitude of the measured reflection coefficient.

7.3 Microwave Reflections from the Surface of a Block of Semiconductor

A theoretical analysis has been made of the microwave reflections from the surface of a block of semiconductor placed at the end of a rectangular waveguide. The following waveguide configurations were considered for the purpose of analysis:

(a) a semiconductor slab placed inside a rectangular waveguide and terminated by a short-circuit metal plate (Figure 1.1);

(b) a semiconductor slab pressed at the end of a rectangular waveguide opening onto a metal flange and terminated by a short-circuit metal plate (Figure 1.2);

(c) a semiconductor slab placed at the end of a rectangular waveguide and followed by free space (Figure 1.3).

The approximate and exact solutions of the reflection coefficients at the plane z=0 of these configurations are presented, together with experimental verifications wherever possible. During the analysis a new method of measurement, involving the placement of a semiconductor sample at the open end of a rectangular waveguide, is developed. The method has been termed the "open-end-waveguide measuring technique".

7.3.1 The Approximate Solution of the Reflection Coefficient for a Finite Semiconductor Medium

The approximate solution for the reflection coefficients at the plane z=0 of Figures 1.2 and 1.3 for a finite medium is developed in Chapter III. This solution, which has been based on the assumption of a z-directed TEM wave propagating in the semiconductor region, is derived from the consideration of the input impedance at the air-semiconductor interface plane. The appropriate expressions for the microwave conductivity and dielectric constant are also derived in terms of the measurable quantities A and ϕ (Equation 3.14).

The assumption that the electromagnetic wave in the semiconductor region is a TEM wave, is approximately justified. It is because of this reason that the solutions are approximate.

Numerical computions, as related to operation at 9.522 and 34.5 GHz, show that these approximate solutions apply only to semiconductors of low resistivity ($\sigma > 2\omega\varepsilon_o\varepsilon_r$).

7.3.2 The Exact Solution of the Reflection Coefficient for a Semi-Infinite Medium

The exact solution of the reflection coefficient at the plane z=0 of Figure 4.1(a) for a semi-infinite medium with complex permittivity is developed in Chapter IV. This solution, which has been based on a radiative propagating wave in the half-space z>0 is arrived at by modifying the original formulation by Lewin[43] in the case of a lossless medium (air). This solution has been extended to the case of rectangular and parallel-plate waveguides with bounded ground planes (Figures 4.2 and 4.3). An alternative solution to the rectangular waveguide with bounded planes, based on the conservation of power similar to that of Harrington[44], is also presented. Further, it is noted that the solutions which are presented are not completely exact and have been obtained on the assumption of an aperture field (field at z=0) equal to that of the dominant incident mode.

Numerical computations, as related to operation at 9.522 and 34.5 GHz are made for the reflection coefficient of the waveguide structure of Figure 4.1(a) with germanium, selectron, and air in the half-space. The results are given in Figures 4.4 through 4.7.

Experimental verifications of the theoretical analysis have been made with n-type germanium of various resistivity (0.1, 1, 5, 10, 25, 50 ohm cm), selectron, and air at the end of the waveguide system of Figure 4.1(a), using a microwave reflection-type bridge discussed in Chapter II.

The results of the reflection coefficient measurements, which are summarised in Figures 4.6 and 4.7, are found to agree with those obtained from calculations.

The values of resistivity as measured by microwave methods at 34.5 GHz show good agreement with those measured by the d.c. 4 probe method. At 9.522 GHz measurements, however, the agreement is not very good. This comparison is shown in Tables 4.2 and 4.3. The possible reason for the discrepancy at X-band is the finite size of the samples used, particularly the 0.26 and 45.76 ohm cm ones, which is insufficient to satisfy the condition of a semi-infinite medium assumed in the theory. At Q-band, the same samples may satisfy the condition of a semi-infinite medium because of the smaller skin depth. The other reasons for the discrepancy have been discussed in Section 4.8.

7.3.3 The Exact Solution of the Reflection Coefficient For a Finite Medium

Heaton and Pal[16], in a recently published paper, derived an expression for the reflection coefficient of a semiconductor slab placed across the open end of a rectangular waveguide. Their theory, which is not essentially different from that of Lindmayer and Kutsko[7], has been based on an unbounded wave propagating in the axial direction in the semiconductor slab. They assume that the z-directed propagation constant in the semiconductor region is of the form $\gamma_z = j\omega\sqrt{\mu\varepsilon_o\hat{\varepsilon}_r}$. This is not completely justified, particularly for semiconductor samples with low $\hat{\varepsilon}_r$, when the wave may propagate in the transverse directions as well.

A more general solution of the reflection coefficient of a slab with complex permittivity, held against the waveguide flange and followed by a short circuit conductivity plate, is developed in the same manner as used by Compton[47] and Crosswell[48] and is given in Chapter V. This technique has also been applied to the admittance of a rectangular waveguide system radiating into a lossless plasma layer.

Numerical computations are made for the Ge slab case for varying values of resistivity and thickness at 9.53 GHz and 34.5 GHz.

Experiments which confirm the theory have been performed at 9.53 GHz. The results, which are shown in Figure 5.5, indicate that the solution given by the cited authors[16] is approximately correct for low resistivity samples and is incorrect for high resistivity ones ($\sigma<2\omega\varepsilon_o\varepsilon_r$).

Numerical calculations are also made for a plasma layer case. The results of these calculations, which agree with those given by the other authors[49-51], are presented in Figures 5.9 through 5.13.

Finally, we must point out that the important results of the microwave reflections have been summarised in Figures 4.6, 4.7, 5.5, and 5.6. The "open-end-waveguide measuring technique", as mentioned earlier, utilizes these design curves for the determination of the microwave conductivity and the dielectric constant.

7.4 Anisotropy of the Small-Signal Microwave Conductivity of N-Type Germanium in the Presence of a High Electric Field

A simple theory of the small-signal microwave conductivity of a semiconductor in the presence of a high electric field directed at an angle Θ to the microwave field vector, is developed. The conductivity is found to depend on the parallel and perpendicular conductivities and also on the angle between the microwave and d.c. field vectors (Equation 6.13). A theoretical analysis has also been made of the parallel and perpendicular conductivities of n-type germanium in the same manner as used by Nag and Das[23] for the calculation of the parallel conductivity (Section 6.3). The solution to the problem is obtained by solving the appropriate Boltzmann equation, taking into account the effect of both acoustic and optical phonon scattering, and assuming an isotropic effective mass as in the analysis of Nag and Das[23].

Numerical calculations have been made of the microwave conductivity and the angle of rotation of the microwave current vector for an 11.4 ohm cm n-type germanium sample at 9.381 GHz as related to experiments. These calculations, which are plotted in Figures 6.3 through 6.5, show that the microwave conductivity increases with Θ and becomes maximum when $\Theta=90^{\circ}$ (Figure 6.3), where as the angle of rotation of the microwave current vector first increases with Θ, then becomes maximum when $\Theta=40^{\circ}$ and finally decreases to zero when $\Theta=90^{\circ}$ (Figure 6.4).

To obtain data to confirm the theory, measurements have been made of the conductance as a function of the electric field intensity in the same germanium sample (11.4 ohm cm) at d.c. and 9.381 GHz. The reasons for choosing 11.4 ohm cm, n-type germanium are that it shows hot electron effects and it has low joule heating for the large samples required for 10 GHz measurements. D.c. measurements which are summarised in Figure 6.9 have been used for the determination of d.c. conductivity J/F and differential conductivity $\partial J/\partial F$. These results are given in Figure 6.10 and provide a basis for comparison with the microwave measurements. The reflection coefficient bridge was used to determine the microwave conductivity as a function of the amplitude of the electric field, applied in the form of short pulses. The method of measurement was the "open-end-waveguide measuring technique", which allowed the angle between the microwave and d.c. field vectors to be varied. The microwave measurements were made at $\Theta=0^{\circ}$, 40° and 90° with applied electric fields up to 1.8 KV/cm. The design charts of Figures 5.5 and 5.6 were used to relate the VSWR or reflection coefficients to the conductivity of the sample.

The results of microwave measurements which are summarised in Figure 6.10, are found to agree with the calculated values. The microwave conductivity for $\Theta=40^{\circ}$ was evaluated from equation 5.13. These results confirm that the microwave conductivity in the presence of a high electric field is indeed dependent on the angle between the microwave and d.c. field vectors. It is to be noted that this measurement for the conditions of the d.c. field vector directed at an angle to the microwave field vector is a unique one.

For future investigation it is recommended that measurements should be made in other materials, such as InSb, in which the anisotropic effect[34, 63] has been reported to be strong at low fields (120 V/cm) and at $77^{\circ}K$. Consequently, the problems of injection of the minority carriers during measurements at high electric fields will not arise.

Finally, we conclude by saying that the results of this investigation, which confirm the existence of the anisotropic effect in n-type germanium, prove the feasibility of operation of a new microwave device, namely "the hot electron microwave rotator". The theoretical performance of such a rotator has been investigated elsewhere by the author[57].

APPENDICES

APPENDIX-A

DERIVATION OF THE EQUATIONS (3.14a) AND (3.14b)

Equations (3.12) and (3.13) yield the following equation

$$\hat{\varepsilon}_r = \left[1 - (f_c/f)^2\right] \left[\frac{1 + e^{-(A + j\phi)}}{1 - e^{-(A + j\phi)}}\right]^2 . \quad \text{(A-1)}$$

It may be shown that[65],

$$\left[\frac{1 + e^{-(A + j\phi)}}{1 - e^{-(A + j\phi)}}\right] = |Y_n| e^{j\Theta} \quad \text{(A-2)}$$

where $$|Y_n| = \left[\frac{\cosh A + \cos\phi}{\cosh A - \cos\phi}\right]^{1/2} \quad \text{(A-3)}$$

and $$\Theta = -\tan^{-1}\left[\frac{\sin\phi}{\sinh A}\right] . \quad \text{(A-4)}$$

Substituting equation (A-2) in equation (A-1),

$$\hat{\varepsilon}_r = \left[1 - (f_c/f)^2\right] \left[|Y_n|^2 \cos 2\Theta + j |Y_n|^2 \sin 2\Theta \right] . \quad \text{(A-5)}$$

Equations (3.14a) and (3.14b) may now be obtained by equating the real and the imaginary parts of (A-5) and subsequently using equation (A-3) and (A-4).

APPENDIX-B

DERIVATION OF THE ADMITTANCE EQUATION (4.15)

Substitution of equations (4.7) and (4.9) in equation (4.14) yields the following identity,

$$\left(\frac{\partial}{\partial x^2} + k_o^2\right) \left[\frac{1}{jk_1} (1-R) \sin(\frac{\pi x}{a}) + \sum_1^\infty \sum_0^{\infty}{}' A_{mn} \sin(\frac{m\pi}{a} x) \cos(\frac{n\pi}{b} y)\right]$$

$$= \frac{1}{2\pi} \int_0^a \int_0^b E(x', y') \left[\frac{\partial^2}{\partial x^2} + \hat{k}^2\right] \frac{e^{-j\hat{k}r}}{r} dx' dy' \tag{B-1}$$

where

$$r\Big|_{z=0} = \left[(x - x')^2 + (y - y')^2\right]^{1/2}. \tag{B-2}$$

Differentiating the first term in the parenthesis of equation (B-1) on the l.h.s. and substituting the equation (4.13) for A_{mn}, we obtain

$$1 - R = \frac{jk_1}{\left\{k_o^2 - (\frac{\pi}{a})^2\right\} \sin(\frac{\pi x}{a})} \left[\frac{1}{2\pi} \int_0^a \int_0^b E(x', y') \cdots\right.$$

$$\left\{\frac{\partial^2}{\partial x^2} + \hat{k}^2\right\} \frac{e^{-j\hat{k}r}}{r} dx' dy' + \sum_1^\infty \sum_0^{\infty}{}' \frac{4}{ab} \frac{\varepsilon_{mn}}{\gamma_{mn}} \left(\frac{\partial^2}{\partial x^2} + k_o^2\right) \cdots$$

$$\left.\int_0^a \int_0^b E(x', y') \sin(\frac{m\pi}{a} x') \cos(\frac{n\pi}{b} y') dx' dy' \sin(\frac{m\pi}{a} X) \cos(\frac{n\pi}{b} y)\right]. \tag{B-3}$$

Application of equations (B-3) and (4.12) results

$$\frac{1-R}{1+R} = \frac{jk_1}{\left\{k_o^2 - (\frac{\pi}{a})^2\right\} \quad \sin(\frac{\pi x}{a})} \quad \frac{ab}{2D_1}\left[\frac{1}{2\pi} \int_0^a \int_0^b E(x', y') \left\{\frac{\partial^2}{\partial x^2} + \hat{k}^2\right\} \cdots \right.$$

$$\frac{e^{-j\hat{k}r}}{r} dx'\, dy' + \sum_1^{\infty} \sum_0^{\infty} \frac{4}{ab} \frac{\varepsilon_{mn}}{\gamma_{mn}} \left(\frac{\partial^2}{\partial x^2} + k_o^2\right) \int_0^a \int_0^b E(x', y')$$

$$\left. \sin(\frac{m\pi}{a} x') \cos(\frac{n\pi}{b} y')\, dx'\, dy' \sin(\frac{m\pi}{a} X) \cos(\frac{n\pi}{b} y) \right] \quad \text{(B-4)}$$

$$\text{where } D_1 = \int_0^a \int_0^b E(x', y') \sin(\frac{\pi}{a} x')\, dx'\, dy' \;. \quad \text{(B-5)}$$

Multiplication of the numerator and denominator of equation (B-4) by $\int_{x=0}^{a} \int_{y=0}^{b} \sin(\frac{\pi x}{a}) dxdy$ gives the desired equation (4.15).

APPENDIX-C

THE TRANSFORMATION OF THE QUADRUPLE INTEGRAL EQUATION (4.20) INTO THE DOUBLE INTEGRAL EQUATION (4.21)

With the change of variables

$$x + x' = a + \upsilon \qquad x - x' = u$$

$$y + y' = b + \eta \qquad y - y' = v$$

we obtain

$$\sin(\frac{\pi}{a}x)\ \sin(\frac{\pi}{a}x') = \frac{1}{2}\left[\cos\frac{\pi}{a}(x - x') - \cos\frac{\pi}{a}(x + x')\right]$$

$$= \frac{1}{2}\left[\cos(\frac{\pi}{a}u) + \cos(\frac{\pi}{a}\upsilon)\right]$$

$$= \cos\frac{\pi}{a}(\frac{u+\upsilon}{2})\ \cos\frac{\pi}{a}(\frac{u-\upsilon}{2})$$

$$= \cos\frac{\pi}{a}(x - \frac{a}{2})\ \cos(x' - \frac{a}{2}) \qquad \text{(C-1)}$$

and replacing $\frac{\partial}{\partial x^2}$ by $-\frac{\partial}{\partial x \partial x'}$, which is permissible as r is a function of x - x' we obtain

$$\left(\hat{k}^2 + \frac{\partial^2}{\partial x^2}\right)\ \sin(\frac{\pi}{a}x)\ \sin(\frac{\pi}{a}x')$$

$$= \hat{k}^2\cos\frac{\pi}{a}(x - \frac{a}{2})\ \cos\frac{\pi}{a}(x' - \frac{a}{2}) - (\frac{\pi}{a})^2\ \sin\frac{\pi}{a}(x - \frac{a}{2})\ \sin\frac{\pi}{a}(x' - \frac{a}{2})$$

$$= \frac{\hat{k}^2}{2}\left[\cos\frac{\pi}{a}(x - x') + \cos\frac{\pi}{a}(x + x' - a)\right] - \frac{1}{2}(\frac{\pi}{a})^2\left[\cos\frac{\pi}{a}(x-x') - \cos\frac{\pi}{a}(x+x'-a)\right]$$

$$= \frac{1}{2}\left[\hat{k}^2 - (\frac{\pi}{a})^2\right]\left[\cos(\frac{\pi}{a}u) + \frac{\hat{k}^2 + (\frac{\pi}{a})^2}{\hat{k}^2 - (\frac{\pi}{a})^2}\cos(\frac{\pi}{a}\upsilon)\right], \qquad \text{(C-2)}$$

Thus equation (4.20) becomes

$$Y_n = j\frac{\left[\hat{k}^2 - (\frac{\pi}{a})^2\right]}{2\pi\ ab\ k_1} \int_0^a \int_0^a \int_0^b \int_0^b \left[\cos(\frac{\pi}{a}u) + \frac{\hat{k}^2 + (\frac{\pi}{a})^2}{\hat{k}^2 - (\frac{\pi}{a})^2}\cos(\frac{\pi}{a}\upsilon)\right] \cdots$$

$$\frac{e^{-j\hat{k}r}}{r}\ dxdx'dydy' . \qquad \text{(C-3)}$$

The change of axes and ranges of integration are shown in Figure C-1. Further†, replacing dxdx' by $\frac{1}{2}$ $du d\upsilon$ and dydy' by $\frac{1}{2}$ $dv d\eta$ and multiplying the result by 4 as the total integration is 4 times the integration in the first quadrant, one obtains

$$\int_0^a \int_0^a dxdx' = \frac{1}{2} \int \int du d\upsilon = 2 \int_0^a \int_0^{a-u} du d\upsilon \qquad \text{(C-4)}$$

and similarly

$$\int_0^b \int_0^b dydy' = \frac{1}{2} \int \int dv d\eta = 2 \int_0^b \int_0^{b-v} dv d\eta . \qquad \text{(C-5)}$$

Substituting equations (C-4) and (C-5) in equation (C-3),

$$Y_n = \frac{\left[\hat{k}^2 - (\frac{\pi}{a})^2\right] j4}{2\pi\ ab\ k_1} \int_0^a \int_0^{a-u} \int_0^b \int_0^{b-v} \left[\cos(\frac{\pi}{a}u) + \frac{\hat{k}^2 + (\frac{\pi}{a})^2}{\hat{k}^2 - (\frac{\pi}{a})^2}\cos(\frac{\pi}{a}\upsilon)\right] \cdots$$

$$\frac{e^{-jkr}}{r}\ du d\upsilon dv d\eta \qquad \text{(C-6)}$$

which can be reduced to equation (4.21).

---

† Page 92, Reference 43.

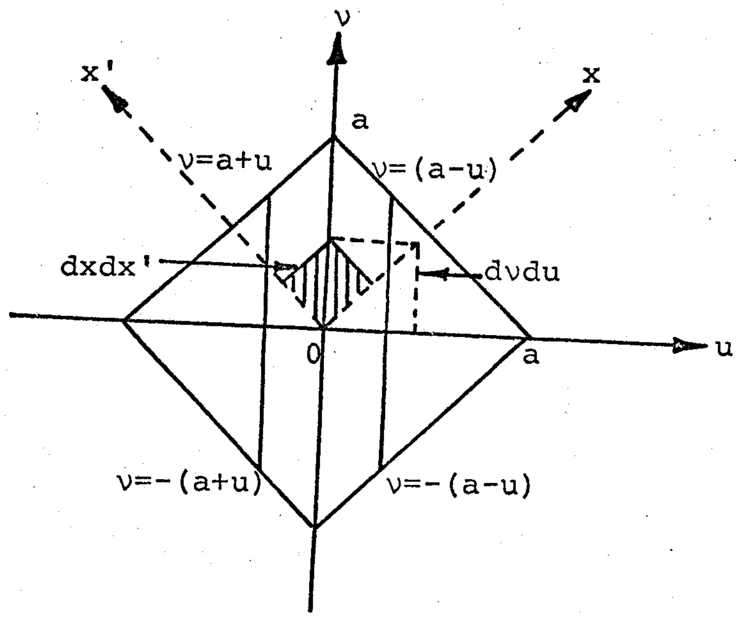

FIGURE C-1: The Change of Axes and the Ranges of Integration.

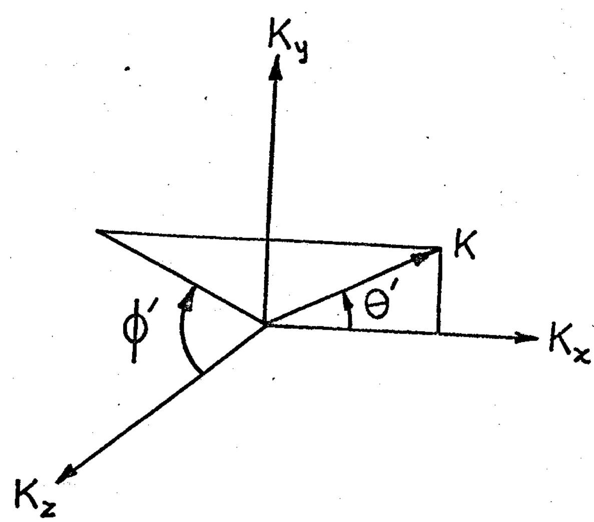

FIGURE D-1: The Wave Vector for the Carriers.

APPENDIX-D

THE ENERGY DISTRIBUTION FUNCTION FOR THE CARRIERS

A non-equilibrium distribution function for the carriers having the wave vector $\vec{k}$ can be represented by spherical harmonics of degree ℓ, which is of this type[66],

$$f(\vec{k}) = \sum_{\ell=0}^{\infty} k^{\ell} \{ a_{\ell} P_{\ell} (\cos\Theta') + \sum_{m=1}^{\ell} [a_{\ell}^{m} \cos m\phi' + b_{\ell}^{m} \sin m\phi'] \cdots$$

$$P_{\ell}^{m} (\cos\Theta') \} \qquad \text{(D-1)}$$

where $P_{\ell}(\cos\Theta')$ is the Legendre Polynomial and is given by

$$P_{\ell} (\cos\Theta') = \frac{(-1)^{\ell}}{\ell!} k^{\ell+1} \frac{\partial^{\ell}}{\partial k_z^{\ell}} \left(\frac{1}{k}\right)$$

$$P_0 (\cos\Theta') = 1$$

$$P_1 (\cos\Theta') = \cos \Theta'$$

$$\cos\Theta' = k_x/k \text{ and } k^2 = k_x^{\,2} + k_y^{\,2} + k_z^{\,2}$$

and the associated Legendre function

$$P_{\ell}^{m} (\cos\Theta') = (1 - \cos^2\Theta')^{m/2} \frac{d^m}{dk_x^{\,m}} \{ P_{\ell} (\cos\Theta')\} \qquad \text{(D-2)}$$

where Θ' is the angle between the wave vector k and k_x-axis, ϕ' is the angle between the projection of the wave vector on the $k_y k_z$ plane and the k_z-axis; a, b are constants and ℓ, m are integers.

The function may be approximately written as

$$f(\vec{k}) \doteq \sum_{\ell=0}^{\infty} \{ k^{\ell} a_{\ell} P_{\ell} (\cos\Theta') + k^{\ell} b_{\ell} \sin\phi' P_{\ell}' (\cos\Theta')$$

$$+ k^{\ell} a_{\ell} \cos\phi' P_{\ell}' (\cos\Theta')\} \qquad \text{(D-3)}$$

$$\doteq k^{o} a_{o} P_{o} (\cos\Theta') + \sum_{\ell=1}^{\infty} k^{\ell} a_{\ell} P_{\ell} (\cos\Theta') + \sum_{\substack{\ell=1 \\ \ell\neq 0}}^{\infty} \Big[k^{\ell} b_{\ell} \sin\phi' \ldots$$

$$P_{\ell}' (\cos\Theta') + k^{\ell} a_{\ell} \cos\phi' P_{\ell}' (\cos\Theta')\Big]$$

$$\doteq f_{o}(E) + f_{1}(E) \cos\Theta' + f_{2}(E) \sin\phi' \sin\Theta' + f_{3}(E) \cos\phi' \sin\Theta' \qquad \text{(D-4)}$$

which is the same as described by Moll[67]. The magnitudes of the coefficients f_1, f_2 and f_3 give the currents in the x, y, and z directions, respectively.

A detailed analysis by Reik and Risken[68] for the case of n-type germanium shows that the distribution function can be given by the approximate expansion of the first term in equation (D-3) for the current flow in the x-direction only. Since an x-directed d.c. field at an angle Θ to the microwave field produces a component of the current in the y-direction also, it is appropriate to include the second term in equation (D-3). Thus for the wave vector $\vec{k}$ lying on the k_x k_y plane, ϕ'=90° and the distribution function for the carriers becomes

$$f(\vec{k}) \doteq \sum_{\ell=0}^{\infty} k^{\ell} a_{\ell} P_{\ell} (\cos\Theta') + \sum_{\substack{\ell\neq 0 \\ \ell=1}}^{\infty} k^{\ell} b_{\ell} P_{\ell}' (\cos\Theta') \sin\phi'$$

$$\doteq a_o P_o (\cos\Theta') + k a_1 P_1 (\cos\Theta') + k a_1 P_1' (\cos\Theta')$$

$$= a_o + k a_1 \cos\Theta' + k a_2 \sin\Theta'$$

$$= a_o + k_x a_1 + k_y a_2 \qquad \text{(D-5)}$$

This may be finally written as

$$f(\vec{k}) = f(E) + k_x g(E) + k_y h(E) \qquad \text{(D-6)}$$

where k_x and k_y are the components of the wave vectors in x and y directions, respectively; g(E) and h(E) are the purturbed values of the distribution functions in the x- and y-directions, respectively; f(E) is the isotropic part of the distribution function and k_x g(E) and k_y h(E) are the anisotropic parts of the distribution function. When the external field is removed, the distribution function restores to the equilibrium, i.e. $f(\vec{k}) = f(E)$.

REFERENCES

1. Bardeen, J. and Brattain, W.H., "The Transistor, A Semiconductor Triode", Phys.Rev., Vol.74, pp.230-231, 1948.
2. Allerton, G.L. and Seifert, J.R., "Resistivity Measurement of Semiconductors at 9000 MC/S", IRE Trans. Instrum. I-g, pp. 175-179, 1960.
3. Jacobs, H., Brand, A.F., Meindl, J.D., Benanti, M. and Benjamin, R., "Electrodeless Measurement of Semiconductor Resistivity at Microwave Frequencies", Proc. IRE, Vol. 49, pp. 928-932, 1961.
4. Champlin, K.S. and Armstrong, D.B., "Explicit Forms For the Conductivity and Permittivity of Bulk Semiconductors", Proc. IRE (Correspondence), Vol. 50, pp. 232-232, 1962.
5. Nag, B.R. and Roy, S.K., "Microwave Measurement of Conductivity and Dielectric Constant of Semiconductors", Proc. IRE, Vol. 50, pp. 2515-2516, 1962.
6. Bhar, J.N., "Microwave Techniques in the Study of Semiconductors", Proc. IEEE, Vol. 51, pp. 1623-1631, 1963.
7. Lindmayer, J. and Kutsko, M., "Reflection of Microwaves from Semiconductors", Solid State Electronis, Vol. 6, pp. 377-381, 1963.
8. Champlin, K.S., "Frequency Dependence of High Frequency Transport Properties of Cubic Crystals", Phy. Rev., Vol. 130, pp. 1374-1377, 1963.

9. Champlin, K.S., Armstrong, D.B. and Gunderson, P.D., "Charge Carrier Inertia in Semiconductors", Proc. IEEE, Vol. 52, pp. 677-685, 1964.

10. Gunn, M.W. and Brown, J.B., "Measurement of Waveguide Properties in a Slotted Waveguide Structure", Proc. IEEE, Vol. 112(3), pp. 463-468, 1965.

11. Brodwin, M.E. and Pau-Sun, Lu, "A Precise Cavity Technique for Measuring Low Resistivity of Semiconductors", Proc.IEEE (Correspondence), Vol. 53, pp. 1742-1743, 1965.

12. Champlin, K.S. and Glover, G.H., "Gap Effect in the Measurement of Large Permittivities", IEEE Trans. MTT (Correspondence), Vol. 14, pp. 397-398, 1966.

13. Champlin, K.S. and Holm, J.D., "Analysis and Calibration of a Reflection Coefficient Bridge for Use with any Waveguide Mode", IEEE Trans. MTT, Vol. MTT-15, pp. 447-448, 1967.

14. Gunn, M.W. and Sheikh, R.H., "Wave Propagation in Rectangular Waveguide with a Semiconducting Wall", Proc. IEE, Vol. 115, pp. 32-36, 1968.

15. Sheikh, R.H., "Complex Permittivity of Germanium at Microwave Frequencies", Doctoral Thesis, McMaster University, pp. 39, 1968.

16. Heaton, A.G. and Pal, D.K., "Determination of Semiconductors Resistivity by Microwave Measurements", Proc. IEE, Vol. 115, pp. 742-746, 1968.

17. Bilenko, D.I., Kats, L.I. and Malinin, L.V., "Reflection of Electromagnetic Energy from Semiconductors in the Millimeter Range of Wavelengths", Soviet Physics - Semiconductors, Vol. 2, pp. 35-38, 1968.

18. Hines, M.E., "Network Integration Approaches for Multiple-Diode High Power Microwave Generation", G-MTT International Microwave Symposium Digest, pp. 46-53, 1968.

19. Arthur, J.B., Gibson, A.F. and Granville, J.W., "The Effect of High Electric Fields on the Absorption of Germanium at Microwave Frequencies", J. Electronics, Vol. 2, pp. 145, 1956.

20. Gibson, A.F., Granville, J.W. and Paige, E.G., "A Study of Energy Loss Processes in Germanium at High Electric Fields Using Microwave Frequencies", J. Phys. Chem. Solids, Vol. 19, pp. 198-217, 1961.

21. Paranjape, B.V., "Behaviour of Hot Electrons in Microwave Fields", Phys. Rev., Vol. 122, pp. 1372-1375, 1961.

22. Schmitd-Teidemann, "Tensor Theory of the Conductivity of Warm Electrons in Cubic Semiconductors", Philips Res. Depts. Vol. 18, pp. 338-360, 1963.

23. Nag, B.R. and Das, P., "Microwave Conductivity of Semiconductors in the Presence of High Electric Fields", Phys. Rev., Vol. 132, pp. 2514-2520, 1963.

24. Gunn, M.W., "Hot Electron Effects in N-type Germanium at 9.392 GC/S", J. of Elect. Control, Vol. 16, pp. 481-491, 1964.

25. Gunn, M.W., "The Microwave Conductivity of Germanium", Proc. IEEE, Vol. 52, pp. 851-851, 1964.

26. Staecker, P.W. and Das, P., "Hot Electron Microwave Rotator", Proc. IEEE, Vol. 52, pp. 1766-1768, 1965.

27. Dykman, I.M. and Tolpygo, E.I., "Microwave Conductivity of Semiconductors with Carriers Heated by D.C. Field", Soviet Physics - Solid State, Vol. 7, pp. 332-338, 1966.

28. Gershenzon, E.M., Gurvich, Yu. A. and Litvak-Gorskaya, L.B., "Anistropic Absorption of Electromagnetic Waves By Hot Carriers in Semiconductors", Soviet Physics - Solid State, Vol. 7, pp. 1111-1113, 1965.

29. Guha, S. and Nag, B.R., "Microwave Conduction in N-type Germanium under Hot Electron Conditions", Proc. Phys. Soc. (G.B.), Vol. 90, pp. 427-434, 1967.

30. Pötzl, H.W. and Richter, K., "Microwave Conductivity Anisotropy of Hot Electrons in n-InSb at 77°k", Proc. IEEE, Vol. 55, pp. 1497-1498, 1967.

31. Nag, B.R., "Hot Carrier Microwave Conductivity of Elemental Semiconductors", Solid State Electronics, Vol. 11, pp. 209-218, 1968.

32. Das, P., Rifkin, R.H. and Poole, J.J., "Microwave Conductivity of Polar Semiconductors in the Presence of High Electric Fields", Electronics Letters, Vol. 3, pp. 515-516, 1967.

33. Kopetz, H. and Pötzl, H.W., "Microwave Conductivity of Polar Semiconductors in the Presence of A High Electric Field", Electronics Letters, Vol. 4, pp. 79-80, 1968.

34. Richter, K. and Bonek, E., "Anisotropy of Small-Signal Microwave Conductivity due to Hot Electrons in InSb", J. of Appl. Physics, Vol. 39, pp. 4035-4036, 1968.

35. Beljers, H.G. and Vander Lindt, W.J., "Dielectric Measurements with Two Magic Tees on Shorted Waveguides", Phillips Research Report, Vol. 6, pp. 96-104, 1951.

36. Altman, J.L., Microwave Circuits, (D. Van Nostrand Co., N.Y. 1964), pp. 64.

37. Collin, R.E., Foundations of Microwave Engineering, (McGraw Hill, N.Y. 1966) pp. 264.

38. Holm, J.D., Johnson, D.L. and Champlin, K.S., "Reflections from Rotary-Vane Precision Attenuators", IEEE Trans. on Microwave Theory and Techniques (Correspondence), Vol. MTT-15, pp. 123-124, 1967.

39. Engen, G.F. and Beatty, R.W., "Microwave Reflectometer Techniques", IRE Trans. on Microwave Theory and Techniques", Vol. MTT-7, pp. 351-359, 1959.

40. Montogomery, C.G., Technique of Microwave Measurements, (Boston Tech. Lithographers, Mass., 1963) pp. 533.

41. Ramo, S., Whinnery, J.R. and Van Duzer, T., Fields and Waves in Communication Electronics, (John Wiley and Sons, Inc., N.Y., 1965) pp. 440.

42. Smith, R.A., Semiconductors, (Cambridge University Press, 1964) pp. 217.

43. Lewin, L., Advanced Theory of Waveguides, (Illiffe and Sons, Ltd., 1951) Chapter 6.

44. Harrington, R.F., Time Harmonic Electromagnetic Fields, (McGraw Hill, N.Y., 1961) pp. 130.

45. Mclachlan, N.W., Bessel Functions for Engineers, (Oxford Press, 1955) Formula 140, pp. 199.

46. Scarborough, J.B., Numerical Mathematical Analysis, (The John Hopkinson Press, 1958) pp. 166.

47. Compton, R.T., "The Admittance of Aperture Antennas Radiating into Lossy Media", Antenna Laboratory, Ohio State University Research Foundation, Columbus, Ohio, Rept. 1691-5, 1964.

48. Croswell, W.F., Rudduck, R. and Hatcher, D.M., "The Admittance of a Rectangular Waveguide Radiating into a Dielectric Slab", IEEE Trans. Antennas and Propagation Vol. AP-15, pp. 627-633, 1967.

49. Villenauve, A.T., "Admittance of Waveguide Radiating into a Plasma Environment", IEEE Trans. Antennas and Propagation, Vol. AP-13, pp. 115-121, 1965.

50. Galjes, J., "Admittance of a Waveguide Radiating into a Stratified Plasma", IEEE Trans. Antennas and Propagation, Vol. AP-13, pp. 64-70, 1965.

51. Galjes, J. and Mentzoni, M.H., "Waveguide Admittance for Radiation into Plasma Layers - Theory and Experiment", IEEE Trans. Antennas and Propagation, Vol. AP-15, pp. 465-470, 1967.

52. Bailey, M.C. and Swift, C.T., "Input Admittance of a Circular Waveguide Aperture Covered by a Dielectric Slab", IEEE Trans. Antennas and Propagation, Vol. AP-16, pp. 386-391, 1968.

53. Croswell, W.F., Taylor, W.C., Swift, C.T. and Cockrell, C.R., "The Input Admittance of a Rectangular Waveguide Fed Aperture Under an Inhomogeneous Plasma: Theory and Experiment", IEEE Trans. Antennas and Propagation, Vol. AP-16, pp. 475-487, 1968.

54. I.B.M., Scientific Subroutine Package, (IBM Tech. Publication Department, N.Y., 1966) pp. 96.

55. Shockley, W., "Hot Electrons in Germanium and Ohm's Law", Bell. Syst. Tech. Journal, Vol. 30, pp. 990-1034, 1951.

56. Engineer, M.H. and Nag, B.R., "On a Semiconductor Microwave Rotator Using Hot Carrier Properties", Proc. IEEE (Correspondence), Vol. 54, pp. 429-230, 1966.

57. Gunn, M.W. and Rahman, M.H., "The Hot Electron Microwave Rotator", Proc. IEEE (Correspondence), Vol. 55, pp. 1082-1084, 1967.

58. Rose, K., "A Microwave Technique for the Study of Deviations from Ohm's Law in High Resistivity Semiconductors", Tech. Report No. 1, University of Illinois, pp. 16, 1962.

59. Acket, G.A. and De Groot, J., "Measurements of the Current Field Strength Characteristics of N-type Gallium Arsenide Using Various High Power Microwave Techniques", IEEE Trans. Electron Devices, Vol. ED-14, pp. 505-511, 1967.

60. Yamashita, J. and Wortanabe, M., "On the Conductivity of Non-polar Crystals in the Strong Electric Field", Progress Theor. Phys. Vol. 12, pp. 443-453, 1954.

61. Stratton, R., Solid State Physics in Electronics and Telecommunications (Vol. 1, Academic Press, N.Y., 1960) pp. 343.

62. Nag, B.R., "Hot Carrier Microwave Conductivity of Elemental Semiconductors", Solid State Electronics, Vol. 11, pp. 209-218, 1968.

63. Conwell, E.M., Fowler, V.J. and Zucker, J., "Final Report on Contract AF 19 (604)-5714, Air Force Cambridge Res. Centre, Cambridge, Massachusetts, 1960.

64. Pinson, W., Private Communication.

65. Sheikh, R.H., "The Microwave Measurement of Semiconductor Permittivity", M.Sc. Thesis, McMaster University, pp. 43, 1965.

66. James, J. and James, R.C., Mathematics Dictionary, (D. Van Nostrand Co., Inc., Princeton, N.J., 1960) pp. 184.

67. Moll, J.L., "Physics of Semiconductors", (McGraw Hill, N.Y., 1964) pp. 63.

68. Reikh, H.G. and Risken, H.,"Distribution Functions for Hot Electrons in Many Valley Semiconductors", Phys. Rev. Vol. 124, pp. 777-784, 1961.